UNIVERSITY OF CALIFORNIA SAN DIEGO

Aging, immortality and persistence produced by phenotypic heterogeneity in bacterial populations

A dissertation submitted in partial satisfaction of the
requirements for the degree Doctor of Philosophy

in

Biology

by

Audrey Menegaz Proenca

Committee in charge:

Professor Lin Chao, Chair
Professor Ronald Burton
Professor Justin Meyer
Professor Scott Rifkin
Professor Gürol Süel

2019

The Dissertation of Audrey Menegaz Proenca is approved, and it is acceptable in quality and form for publication on microfilm and electronically:

_____

_____

_____

_____

_____

Chair

University of California, San Diego

2019

TABLE OF CONTENTS

LIST OF FIGURES

LIST OF TABLES

ACKNOWLEDGEMENTS

Foremost, I would like to express my gratitude to the Chao Lab show-runners, Dr. Lin Chao and Dr. Camilla Rang. From the moment Lin and I chatted about bacterial aging, back when I was an undergraduate exchange student, being part of your research group has been a most exciting and gratifying experience. Thank you both for teaching me so much over the years, for helping me grow as a scientist and as a person. For the mentoring, advice, and friendship. Lin, thank you for challenging me, for guiding me through all of our crazy explorations, and for making sure I always had a safe course in case the explorations failed. Camilla, thank you for the technical guidance, for the encouragement face any challenge, and for making research always a fun experience. Thank you both for this awesome lab, for keeping me inspired and caffeinated the last five years.

I thank all past and present members of the Chao Lab for sharing so many hours of relentless cell-tracing on ImageJ, endlessly solving the weirdest microscopy issues, and for support through all the hardships of this work. Thank you all: Justin Ang, Sarah Ardell, Christen Buetz, Matt Campos, Jeff Chen, Sophia Cheung, Jason Darvis, Siyu Grace, Ida Ivanova, Josh Kenchel, Annie Li, Xiyu Liu, Andrew Qiu, Chao Shi, and Brandon Tang. And special thanks to Lexi, the best lab dog, for sharing my lunch so many times — long before my cooking was anywhere near palatable.

I would like to thank my thesis committee, Dr. Ron Burton, Dr. Justin Meyer, Dr. Scott Rifkin, and Dr. Gurol Suel, for the immensely helpful feedback provided over the years. Your guidance, insights and suggestions were essential in shaping this work from the very start. Thank you for sharing our excitement for each new project and for encouraging my ambitions for this

research and beyond. My sincere thanks to collaborators at the Jeff Hasty Lab, Omar Din, Ryan Johnson and Garret Graham, for the inestimable assistance with experimental setup and microfluidic expertise throughout this work.

I would like to thank all wonderful people of the Section of Ecology, Behavior and Evolution. My most sincere gratitude for your support through the ups and downs of Science, for the discussions and ceaseless incentive. To my fellow students, thank you for being such kind and incredible people. The encouragement and fellowship I found among you is a most treasured memory from this degree.

Finally, I am extremely grateful for the friends this PhD brought my way, Christen, Hamanda, Andrew, and Henry, and my talented husband Cesar. Thank you for the encouragement and support through every hardship, every failure, and for the many shared beers when everything worked out in the end. My most sincere thanks for keeping me sane throughout this research, for reminding me there is a life outside the lab, and for always being there when I needed you. You guys are amazing!

I thank all funding sources for this research, provided by the Ministry of Education of Brazil through the Science Without Borders Fellowship/CAPES; National Science Foundation; Chris Wills Endowed Graduate Student Research Award; and UC San Diego Goeddel Chancellor's Award. I am also grateful for the support provided via conference funding by the UC San Diego Division of Biological Sciences and Section of Ecology, Behavior and Evolution; Dr. Donald Helinski; UC San Diego Graduate Student Association; and the Society for the Study of Evolution.

Chapter 1, in full, is a reprint of the material as it appears in Proenca AM, Rang CU, Buetz C, Shi C, Chao L (2018). Age structure landscapes emerge from the equilibrium between aging

and rejuvenation in bacterial populations. *Nature Communications* 9:3722. The dissertation author was the primary investigator and author of this paper.

Chapter 2, in full, is a reprint of the material as it appears in Proenca AM, Rang CU, Qiu A, Shi C, Chao L (2019). Cell aging preserves cellular immortality in the presence of lethal levels of damage. *PLoS Biology* 17(5): e3000266. The dissertation author was the primary investigator and author of this paper.

Chapter 3, in part, is currently being prepared for submission for publication of the material. Proenca AM, Rang CU, Chao L. The dissertation author was the primary investigator and author of this material.

VITA

2014	Licentiate Bachelor of Science in Biological Sciences *summa cum laude*, Pontifical Catholic University of Rio Grande do Sul, Porto Alegre, Brazil
2014-2018	Science without Borders Fellow, CAPES Foundation, Ministry of Education of Brazil
2019	Doctor of Philosophy in Biology, University of California San Diego, La Jolla, CA

PUBLICATIONS

Azevedo, L.S., Moraes, F.P., Proenca, A.M., Xavier, M.M., Pantoja, E.O., Villavicencio, B., Finck, J.A., Rocha, K.B., Azevedo, W.F. 2012. Recent progress of molecular docking simulations applied to development of drugs. *Current Bioinformatics* 7: 352-365.

Chao, L., Rang, C.U., Proenca, A.M., Chao, J.U. 2016. Asymmetrical damage partitioning in bacteria: A model for the evolution of stochasticity, determinism, and genetic assimilation. *PLoS Computational Biology* 12(1): e1004700.

Proenca, A.M., Rang, C.U., Buetz, C., Shi, C., Chao, L. 2018. Age structure landscapes emerge from the equilibrium between aging and rejuvenation in bacterial populations. *Nature Communicatons* 9:3722.

Rang, C.U., Proenca, A.M., Buetz, C., Shi, C., Chao, L. 2018. Minicells as a damage disposal mechanism in *Escherichia coli*. *mSphere* 3(5): e00428-18.

Proenca, A.M., Rang, C.U., Qiu, A., Shi, C., Chao, L. 2019. Cell aging preserves cellular immortality in the presence of lethal levels of damage. *PLoS Biology* 17(5): e3000266.

ABSTRACT OF THE DISSERTATION

Aging, immortality and persistence produced by phenotypic heterogeneity in bacterial populations

by

Audrey Menegaz Proenca

Doctor of Philosophy in Biology

University of California San Diego, 2019

Professor Lin Chao, Chair

Senescence, the process of age-specific decrease of fitness, has puzzled evolutionary biologists ever since the publication of On the Origin of Species. How ubiquitous among living creatures is this phenotypic decline that arises with age? Up until the last decade aging seemed limited to multicellular organisms with a clear separation between soma and germline, as stated by the Evolutionary Theory of Aging. Bacteria were considered functionally immortal. However, with the improvement of single-cell microscopy techniques, studies revealed that prokaryotes are,

indeed, susceptible to aging. Bacteria inheriting a conserved cell pole, harboring larger non-genetic damage loads, display an aging phenotype, while its sibling rejuvenates through the inheritance of a reduced damage load. My research shows that aging and rejuvenation represent deterministic aspects of bacterial physiology, deriving from the stabilization of a population around states of growth equilibrium. The maintenance of this equilibrium allows for proliferative immortality. I demonstrate that equilibrium can be disrupted by extrinsic damage, leading to the mortality of aging lineages while rejuvenating lineages remain immortal. Thus, the phenotypic heterogeneity produced by asymmetric damage partitioning leads to differential mortality in a bacterial population. Finally, I offer evidence for the connection between aging and the phenotype of bacterial persistence, where transiently dormant cells survive antibiotic treatments. This work demonstrates the emergence of deterministic age structures in bacterial populations, its relevance for the maintenance of cellular proliferation, and offers a potential application of this research for a pressing public health concern.

INTRODUCTION

The evolutionary theory of aging

Aging is defined as a decline in fitness over time, with a decrease of reproductive outputs and survival rates due to the internal deterioration of an organism (Rose 1991). In essence, the prevalence of aging seems an evolutionary contradiction: why would natural selection not oppose a decrease of fitness with age, when it was shown that organisms are capable of evolving longer lifespans (Luckinbill et al. 1984)? The most accepted explanation, stated by the evolutionary theory of aging, is that mutations with deleterious effects late in life tend to accumulate because of the declining strength of natural selection with age (Freeman and Herron 2007). Such mutations may also display antagonistic pleiotropic effects —beneficial for young organisms and harmful for old individuals —, thus being favored by selection while manifested by the most abundant age class of the population (Ackermann, Schauerte, et al. 2007).

An essential requirement of the evolutionary theory, to ensure the declining strength of natural selection on aging organisms, is a clear differentiation between soma and germ lines. The disposable soma theory is considered a mechanism of the evolutionary theory of aging, specifying that somatic cells accumulate various forms of damage (López-Otín et al. 2013), while the germline must remain intact (Kirkwood 2008). In this perspective, is seemed reasonable to believe that unicellular organisms were immune to aging. Without a separation between soma and germline, a cell would divide symmetrically and produce two organisms with similar levels of damage. Until recently, the only way of aging known to prokaryotes was conditional senescence, when organisms become unculturable due to nutrient depletion and accumulation of toxic metabolites (Ksiązek 2010b, 2010a).

The immortality of bacteria was first questioned with the advancement of single-cell microscopy techniques, revealing unexpected patterns within populations. The clearly asymmetric division of *Caulobacter crescentus* (Ackermann, Stearns, and Jenal 2003) was shown to create distinct fates for mother and daughter cells, which was surprisingly seconded by the morphologically symmetric *Escherichia coli* (Stewart et al. 2005). These studies demonstrated that bacteria also suffer an age-related loss of fitness, with lower probability of survival, growth rate and reproductive output. For rod-shaped bacteria, aging depends on which cellular pole is inherited at the time of division: a newly synthesized pole or a conserved one, with the latter accumulating damage in the form of protein aggregates (Lindner et al. 2008). In other words, at each division one of the two siblings acts as the somatic lineage, aging and storing damage while the other sibling rejuvenates. In the next section, we shall discuss in detail the role of asymmetry and current findings on bacterial aging.

Aging in asymmetrically dividing bacteria

Long before aging was a recognized phenomenon in prokaryotes, when bacteria were still considered functionally immortal, it was clear that these organisms exhibited patterns of asymmetry between sister cells and well-defined cell polarity (Maddock, Alley, and Shapiro 1993). *C. crescentus* was already a model organism for the study of polarity and asymmetry due to its curious life cycle: at each division, a stalked cell generates a juvenile swarmer, which disperses and differentiates into a stalked cell in order to reproduce (Poindexter 1964). The study of asymmetry mechanisms in this species led to the finding of an actin-like protein, MreB, involved in determination of cell polarity, cell shape regulation and positioning of origins of replication (Gitai, Dye, and Shapiro 2004). *C. crescentus* revealed a fine regulation of asymmetry through the

inhibition of replication in the juvenile swarmer stage (Chen et al. 2010), with a clear polarity already implemented in predivisional cells (Tsokos and Laub 2012). The distinct stages of development in *C. crescentus* made it the first model organism for bacterial aging.

Bacterial aging was described through single-cell microscopy, tracking individuals over generations. *C. crescentus* aging was first observed by following stalked mother cells for 300 h of cultivation, as it produced swarmer daughter cells. Mother cells exhibited a decrease in age-specific reproductive output, in a rate that exceeded linear damage accumulation (Ackermann, Stearns, and Jenal 2003), thus aging throughout the experiment. This pioneer study was quickly followed by the reporting of aging in *E. coli*, known for its morphologically symmetric division (Stewart et al. 2005). In this case, although the two daughter cells look identical, the inheritance of distinct cells poles produced physiologically distinct individuals. Stewart and colleagues thus defined bacterial age as a function of pole inheritance. At each division, one of the daughter cells (old daughter) inherits a conserved pole from its mother, while the other (new daughter) receives a newly synthesized pole. Old daughters exhibit lower growth rates than their siblings, effect that accumulates with increasing pole age; they also produce less offspring biomass and have higher probability of dying, reflecting a loss of fitness with increased age. On the other hand, the new daughter rejuvenates at each division, diminishing the need of cellular repair through damage partitioning.

A recurring limitation of early aging experiments, however, was the analysis of long-term asymmetry. In this context, mathematical models and simulations play an important role on predicting outcomes over many bacterial generations (Nyström 2007). An early model addressed the data collected by Stewart et al., accounting for asymmetric cell division and the possibility of cellular repair (Ackermann, Chao, et al. 2007). Considering the chance of survival as a function of

accumulated damage, the model and simulations indicated that organisms with asymmetric division have an advantage over those with symmetric division, even when the likelihood of survival is the same for both. This study presented another side of the evolutionary theory of aging, in which senescence could also evolve from non-genetic damage.

Aging depends on asymmetric damage accumulation

Bacteria dispose of non-genetic damage through the formation of protein aggregates, composed of misfolded proteins. Bacterial aggregates are classified as inclusion bodies, amorphous and induced by stress responses (Sabate, De Groot, and Ventura 2010), although in some cases amyloid aggregates, composed by insoluble fibrils, can also form (Lindner and Demarez 2009). Bacteria are therefore not only a model for the evolution of aging, with the simplest form of soma-germline separation, but also for the study of age-related phenotypes such as loss of proteostasis (López-Otín et al. 2013). The formation of aggregates can be beneficial by clearing the cell of misfolded (Lindner et al. 2008; Rokney et al. 2009) or foreign (Lloyd-Price et al. 2012) proteins and concentrating the damage at the poles. Once small foci of misfolded proteins cluster into a large polar aggregate, it becomes anchored at the cell pole and is inherited by a daughter cell. Therefore, an older pole tends to accumulate larger aggregates and favor the generation of a new daughter free of damage (Lindner et al. 2008).

Old daughters, due to the inheritance of a conserved cell pole over generations, tend to inherit larger damage loads. The polar localization of aggregates is attributed to a passive mechanism, where freely diffusing misfolded proteins tend to aggregate in the cellular regions free of the nucleoid (Winkler et al. 2010; Coquel et al. 2013), usually the poles. A sufficiently large aggregate can no longer diffuse, remaining trapped at the pole. This mechanism is advantageous

because the aggregation of damage has lower energy cost than repair or solubilization of misfolded proteins (Winkler et al. 2010). On a longer time frame, the process of repair and disaggregation takes place through polar chaperones and proteases (Rokney et al. 2009; Sabate, De Groot, and Ventura 2010; Baig et al. 2014), allowing for the survival of old daughters despite its larger damage inheritance.

Despite the strong support for protein aggregation correlating with bacterial aging, a series of discrepant results questioned the generality of this phenomenon. Early models considered asymmetric partitioning a strategy depending on environmental conditions (Watve et al. 2006), and microscopy experiments suggested that aging could be dependent on the infliction of extrinsic damage (Rang et al. 2012). Similarly, *E. coli* lineages were shown to display remarkably stable growth over hundreds of generations when observed in a microfluidic device (Wang et al. 2010; Taheri-Araghi et al. 2015), which promotes unstressed growth conditions. The replicative immortality reported by Wang et al. seemed in direct conflict with the idea that old lineages accumulate damage over generations, since their results showed no decline in function with the consecutive inheritance of old poles. Although conciliatory explanations were offered by modeling (Chao 2010) and a re-evaluation of microfluidic growth data (Rang, Peng, and Chao 2011), the prevalence of aging in prokaryotes remained controversial. All these contradictory findings raised questions on whether bacteria experience a deterministic form of aging, and whether physiological asymmetry could be considered an aging phenotype. Addressing these issues was therefore essential for the advancement of the field, and for the establishment of bacteria as model organisms for the study of aging.

Chapter summaries

The present work addresses the controversies surrounding bacterial aging, conciliating the discrepancies raised in the literature and establishing the connection between aging in bacterial and eukaryotic systems.

In Chapter 1, we show that aging and rejuvenation represent a deterministic aspect of bacterial physiology. By following *E. coli* lineages in the stable environment of microfluidic devices, we demonstrate that asymmetric cell division occurs in the absence of extrinsic damage. In these conditions, new and old lineages reach distinct states of growth equilibrium, thus remaining proliferative and stable over time while displaying asymmetric physiology. Because cells in equilibrium continuously generate daughters of the opposite polarity, we show that deterministic aging structures emerge from bacterial populations, where immortal new and old lineages are constantly connected by processes of aging and rejuvenation.

In Chapter 2, we show that cellular aging determines the transition from immortality to mortality in bacterial populations. We demonstrate that the infliction of extrinsic damage disrupts stable equilibrium with a dosage-dependent response. When the rates of damage accumulation surpass a certain threshold, old lineages lose stability and become mortal. New lineages within the same population, however, retain immortal proliferation due to physiological asymmetry. Thus, the asymmetric partitioning of damage is a key process determining the immortality or mortality of a cell lineage facing environmental pressures. This study provides further evidence for the ubiquitousness of the aging process, identifying similarities between bacterial and eukaryotic aging cell lineages.

In Chapter 3, we explore the potential implications of bacterial aging for a critical public health issue, antibiotic persistence. Most chronic infections are caused by subpopulations of

antibiotic susceptible bacteria in a transient state of dormancy, defined as persistence. This phenotype arises due to a natural and ubiquitous heterogeneity of growth states in bacterial populations. Nonetheless, the origin and unifying mechanism of this dormancy remains unknown, with several unrelated pathways being able to trigger persistence. We show that asymmetric damage partitioning, by producing deterministic phenotypic heterogeneity in bacterial populations, could be a driver of bacterial persistence. Elucidating the link between asymmetry and persistence may provide a new perspective in the treatment of recalcitrant infections.

References

Ackermann, Martin, Lin Chao, Carl T Bergstrom, and Michael Doebeli. 2007. "On the Evolutionary Origin of Aging." *Aging Cell* 6 (2): 235–44. doi:10.1111/j.1474-9726.2007.00281.x.

Ackermann, Martin, Alexandra Schauerte, Stephen C Stearns, and Urs Jenal. 2007. "Experimental Evolution of Aging in a Bacterium." *BMC Evolutionary Biology* 7 (January): 126. doi:10.1186/1471-2148-7-126.

Ackermann, Martin, Stephen C. Stearns, and Urs Jenal. 2003. "Senescence in a Bacterium with Asymmetric Division." *Science* 300: 1920.

Baig, Ulfat I, Bharati J Bhadbhade, Dincy Mariyam, and Milind G Watve. 2014. "Protein Aggregation in *E. coli*: Short Term and Long Term Effects of Nutrient Density." *PLoS ONE* 9 (9): e107445. doi:10.1371/journal.pone.0107445.

Chao, Lin. 2010. "A Model for Damage Load and Its Implications for the Evolution of Bacterial Aging." *PLoS Genetics* 6 (8): e1001076. doi:10.1371/journal.pgen.1001076.

Chen, Y Erin, Carolina Tropini, Kristina Jonas, Christos G Tsokos, and Kerwyn C Huang. 2010. "Spatial Gradient of Protein Phosphorylation Underlies Replicative Asymmetry in a Bacterium." *Proceedings of the National Academy of Sciences* 108 (3): 1052–57. doi:10.1073/pnas.1015397108/-/DCSupplemental.www.pnas.org/cgi/doi/10.1073/pnas.1015397108.

Coquel, Anne Sophie, Jean Pascal Jacob, Mael Primet, Alice Demarez, Mariella Dimiccoli, Thomas Julou, Lionel Moisan, Ariel B. Lindner, and Hugues Berry. 2013. "Localization of Protein Aggregation in *Escherichia coli* Is Governed by Diffusion and Nucleoid Macromolecular Crowding Effect." *PLoS Computational Biology* 9 (4). doi:10.1371/journal.pcbi.1003038.

Freeman, Scott, and Jon C. Herron. 2007. “Why Do Organisms Age and Die?” In *Evolutionary Analysis*, 4th ed., 487–502. Upper Saddle River, NJ: Pearson Prentice Hall.

Gitai, Zemer, Natalie Dye, and Lucy Shapiro. 2004. “An Actin-like Gene Can Determine Cell Polarity in Bacteria.” *Proceedings of the National Academy of Sciences of the United States of America* 101 (23): 8643–48. doi:10.1073/pnas.0402638101.

Kirkwood, T. B. L. 2008. “Understanding Ageing from an Evolutionary Perspective.” *Journal of Internal Medicine* 263 (2): 117–27. doi:10.1111/j.1365-2796.2007.01901.x.

Książek, Krzysztof. 2010a. “Bacterial Aging: From Mechanistic Basis to Evolutionary Perspective.” *Cellular and Molecular Life Sciences* 67 (18): 3131–37. doi:10.1007/s00018-010-0417-4.

———. 2010b. “Let’s Stop Overlooking Bacterial Aging.” *Biogerontology* 11 (6): 717–23. doi:10.1007/s10522-010-9278-3.

Lindner, Ariel B., and Alice Demarez. 2009. “Protein Aggregation as a Paradigm of Aging.” *Biochimica et Biophysica Acta - General Subjects* 1790 (10). Elsevier B.V.: 980–96. doi:10.1016/j.bbagen.2009.06.005.

Lindner, Ariel B, Richard Madden, Alice Demarez, Eric J Stewart, and François Taddei. 2008. “Asymmetric Segregation of Protein Aggregates Is Associated with Cellular Aging and Rejuvenation.” *Proceedings of the National Academy of Sciences of the United States of America* 105 (8): 3076–81. doi:10.1073/pnas.0708931105.

Lloyd-Price, Jason, Antti Häkkinen, Meenakshisundaram Kandhavelu, Ines J. Marques, Sharif Chowdhury, Eero Lihavainen, Olli Yli-Harja, and Andre S. Ribeiroa. 2012. “Asymmetric Disposal of Individual Protein Aggregates in *Escherichia coli*, One Aggregate at a Time.” *Journal of Bacteriology* 194 (7): 1747–52. doi:10.1128/JB.06500-11.

López-Otín, Carlos, Maria A. Blasco, Linda Partridge, Manuel Serrano, and Guido Kroemer. 2013. “The Hallmarks of Aging.” *Cell* 153: 1194–1217. doi:10.1016/j.cell.2013.05.039.

Luckinbill, Leo S., Robert Arking, Michael J. Clare, William C. Cirocco, and Steven A. Buck. 1984. “Selection for Delayed Senescence in *Drosophila melanogaster*.” *Evolution* 38 (5): 996–1003. doi:10.5274/jsbr.31.3.143.

Maddock, Janine R., M. R. K. Alley, and Lucille Shapiro. 1993. “Polarized Cells, Polar Actions.” *Journal of Bacteriology* 175 (22): 7125–29.

Nyström, Thomas. 2007. “A Bacterial Kind of Aging.” *PLoS Genetics* 3 (12): 2355–57. doi:10.1371/journal.pgen.0030224.

Poindexter, Jeanne Stove. 1964. “Biological Properties and Classification of the *Caulobacter* Group1.” *Bacteriological Reviews* 28 (3): 231–95.

Rang, Camilla U, Annie Y Peng, and Lin Chao. 2011. “Temporal Dynamics of Bacterial Aging and Rejuvenation.” *Current Biology* 21 (21): 1813–16. doi:10.1016/j.cub.2011.09.018.

Rang, Camilla U, Annie Y Peng, Art F Poon, and Lin Chao. 2012. “Ageing in *Escherichia coli* Requires Damage by an Extrinsic Agent.” *Microbiology* 158 (Pt 6): 1553–59. doi:10.1099/mic.0.057240-0.

Rokney, Assaf, Merav Shagan, Martin Kessel, Yoav Smith, Ilan Rosenshine, and Amos B. Oppenheim. 2009. “*E. coli* Transports Aggregated Proteins to the Poles by a Specific and Energy-Dependent Process.” *Journal of Molecular Biology* 392 (3). Elsevier Ltd: 589–601. doi:10.1016/j.jmb.2009.07.009.

Rose, Michael R. 1991. *Evolutionary Biology of Aging*. New York: Oxford University Press.

Sabate, Raimon, Natalia S. De Groot, and Salvador Ventura. 2010. “Protein Folding and Aggregation in Bacteria.” *Cellular and Molecular Life Sciences* 67 (16): 2695–2715. doi:10.1007/s00018-010-0344-4.

Stewart, Eric J, Richard Madden, Gregory Paul, and François Taddei. 2005. “Aging and Death in an Organism That Reproduces by Morphologically Symmetric Division.” *PLoS Biology* 3 (2): e45. doi:10.1371/journal.pbio.0030045.

Taheri-Araghi, Sattar, Serena Bradde, John T. Sauls, Norbert S. Hill, Petra Anne Levin, Johan Paulsson, Massimo Vergassola, and Suckjoon Jun. 2015. “Cell-Size Control and Homeostasis in Bacteria.” *Current Biology* 25 (December). Elsevier Ltd: 385–91. doi:10.1016/j.cub.2014.12.009.

Tsokos, Christos G, and Michael T Laub. 2012. “Polarity and Cell Fate Asymmetry *in Caulobacter crescentus*.” *Current Opinion in Microbiology* 15 (6). Elsevier Ltd: 744–50. doi:10.1016/j.mib.2012.10.011.

Wang, Ping, Lydia Robert, James Pelletier, Wei Lien Dang, Francois Taddei, Andrew Wright, and Suckjoon Jun. 2010. “Robust Growth of *Escherichia coli*.” *Current Biology* 20 (12). Elsevier Ltd: 1099–1103. doi:10.1016/j.cub.2010.04.045.

Watve, Milind, Sweta Parab, Prajakta Jogdand, and Sarita Keni. 2006. “Aging May Be a Conditional Strategic Choice and Not an Inevitable Outcome for Bacteria.” *Proceedings of the National Academy of Sciences of the United States of America* 103 (40): 14831–35. doi:10.1073/pnas.0606499103.

Winkler, Juliane, Anja Seybert, Lars König, Sabine Pruggnaller, Uta Haselmann, Victor Sourjik, Matthias Weiss, Achilleas S Frangakis, Axel Mogk, and Bernd Bukau. 2010. “Quantitative and Spatio-Temporal Features of Protein Aggregation in *Escherichia coli* and Consequences on Protein Quality Control and Cellular Ageing.” *The EMBO Journal* 29 (5): 910–23. doi:10.1038/emboj.2009.412.

CHAPTER 1

Age structure landscapes emerge from the equilibrium between aging and rejuvenation in bacterial populations

1.1 Abstract

The physiological asymmetry between daughters of a mother bacterium is produced by the inheritance of either old poles, carrying non-genetic damage, or newly synthesized poles. However, because bacteria display long-term growth stability leading to physiological immortality, there is controversy on whether asymmetry corresponds to aging. Here we show that deterministic age structure landscapes emerge from physiologically immortal bacterial lineages. Through single-cell microscopy and microfluidic techniques, we demonstrate that aging and rejuvenating bacterial lineages reach two distinct states of growth equilibria. These equilibria display stabilizing properties, which we quantified according to the compensatory trajectories of continuous lineages throughout generations. Finally, we show that the physiological asymmetry between aging and rejuvenating lineages produces complex age structure landscapes, resulting in a deterministic phenotypic heterogeneity that is not artifact of starvation, neither a strategy induced by extrinsic damage. These findings indicate that physiological immortality and cellular aging can coexist in a single cellular context.

1.2 Introduction

Aging, defined broadly as the decline of function and consequent loss of fitness with time, is a ubiquitous characteristic of biological organisms (Rose 1991; Kirkwood 2008). Although bacteria were traditionally thought not to age, recent studies have suggested that the phenotype is

present in asymmetrically dividing Caulobacter crescentus and Escherichia coli (Ackermann, Stearns, and Jenal 2003; Stewart et al. 2005; Ackermann, Chao, et al. 2007; Lindner et al. 2008). Because rod-shaped bacteria such as E. coli divide at the middle, a new pole is synthesized at the division plane with every replication, while the distal old poles are conserved from the mother (Figure 1.1A). Thus, each *E. coli* cell has an old and a new pole. Upon division, cells inheriting the maternal old pole are called old daughters, while the ones inheriting the newly synthesized pole are called new daughters. Old poles are consecutively inherited over generations, carrying accumulated non-genetic damage in the form of inclusion bodies, which are aggregates of misfolded proteins (Lindner et al. 2008; Lindner and Demarez 2009; Winkler et al. 2010; Coquel et al. 2013). Old daughters, inheriting larger damage loads along with old poles, display a decline in growth rates associated with aging, while new daughters rejuvenate by receiving less damage.

Nonetheless, despite a succession of reports on bacterial aging (Ackermann, Stearns, and Jenal 2003; Stewart et al. 2005; Ackermann, Chao, et al. 2007; Lindner et al. 2008; Winkler et al. 2010; Coquel et al. 2013; Rang, Peng, and Chao 2011; Rang et al. 2012) and the identification of similar asymmetry in other systems (Laney, Olson, and Sosik 2012; Coelho et al. 2013; Coelho et al. 2014; Fuentealba et al. 2008), the validity and significance of the phenomenon remains controversial. While protein aggregates are strongly biased towards old poles in E. coli and reportedly correlate with functional decline (Lindner et al. 2008; Rokney et al. 2009; Winkler et al. 2010; Coquel et al. 2013), this association was often found to be equivocal in similar systems, such as fission yeast (Coelho et al. 2013; Nakaoka and Wakamoto 2017). Studies in both E. coli and fission yeast suggested that aging is a consequence of extrinsic damage (Rang et al. 2012; Coelho et al. 2013), configuring their divisional asymmetry as a conditional strategy (Watve et al. 2006) as opposed to a deterministic process. Moreover, studies following up on the first reports of

bacterial aging found no reduction in the growth rate of cell lineages over hundreds of generations, and no physiological asymmetry between old and new daughters (Wang et al. 2010). Finally, even when deterioration or growth rate decreases were observed, the decline could be accounted by starvation. The problem arises because agar pads (Stewart et al. 2005; Lindner et al. 2008; Rang et al. 2012) and small microfluidic devices (such as the mother machine (Wang et al. 2010; Taheri-Araghi et al. 2015)) were used to sustain the bacteria during time-lapse microscopy. With agar pads, bacteria form mini-colonies and cells located in the center could become nutrient-limited within a few generations. With the mother machine old daughters always reside at the blind end of growth channels, which is most removed from the nutrient source at the opposite and open end. Therefore, starvation could be present in previous bacterial aging studies.

Despite these conflicting results on bacterial aging, diverse studies have suggested asymmetric damage partitioning as a common mechanism of cell maintenance. Besides bacteria and yeast, the physiological asymmetry between daughter cells has been observed in diatoms (Laney, Olson, and Sosik 2012), nematodes (Valfort et al. 2018), stem cells (Moore et al. 2015; Bufalino, DeVeale, and van der Kooy 2013; Ogrodnik et al. 2014), and others. Thus, the identification of a deterministic divisional asymmetry in bacteria, leading to aging and rejuvenation in clonal populations, could further characterize aging at the cellular level as a ubiquitous process in living organisms.

In this study, we show that deterministic age structures emerge within single populations of unstressed E. coli, while maintaining long-term growth stability and proliferative immortality. We employed two microfluidic designs to ensure culturing of bacteria in the absence of extrinsic damage and to avoid starvation. Our results indicate that the asymmetry between new and old daughters does not correspond to differential nutrient deprivation. By following bacterial

populations over several generations, we show that new and old lineages stabilize around two distinct growth equilibrium attractors, thus exhibiting stable growth over time while displaying consistent asymmetry. Moreover, sister lineages are constantly generated from these equilibria. With every division, a new mother in equilibrium generates a new daughter like itself, and an old daughter that loses function over generations as it ages towards the equilibrium attractor of old lineages. The opposite pattern is verified when new daughters generated from old mothers rejuvenate towards their own equilibrium attractor. Therefore, constant patterns of aging and rejuvenation connect distinct growth equilibria within clonal populations, providing evidence for deterministic age structures in bacteria. These results suggest that key aspects of biological aging may have originated in single cell organisms, such as bacteria. We propose that the emergence of age structures allowed bacteria to evolve a more complex life history by adapting different stages to different ecological challenges.

1.3 Results

1.3.1 Physiological asymmetry does not derive from starvation

To determine the presence of asymmetric damage partitioning in the absence of extrinsic damage, and to test if starvation — rather than aging — could account for the difference between old and new daughters, we measured bacterial growth in microfluidic devices. Our measurements are hereby presented as doubling times, corresponding to elongation rates, which represents a physiologically meaningful parameter, while exhibiting lower variance than division intervals (Figure 1.A.1). Our first microfluidic design, known as the mother machine (Wang et al. 2010; Taheri-Araghi et al. 2015) (Figure 1.1B), is designed to trap cells in a narrow linear channel (oriented vertically for reference) with a blind end at the bottom. A constant supply of nutrient

media flows horizontally, carrying away cells growing out of the traps and delivering nutrients through the open end of the features. Thus, the bottom cells are located farthest from the nutrient source and a starvation gradient could exist. An attractive feature of the mother machine is that the linear channel reduces the tracking of cells to a one-dimensional problem.

In our design of the mother machine, the growth traps harbored four cells for complete division cycles. These bacterial cells were ordered as old, new, new, and old daughters, and denoted as OO, ON, NN, and NO (Figure 1.1C), since the channel is too narrow for the cells to switch places. OO represents the cell that was an old daughter the last two generations, ON is a new daughter born of an old mother, and so forth. We found that ON cells displayed faster doubling times than OO (two-tailed paired t test, $t = -23.152$, $df = 555$, $p < 0.001$; Figure 1.A.2), reflecting the expected asymmetry between new and old daughters. However, the fact that ON is also closer to the nutrient source than OO (Figure 1.1C) suggests that either starvation or asymmetry could produce this pattern. Adding the third cell NN is still confounding because both starvation and aging predict that it has a shorter doubling time. It is only the inclusion of NO, and its comparison to NN, that distinguishes between the two explanations. While aging predicts that the rank of doubling times is NN < NO, since NN is the new daughter, starvation predicts the opposite due to NO being closest to the nutrient source. Our measurements of these cells provided clear support for aging over starvation, with a pair-wise comparison finding NO to display a significantly longer doubling time than NN (Figure 1.2A, Figure 1.A.2 and Table 1.A.1).

The above result alone should eliminate starvation as the explanation for the observed physiological differences between old and new daughters, but we tested this conclusion even more rigorously. We employed a second microfluidic design (Mondragón-Palomino et al. 2011; Ullman et al. 2012), comprising large growth chambers and controlling for positional nutrient deprivation

by opening both ends of the traps (Figure 1.1D). In these chambers, the larger width spread cells into a monolayer of approximately 300 bacteria, which pushed against each other and shuffled positions as they elongated. Unlike the mother machine, this device did not preferentially retain either the old or the new daughter. Thus, we named this design, for the purpose of this study, the daughter device, and used it to test whether the doubling time relationship observed for OO, ON, NN, and NO in the mother machine could be replicated. To assemble a data set equivalent to Fig. 2A, we identified OO cells in the daughter device as those that had been old for at least two generations, and then followed them forward in time to obtain the series OO, ON, NN, and NO. The relationships measured for OO, ON, NN, and NO in the mother machine (Figure 1.2A) and the daughter device (Figure 1.2B, Figure 1.A.2 and Table 1.A.1) were nearly identical. Most importantly, NO (20.18±0.97 min, mean ± s.d., n = 620) still had a significantly longer doubling time than NN (19.60±0.94 min, n = 620) in the latter device. To ensure that the shuffling was effective, we measured cell positions in the daughter device and found that OO, ON, NN, and NO experienced the same average distances from the open sides and nutrient sources (Figure 1.2C-D). Thus, these results indicate that bacterial populations display asymmetric physiology in the absence of both extrinsic damage and starvation.

The strongest evidence that aging rather than starvation accounts for the difference between old and new daughters comes from a comparison of the rank order of OO, ON, NN, and NO doubling times. In both microfluidic devices, the rank was OO > NO > ON > NN (Figure 1.2A-B), indicating that bacterial aging is more quantitative than just new daughters growing faster than old daughters. Rather, because OO and NO are not equivalent old daughters (mother machine: $t = -6.831$, $df = 119.72$, $p < 0.001$; daughter device: $t = -7.876$, $df = 1125.5$, $p < 0.001$; one-tailed t tests), history and time also matter. In the next sections, we explore and quantify the effects of

time on bacterial aging.

1.3.2 Determinism and stochasticity explain doubling time variance

The relationship between the doubling times of mother and daughter cells can be examined by a phase plane on which the doubling times of the new (*T1*) and old (*T2*) daughters are plotted against the doubling time *T0* of their mother (Figure 1.3A and Table 1.A.2). Due to the large variance present in the data, we observed minimal improvement of fit for different non-linear models Figure 1.A.3A). Mother machine data, thus analyzed through linear regression, revealed a positive relationship between *T0* and the pooled doubling times of the daughters (Figure 1.3A, black line; $\beta = 0.28$, $t = 13.34$, $p < 0.001$). Nonetheless, as mentioned above and in Figure 1.A.2, new and old daughters exhibited distinct doubling times. In the phase plane, this physiological distinction produces a visual separation between new and old subpopulations.

To verify whether *T1* and *T2* subpopulations would be better explained by individual models, we performed a two-way ANCOVA evaluating the effect of *T0* and age (new or old) on daughter doubling times. While both *T0* ($F = 209.15$, $p < 0.001$) and age ($F = 336.69$, $p < 0.001$) had a significant effect on *T1* and *T2*, there was also interaction between factors ($F = 10.67$, $p = 0.001$). This indicates that the relationship between *T1* or *T2* and *T0* is best described by distinct slopes for each subpopulation. The independent models for new (linear regression; $\beta = 0.22$, $t = 8.85$, $p < 0.001$) and old daughters ($\beta = 0.35$, $t = 11.44$, $p < 0.001$) are shown in Figure 1.3A. Thus, slow growing mothers produced daughters that were also slow, a pattern consistent with the prevalence of aging generated by asymmetric damage partitioning. Most importantly, the *T2*

regression line lay above and had a larger slope than the line for *T1*, which are expected signatures of aging affecting old daughters more.

Despite following the trends described by linear regression, new and old subpopulations displayed large variance. To determine the sources of this variance, we partitioned the sums of squared deviations for *T1* and *T2* doubling times (see Methods). We started by identifying the total sum of squares as the deviation of each doubling time from the population mean, obtaining SS_T = 6737.66. Some of this total variance was produced by the positive relationship between a mother and its daughters ($\beta = 0.28$; Figure 1.3B, bottom panels). This fraction of the variance, SS_M, was determined as the deviation of predicted pooled *T1* and *T2* from the population mean doubling time, 22.45 min. Thus, the sum of squared deviations due to maternal inheritance was obtained as SS_M = 557.76. Due to asymmetry, however, doubling times predicted by two separate linear models deviated from the values predicted by the mother alone (Figure 1.3B, middle panels). This deviation, produced by asymmetry, was determined as SS_A = 926.32. Finally, observed doubling times deviated from predicted values due to stochasticity, with SS_S = 5253.58 (Figure 1.3B, top panels). By combining these values, the fraction of the variance determined by deterministic sources is given as $(SS_M + SS_A)/SS_T = 0.22$, while the remaining variance was explained by stochastic factors $SS_S/SS_T = 0.78$. Daughter device populations obtained similar results, with 24.9% of the variation explained by non-genetic maternal inheritance and asymmetry (Table 1.A.3).

These analyses suggest that the inheritance of damage across generations produces variance in doubling times of new and old daughters. Mother bacteria with longer doubling times likely carry larger accumulated damage loads, thus producing daughters with longer doubling times as well. Since these mothers partition damage asymmetrically upon division, asymmetry is

also a source of deterministic variance in bacterial populations. In the following sections, we further analyze the patterns emerging from deterministic sources in our populations.

1.3.3 Cell lineages are predicted to achieve growth equilibrium

To investigate stable patterns arising from lineages in the mother machine, we investigated predictions observed in the phase plane. The regression lines of new and old subpopulations displayed slopes shallower than the identity line, indicating that conditions $T1 = T0$ or $T2 = T0$ must exist where each linear model crosses identity (Figure 1.3C). This intersection is predicted to be a stable point (May 1976), to which lineages converge by inheriting either pole consecutively over generations (Figure 1.3D). Importantly, this property does not depend on a linear relationship between doubling times of a mother and its daughters. The same prediction arises from non-linear relationships (Figure 1.A.3), provided that the slope at the intersect with identity is less than 1. Thus, bacterial populations are expected to stabilize around two equilibrium points where the doubling time of the daughter equals the doubling time of the mother, or $T1 = T0 = 21.4$ and $T2 = T0 = 23.1$ min. Old and new subpopulations from the mother machine concentrated around these predicted equilibrium values in the phase plane (Figure 1.3E).

The verification of *T1* and *T2* equilibria requires long term lineage data. The longest old daughter lineages were obtained from the mother machine, since old daughters remain trapped at the bottom of growth wells (Figure 1.1C) for the length of the experiment. Our results revealed that the doubling times of old lineages remained remarkably stable over 53 to 60 generations (Figure 1.3F), which is expected in the presence of equilibrium. By following lineages in the phase plane, we observed that doubling times consistently cycled around an equilibrium value of 23.1 min, despite stochastic patterns being also present (Figure 1.3G). Thus, these results suggest the

existence of a *T2* equilibrium. Since new daughters are only present in the mother machine traps for two generations, new lineages from this device were too short to verify the *T1* equilibrium.

1.3.4 Stable equilibria are connected by aging and rejuvenation

Although the mother machine provided data for a strong characterization of the *T2* equilibrium, it could not harbor enough new daughter divisions to verify the *T1* equilibrium. Thus, we switched to the daughter device, which retains equally well both daughters (Figure 1.2C-D). Following the approach used for characterizing the *T2* equilibrium in the mother machine, we tracked *T1* and *T2* lineages inheriting the same pole consecutively over generations. The same general pattern seen in the mother machine was observed, except that two equilibria were now detected. Old and new daughter lineages achieved distinct equilibrium values of 20.6 and 19.5 min respectively, displaying doubling time stability over time (Figure 1.4A). On the phase plane, new and old lineages cycled around their respective equilibrium point (Figure 1.4B), corresponding to the distinct physiological states produced by asymmetric division.

Because the doubling times of old lineages remain centered around the *T2* equilibrium, the mean value of old daughters in equilibrium does not manifest signs of progressive deterioration or aging over time (Figure 1.3F and Figure 1.4A). Instead, observing aging in a bacterial population requires that lineages are displaced from the *T2* equilibrium. Such displacements will continuously occur when the population harbors both the *T1* and *T2* equilibria. When a new daughter at the *T1* equilibrium becomes a mother, its new daughter remains at the same equilibrium, but its old daughter is now far removed from the *T2* equilibrium (Figure 1.4C). The old lineage generated from this daughter will converge over generations to the *T2* equilibrium (Figure 1.3D), displaying longer doubling times with each division, thus manifesting aging. As a result, aging is predicted

by the phase planes to be an integral part of bacterial populations if the *T1* and *T2* equilibria are present.

To test this prediction, we tracked lineages emerging from either equilibrium in the daughter device. These lineages belong to the same population as presented above, but following cells that are displaced from their correct equilibrium. We identified new daughters at equilibrium (Figure 1.4B) and tracked a lineage of old daughters produced by these new daughters. We followed these old lineages over generations, and their trajectories confirmed a steady aging trend that connected the two equilibria (Figure 1.4D-E, Table 1.A.4). The transition from one equilibrium to the other required about three generations (Figure 1A.4). Similarly, we followed new daughter lineages emanating from the *T2* equilibrium as they converged towards the *T1* equilibrium. Because this convergence was now downwards, doubling times decreased with each generation. Thus, the emanating new lineages were rejuvenated (Figure 1.4D-E), connecting the two equilibria in the opposite direction. The same trend shown in Figure 1.4D was observed when expanding our analysis to 5 generations (Figure 1A.4).

We tested whether these observations corroborated the characterization of the equilibria as stable attractors. By analyzing the doubling time distributions of each generation presented in Figure 1.4D, we followed lineages leaving the opposite equilibrium and approaching their own. Following new lineages originated from the *T2* equilibrium for three generations, we observed that these doubling time distributions varied significantly (Figure 1.5A; one-way ANOVA, $F = 17.69$, $p < 0.001$). A post-hoc analysis confirmed our observation that each new daughter distribution was increasingly displaced from the *T2* equilibrium (Figure 1.A.4). This displacement happens gradually, with each generation displaying doubling times closer to the *T1* equilibrium. In fact, the predicted equilibrium value of 19.5 min represented the true mean of the third new daughter

generation OONNN (one-sample t test, $t = 0.512$, $p = 0.610$), but not of its mother or grandmother (OONN and OON) (Table 1.A.5). This structure was also verified for old lineages leaving the *T1* equilibrium towards the *T2* stable value of 20.6 min (Figure 1.5B, Figure 1.A.4, and Supplementary Table 1A.5; one-way ANOVA, $F = 12.88$, $p < 0.001$). These analyses suggest the presence of a structured doubling time increase or decrease as cells transition between equilibria through processes of aging and rejuvenation.

The convergence of the emanating lineages reconfirmed the stability of the system. Our results showed that, besides representing equilibrium states for long term lineages, the *T1* and *T2* equilibria also behave as attractors that serve as targets for displaced lineages.

1.3.5 Maintenance of equilibrium in the presence of stochasticity

To verify the stability of equilibrium attractors in the presence of stochasticity, we performed a mathematical analysis based on long-term old lineage data (Figure 1.3). For mother machine lineages, which represent the longest observation of the old lineage equilibrium, we had shown that stochasticity represents 78% of the doubling time variance. Although our deterministic factors predict stability (Figure 1.3 and Figure 1.A.3), we considered whether stochasticity would prevent cell lineages from remaining in equilibrium over generations. The complete mathematical analysis is provided in Note 1A.1.

The combined effect of maternal doubling times and asymmetry estimate old daughter doubling times through a linear model of slope $a = 0.347$ and intercept $b = 15.091$ (Figure 1.3A). Because the slope predicted by these deterministic sources is shallower than 1, we observed the attractor $T0 = T2 = 23.12$ min. However, stochasticity could produce the variability observed in *T2* by acting on either a (σ_1) or b (σ_2) (Figure 1A.4). In this case, $T2 = T0*(a + \xi_1) + b + \xi_2$, where

ξ_1 and ξ_2 are random variables drawn each generation from a Gaussian distribution with standard deviation of σ_1 and σ_2, respectively. σ_1 could originate from stochasticity in processes such as asymmetric damage partitioning. A large σ_1 could lead to a continuous displacement of the old lineage if $a^2 + \sigma_1^2 \geq 1$, thus not allowing for stabilization (Note 1.A.1). σ_2, on the other hand, represents an additive source of noise that does not disrupt stability.

To estimate the values of σ_1 and σ_2, we considered the linear model for our mother machine old lineages. If we assume stochasticity to act only on the slope a = 0.374, then $\sigma_1 \neq 0$ and $\sigma_2 = 0$. We can estimate σ_1 by calculating the deviation from a for slopes calculated for each experimental pair of *T0* and *T2* in equilibrium, or (*T2* – b) / *T0* = a + σ_1. By performing this calculation, we obtained $\sigma_1 = 0.07$. The opposite scenario where $\sigma_1 = 0$ and $\sigma_2 \neq 0$ is also possible, in which case *T2* – *T0**a = b + σ_2. In this case, our experimental doubling times indicated that $\sigma_2 = 1.62$. A biologically realistic scenario would likely exhibit stochasticity in both σ_1 and σ_2, resulting in $0 < \sigma_1 < 0.07$ and $0 < \sigma_2 < 1.62$. Thus, $\sigma_1 = 0.07$ represents the maximum stochasticity that could influence the stability of our population. This value satisfies the condition for stabilization where $a^2 + \sigma_1^2 < 1$, for $0.3472 + 0.072 = 0.125$. Therefore, the old lineage equilibrium observed in Fig. 3 behaves as a stable attractor.

We further tested this assertion by estimating the doubling times of simulated old lineages for different starting of σ_1 (Figure 1.5C-D). While an increase in stochasticity dramatically disrupts the stability of *T2* over time, $\sigma_1 = 0.07$ reproduces the pattern observed in our data (compare Figure 1.5D to Figure 1.3F). Because lineages maintain stability when $a^2 + \sigma_1^2 < 1$, equilibrium will be present for $\sigma_1 < 0.94$. The disruption of stability is easily visualized in Figure 1.5E, where we simulated doubling times for a range of σ_1 values, following old lineages for 100 generations (5,000 replicates for each σ_1). As σ_1 approaches 0.94, the doubling time variance increases sharply,

indicating the loss of stabilizing properties. In this scenario, old daughter doubling times would become increasingly large, which in real bacteria would mean the arrest of growth and proliferation. As Figure 1.5E demonstrates, this threshold occurs for a much larger stochasticity than observed in our experiments.

Taken together, the data from this study indicates that bacterial populations displaying immortal proliferation reach states of physiological equilibrium for new and old lineages. These equilibria behave as attractors, to which displaced lineages constantly converge through aging and rejuvenation. Moreover, the equilibria display stabilizing properties despite the presence of stochasticity in the system. Therefore, deterministic patterns of stability connected by constant aging and rejuvenation emerge from bacterial populations in the presence of biological stochasticity.

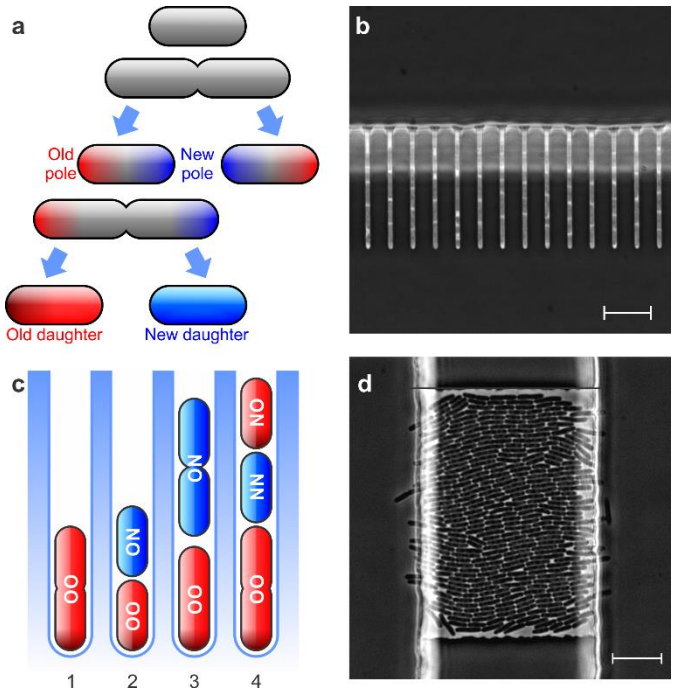

Figure 1.1 - Polarity structure of rod-shaped cells in microfluidic devices.
(A) Upon division, E. coli inherit a conserved old pole, along with a newly synthesized pole formed at the site of fission. On the next division, the old pole is again segregated to one sibling, which is called an old daughter, while the maternal new pole is inherited by the other sibling, called a new daughter. Old poles are consecutively inherited throughout generations, carrying accumulated non-genetic damage. (B) The mother machine design allowed imaging of ~30 growth wells per experiment, with each well harboring an old daughter lineage. Large flow channels (top) provided fresh nutrients to the traps, with the flow preventing the formation of biofilms on the device. (C) Within the mother machine traps, the structure of bacterial lineages maintains a constant pattern. The oldest cells (OO) remain at the closed end, generating another daughter like itself and a new daughter (ON) upon division. When this new daughter divides, its old daughter (NO) will be located by the opening of the well, therefore closer to the nutrient source than its young sibling (NN). A doubling time asymmetry generated solely by starvation would predict that NO cells grow faster than NN. (D) The daughter device consisted of large growth chambers, flanked by two wide flow channels providing fresh medium to the colony. Since two-dimensional colonies can grow feely in this device, the lineages exhibit no rigid polarity structure. Scale bars = 10 µm.

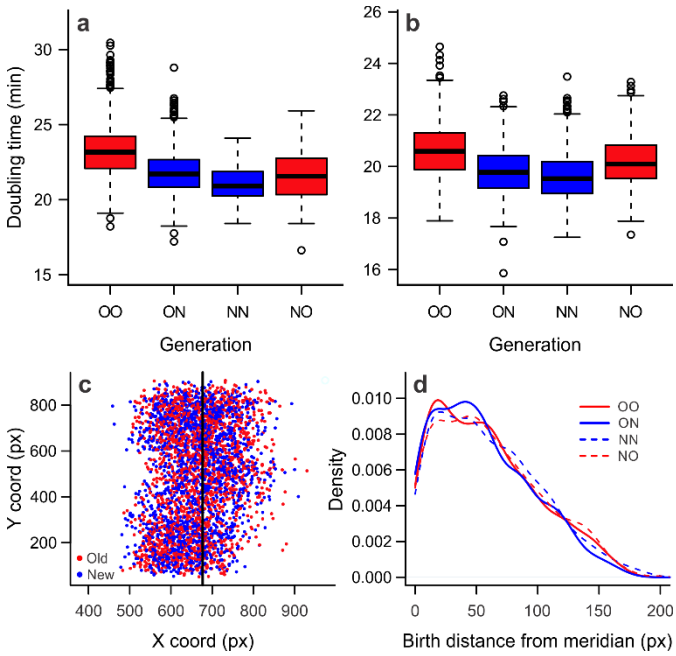

Figure 1.2 - Doubling time asymmetry in the absence of starvation and stress.
(A) Bacteria from the mother machine were categorized as OO, ON, NN and NO (n = 882, 882, 105, 105 cells), reflecting their polarity and position within the growth traps. ON cells displayed faster doubling times than OO. Similarly, NN grew faster than NO (two-tailed paired t test, t = -2.308, df = 104, p = 0.023) despite the latter being closer to the nutrient source. (B) Doubling times of OO, ON, NN and NO cells (n = 556, 556, 620, 620 cells) from the daughter device showed the same pattern as in the mother machine. The doubling time relationships OO > ON (t = -17.219, df = 555, p < 0.001) and NO > NN (t = -13.564, df = 619, p < 0.001) were again verified by two-tailed paired t tests. Boxplots show median (center line), first and third quartiles (box limits), and minimum and maximum (whiskers) (C) Representation of cells within the chamber, according to their coordinates at birth. The vertical line represents the midline of the chamber, which is open along the Y axis on both sides. (D) We analyzed the data from (C) by measuring the distance of each cell from the midline of the chamber at the moment of birth, and verified no localization bias among sibling pairs within the daughter device (OO-ON p = 0.12, and NO-NN p = 0.98, Wilcoxon Signed-Ranks Test). Therefore, doubling time differences represent and effect of aging as opposed to starvation.

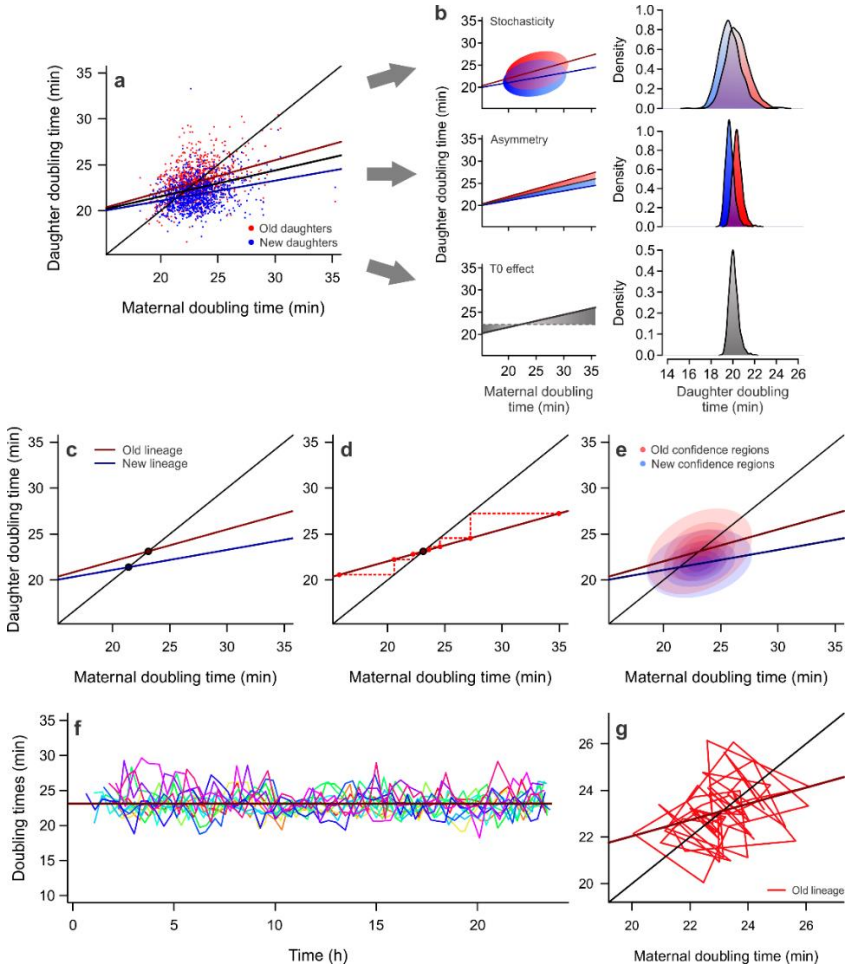

Figure 1.3 - Doubling time relationships predict stabilization at equilibrium points.
(A) Old daughters (23.127 ± 1.903 min, n = 987 cells) displayed longer doubling times than their new siblings (21.778 ± 1.517 min, n = 987 cells) in the mother machine (t = -21.884, df = 986, p < 0.001, paired one-tailed t test), resulting in a separation between new and old subpopulations in the phase plane. (B) The variance in *T1* and *T2* was partitioned into three components through the estimation of sum of squared deviations. Left: Shaded areas represent the variability explained by each component. Maternal doubling times explain the deviation from the population mean; asymmetry explains the deviation from values predicted by *T0* alone; and stochasticity explains the deviation of observed *T1* and *T2* from values predicted by asymmetry. Right: Density distributions showing increasing variance as more components are added to doubling time estimates. (C) Because the slopes of linear models between *T0* and *T1* or *T2* are shallower than the identity line, stable points arise at the intersection between these lines and identity. (D) Graphical representation of *T2* lineages converging toward the predicted equilibrium through the continuous inheritance of old poles. (E) Most of the data points concentrated around the predicted attractors, as shown by ellipse-like confidence regions ranging from 15% to 95% confidence. (F) Doubling times of old lineages from the mother machine shown over 24 h, as 13 independent lineages (n = 745 cells) remain stable over time. (G) Progression of a randomly chosen old lineage around the predicted equilibrium, which behaves as an attractor for the dynamic trajectory of the lineage over 60 generations.

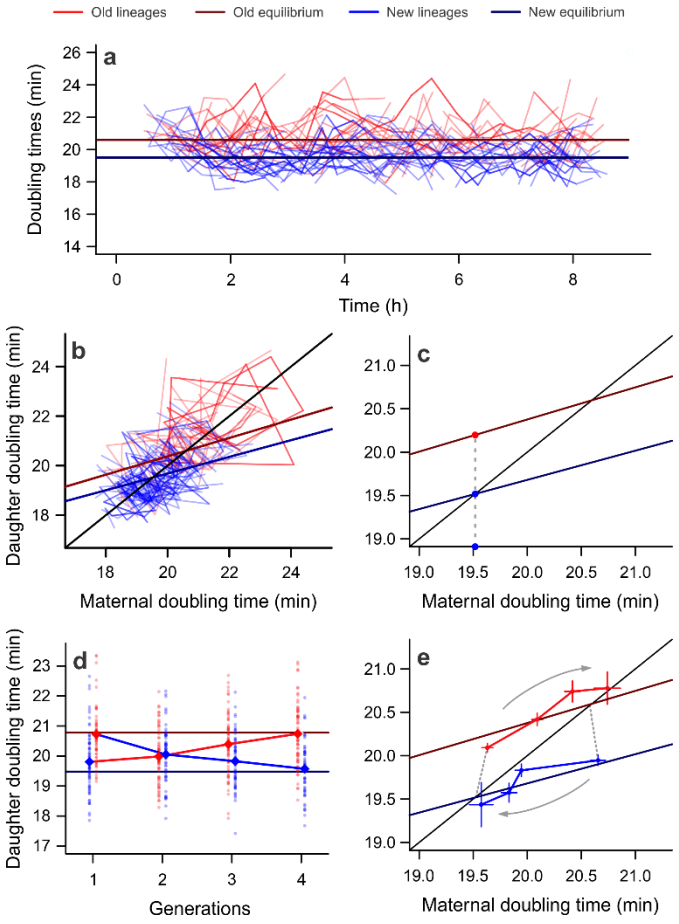

Figure 1.4 - New and old daughters reach equilibrium in the daughter device.
(A) New (19.365±0.907, n = 158) and old lineages (21.177±1.237, n = 116), represented by those inheriting the same pole for at least 4 generations, exhibited stably distinct doubling times (t = 13.354, df = 200.66, $p < 0.001$, one-tailed t test) over time. (B) By following these lineages on the phase plane, we determined the equilibrium points based on the linear relationships between T0 and T1 or T2. A two-way ANCOVA revealed a significant effect of T0 ($F = 460.3$, $p < 0.001$) and age ($F = 334.2$, $p < 0.001$) on daughter doubling times (n = 2400), with both linear models displaying similar slope ($F = 1.051$, $p = 0.305$). (C) Graphical representation of two daughters born from a mother at T1 equilibrium. While its new daughter remains at equilibrium, its old daughter displays a longer doubling time. (D) Old lineages born from T1 equilibrium (generation 1) converge towards T2 equilibrium over three generations. The same is observed for new lineages born from T2 equilibrium, which converge towards T1 equilibrium over time. (E) In the phase plane, we can observe the trajectory of cells born from the opposite equilibrium as they consecutively approach the equilibrium that matches their polarity. Error bars represent mean ± s.e.m. Old lineage n = 370, 179, 70, 30; new lineage n = 291, 139, 62, 24 cells.

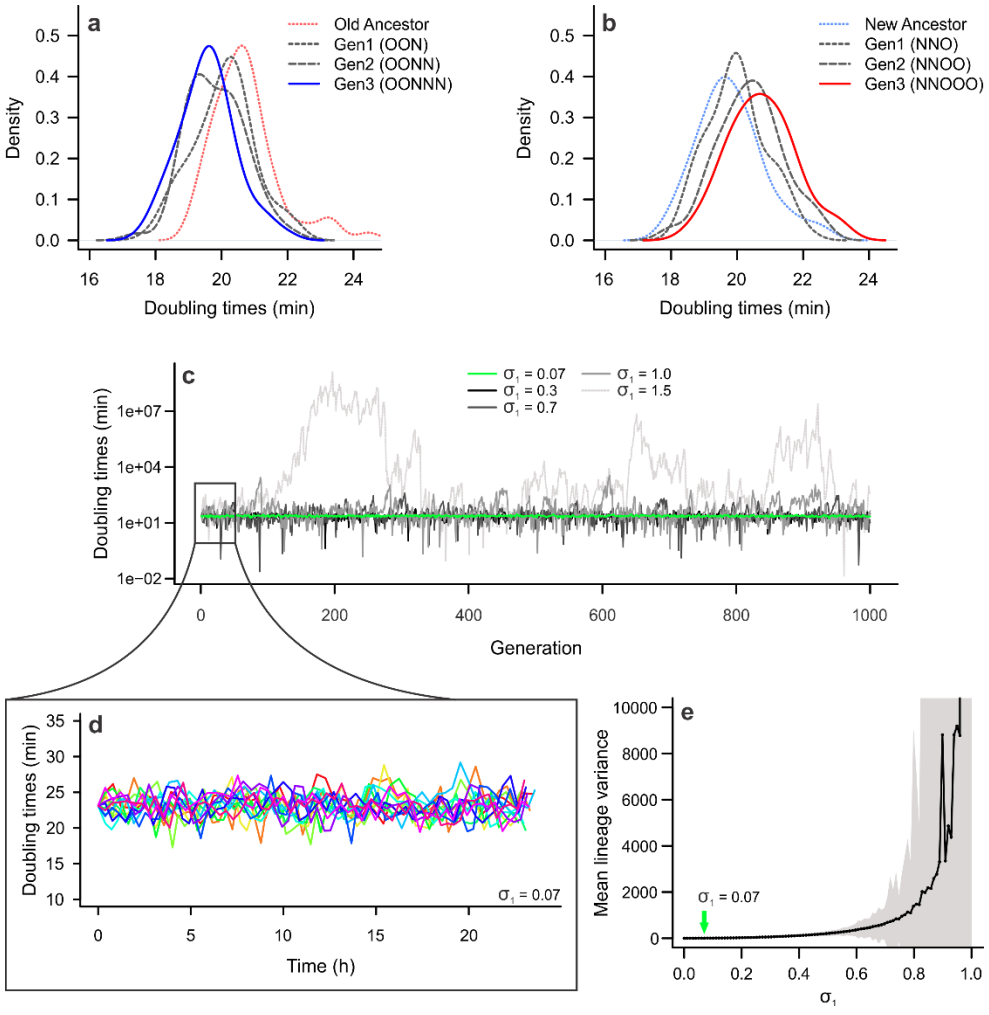

Figure 1.5 - Doubling time equilibria have attractive properties for displaced and stable lineages.
(A and B) Displaced lineages from the daughter device. (A) The doubling time distribution of a new lineage born from an old ancestor at the *T2* equilibrium shifts towards shorter doubling times with each generation. After three generations of rejuvenation, the distribution becomes centered at the *T1* equilibrium. (B) The opposite pattern appears from old lineages generated from the new equilibrium, which converge towards the *T2* attractor over generations (Table 1.A.5). (C, D and E) Evaluation of stochasticity in silico based on mother machine data (Figure 1.3). (C) Doubling times of in silico old lineages starting from the *T2* equilibrium, for increasing values of σ_1 in $T2 = T0^*(a + \sigma_1) + b + \sigma_2$ (Note 1.A.1). Stochasticity disrupts stability if $a^2 + \sigma_1^2 \geq 1$. (D) Doubling times generated for $\sigma_1 = 0.07$, the maximum stochasticity expected from our experimental data. (E) Mean doubling time variance of in silico old lineages followed for 100 generations (5,000 replicates) for a range of σ_1 values (0.0001 to 1). When $\sigma_1 > 0.94$, the stability requirement $a^2 + \sigma_1^2 < 1$ is no longer fulfilled. Shaded area represents standard deviation.

1.4 Discussion

In this study, we showed that the asymmetric partitioning of damage by mother bacteria explains the phenotypic distinction between old and new bacterial daughters, resulting in a landscape of aging and rejuvenation due to the transmission of damage down the daughter lineages. This landscape, quantified in the absence of stress or starvation, is visualized on a phase plane showing the doubling times of the old and new daughters as a function of the doubling time of the mother (Figure 1.3A). We found that the doubling times of new and old lineages converged to distinct equilibrium values, *T1* and *T2* respectively, where they remained stable over time. Doubling times at the *T1* equilibrium are shorter due to the inheritance of lower damage loads by new daughters. However, many cells within a mixed population exhibit doubling times that do not reside at equilibrium. For example, when a new daughter in equilibrium divides, it produces both a new and an old daughter. While the new daughter doubling time remains at the *T1* equilibrium, the old daughter is born at a distance from the *T2* equilibrium (Figure 1.5C). As this old daughter reproduces, the lineage it creates converges onto the *T2* equilibrium (Figure 1.3C and Figure 1.5D). During the convergence, it experiences increasing doubling times and aging. Reproduction by old daughters in equilibrium, likewise, produces lineages of new daughters that experience rejuvenation through decreasing doubling times, as they converge to the *T1* equilibrium (Figure 1.5D). Thus, the equilibria are stable attractors at which equilibrium lineages remain and to which displaced lineages converge. It is the behavior of these lineages, which emanate from one equilibrium and converge onto the other, that drives the dynamics of constant aging and rejuvenation in bacterial populations.

We interpret these equilibria to result from the opposing effects of aging and rejuvenation. All bacterial cells experience aging and rejuvenation as they grow and divide. Aging is driven by

the acquisition of damage through the amount a cell receives from its mother, and the de novo amount it accumulates during its lifetime (Chao 2010; Rang, Peng, and Chao 2011). This maternal contribution is evidenced by the positive slope for the regression of the doubling times of daughters onto their mothers (Figure 1.3A). Mothers with longer doubling times generate daughters that also take longer to divide, presumably because these mothers transmit larger damage loads. This relationship is the bacterial version of the Lansing effect of rotifers, in which the offspring of older parents have shorter lifespan than the offspring of younger (Albert I. Lansing 1947; A. I. Lansing 1948). Rejuvenation results from the dilution of damage caused by the synthesis of new and damage-free materials by a cell, as indicated by the inheritance of a newly synthesized cell pole. The two stable equilibria are achieved when the dilution and acquisition of damage balance each other, such that a lineage allocates the same amount of damage from mother to daughter every generation. Because asymmetric partitioning allocates less damage to new daughters, dilution is a stronger factor in these cells, resulting in a shorter doubling time at equilibrium. For the same reasons, new daughters produced by old daughters in equilibrium experience a sudden increase in dilution, displaying doubling time rejuvenation as they approach the *T1* equilibrium. On the other hand, because old daughters receive larger damage loads by asymmetric partitioning, they experience the opposite of new daughters. Rejuvenation also demonstrates that the distinct physiological states of new and old daughters are not produced by mutations. If mutations accounted for this difference, new daughter lineages produced by the *T2* equilibrium could not be rejuvenated.

The observation of large bacterial populations comprising both the *T1* and *T2* equilibria is essential for understanding the processes of bacterial aging and rejuvenation. The critical role of the two equilibria is demonstrated by the effect of witnessing only one equilibrium, through the

hypothetical case of a symmetrical bacterium (Figure 1.3B). With symmetry, identical old and new daughters are produced upon division and the population stabilizes around a single equilibrium. As a result, any observed variation of doubling times around equilibrium is properly attributed to stochastic noise, rather than aging and rejuvenation (Chao et al. 2016). A similar observation derives from the observation of the *T2* equilibrium in the mother machine. While this design was extraordinarily innovative for the study of bacteria in physiological steady states (Wang et al. 2010), the stability of the single *T2* equilibrium, when viewed in isolation (Figure 1.3D-E), can give the impression that bacterial aging does not occur. Without a *T1* equilibrium to create emanating lineages converging to *T2* equilibrium, the cells in a mother machine appear to behave as symmetrical bacteria that do not age.

The emergence of age structures in bacterial populations through lineages of old and new daughters brings a new perspective to traditional views of biological aging. Although the progressive functional decline in old-pole bacteria comes to a halt once the lineage reaches equilibrium, we anticipate that an increased damage accumulation induced by extrinsic stress could result in a continuous deterioration leading to mortality — a more traditional definition of aging. In fact, the inheritance and accumulation of non-genetic damage is associated with aging in both bacteria (Lindner et al. 2008; Lindner and Demarez 2009; Winkler et al. 2010) and traditional cellular systems (Fuentealba et al. 2008; López-Otín et al. 2013; Moore et al. 2015), which could propose a unifying cause for aging at the cell lineage level. By redefining the old daughter as the continuation of the mother (Stewart et al. 2005; Ackermann, Chao, et al. 2007; Ackermann, Schauerte, et al. 2007), bacterial replication can be seen as an individual mother bacterium budding off new daughters, thus retaining damage to produce rejuvenated individuals. Comparably to budding yeast (Higuchi-Sanabria et al. 2014) and the bacterium *Caulobacter crescentus*

(Ackermann, Stearns, and Jenal 2003; Ackermann, Schauerte, et al. 2007; Tsokos and Laub 2012), the rejuvenated new daughters of *E. coli* represent a physiological juvenile, although morphologically indistinguishable from the mother. With the evolution of a distinction between a mother and a juvenile state in bacteria and other systems, partly due to asymmetric damage partitioning, age structure emerges in the population. As a juvenile daughter ages, its different life stages could experience different ecology and selection pressures. Future explorations remain necessary to determine the resilience of these age structures in face of such extrinsic pressures. Taking these notions together, bacteria could serve as a model for the evolutionary origins of aging, providing quantifiable long-term data on cellular aging and rejuvenation. While aging in bacteria and traditional organisms will always have their differences, it may be that some key features of biological aging arose with the first microbes.

1.5 Materials & Methods

1.5.1 Bacterial strains and growth conditions

All experiments were performed with K-12 *E. coli* wild-type strain MG1655. Before each experiment, cultures were inoculated in Luria-Bertani medium (LB broth; per liter: 10 g tryptone, 5 g yeast extract, 5 g NaCl; Sigma-Aldrich) and grown overnight at 37° C with agitation. For culturing within microfluidic devices, the medium was supplemented with 0.075% Tween 20 to prevent the formation of biofilms.

1.5.2 Microfluidic device design

Two designs of microfluidic devices were used in this study. The first was based on the original mother machine design (Wang et al. 2010), modified for the inclusion of more flow

channels and kindly provided by Ryan Johnson (University of California, San Diego). This design consisted of 16 flow channels bearing 2000 wells (1.25 x 30 x 1 m) each. When loaded into the device, bacteria enter the growth wells and remain trapped at the closed edge, consecutively inheriting old poles throughout the experiment. The wells comported up to seven cells at a time, before cells were washed into the large flow channel. The second design, here called the daughter device, was originally designed for the study of genetic oscillators (Mondragón-Palomino et al. 2011) and comprises 48 growth chambers (40 x 50 x 0.95 µm) distributed in four columns; the chambers are flanked by 10 µm wide channels that provided fresh culture medium to bacteria throughout the experiment. For both devices, master silicon wafers were used as negative molds for the construction of polydimethylsiloxane (PDMS) microfluidic chips. Each soft lithography process yields 8 to 12 devices, which are attached to 24 x 40 mm coverslips through a Si-O-Si covalent bond, after exposure to O2 and UV light.

1.5.3 Cell loading and experimental conditions

For loading the devices, overnight grown cultures were centrifuged for 2 min at 5300 g and supernatant media discarded, followed by pellet resuspension in 50 µL LB-Tween 20 medium. Microfluidic devices were placed in a vacuum chamber for 10 min, and then loaded with bacteria by laying 3 µL of culture over the loading port. After verifying successful filling of the channels, input and output 60 ml syringes, containing 30 ml of culture medium and 10 ml of MilliQ water respectively, were attached to the ports. The medium inlet was refilled as needed for the length of each experiment. All experiments were performed at 37º C with constant supply of growth medium to ensure stable growth conditions. Replicates were performed in four independent microfluidic devices, and imaging began immediately after loading bacteria into the chambers.

1.5.4 Time-lapse image acquisition

Cell movies were collected by a Nikon Eclipse Ti-S microscope, with imaging intervals controlled by NIS-Elements AR software. Phase imaging of mother machine devices followed 2 min intervals, while 20 s intervals were used for the daughter device to ensure the correct tracking of all lineages.

1.5.5 Image analysis for the quantification of bacterial growth

Images were analyzed with the free software ImageJ (NIH, https://imagej.nih.gov/ij). By following microscopy images over time, we obtained growth and position information for each individual cell present in the field of acquisition. Cell coordinates were recorded as Regions of Interest (ROI) and annotated according to pole inheritance. From the ROIs, we determined the cell centroids, its length immediately before and after division, and the interval between cell divisions. Elongation rates (r) and corresponding doubling times (ln(2)/r) were calculated from the data, and from the polarity annotation we determined maternity, sibling pairs and lineage trees. To ensure that the measurements were unbiased, we also performed blind data collections where cell length and time of division were recorded without previous knowledge of asymmetry and pole inheritance.

1.5.6 Doubling time analysis

Statistical analysis was performed using the software R version 3.4.1 (R Core Team 2017). p-values < 0.05 were considered statistically significant. Sample sizes were determined according to previous studies in microfluidic devices (Wang et al. 2010), which reported doubling times of old and new daughters in the mother machine for the strain MG1655. Doubling times were

recorded as defined above, and statistically analyzed without data transformations or corrections. Doubling times of new-old sibling pairs were compared through paired t tests as indicated in the figure legends. When analyzing doubling time relationships in the phase plane, linear regressions were performed between *T0* and *T1* or *T0* and *T2*. Two-way analyses of covariance (ANCOVA) were performed to evaluate the effect of *T0* and age (new or old) over *T1* and *T2*. From the linear regressions, we determined the equilibrium points as the intersection between each linear model and the identity line, thus indicating a stable point where *T0 = T1* or *T0 = T2*. Sample sizes (individual cells) are indicated along with reports of statistical analyses, usually located in the figure legends.

Determination of cell positioning within the daughter device. Centroids obtained for each cell at birth were evaluated according to their distance from the meridian of the growth chamber (horizontal axis). The chambers are open on both sides along the vertical axis, therefore only the localization along the horizontal axis is relevant for starvation analyses.

1.5.7 Partitioning the sum of squared deviations

We partitioned the variance present in our data according to deterministic and stochastic sources. Using the sum of squared deviations method, the total variability (SST) of daughter doubling times was determined as the sum of *T1* and *T2* deviation from the population mean doubling times, or

$$SS_T = \sum_{i=1}^{n}(T1_i - \bar{T}_i)^2 + \sum_{i=1}^{n}(T2_i - \bar{T}_i)^2 \qquad (1)$$

The first component of the total variance comprised the variability produced by the positive relationship between *T0* and pooled *T1* and *T2*, described by the line equation

$$\hat{T}_i = 0.283 \times T0 + 15.897 \qquad (2)$$

The deviation of values predicted by the equation above from the mean daughter doubling times thus represent the variability introduced by the effect of a mother on its daughters:

$$SS_M = 2 \times \sum_{i=1}^{n} (\hat{T}_i - \bar{T}_i)^2 \qquad (3)$$

Because new and old subpopulations are best described by individual linear models rather than a single one, variability is also introduced by asymmetry. We determined this component as the deviation of predicted *T1* and *T2* from the central line in equation (2):

$$\widehat{T1} = 0.219 \times T0 + 16.703 \qquad (4)$$

$$\widehat{T2} = 0.347 \times T0 + 15.091 \qquad (5)$$

$$SS_A = \sum_{i=1}^{n} (\widehat{T1}_1 - \hat{T}_i)^2 + \sum_{i=1}^{n} (\widehat{T2}_i - \hat{T}_i)^2 \qquad (6)$$

The last component of the total variability is determined as the deviation due to stochasticity, estimating the level of noise in doubling times. It is defined as the deviation of observed *T1* and *T2* from the values predicted by asymmetry, or

$$SS_S = \sum_{i=1}^{n} (T1_i - \widehat{T1}_i)^2 + \sum_{i=1}^{n} (T2_i - \widehat{T2}_i)^2 \qquad (7)$$

Thus, by combining the sum of squares deviations, the fraction of the variation explained by deterministic factors is given as $(SS_M + SS_A)/SS_T$, and the fraction explained by stochasticity is determined as SS_S/SS_T.

1.5.8 Analysis of stability in the presence of stochasticity

The values of σ1 and σ2 were calculated from experimental doubling times of old lineages in equilibrium, grown in the mother machine device. For each pair of mother (*T0*) and daughter (*T2*), the effective slope was calculated as (*T2* – b) / *T0* = a + ξ_1, where a and b were obtained from a linear regression. σ1 was calculated as the standard deviation of ξ_1. A similar approach was performed for σ_2, given *T2* – *T0**a = b + σ_2. The resulting values were validated from an exploration of the parameter space for *T2* = *T0**(a + ξ_1) + b + ξ_2, where ξ_1 and ξ_2 are random

variables drawn each generation from a Gaussian distribution with standard deviation of σ_1 and σ_2, respectively. To obtain a combination of σ_1 and σ_2 that satisfied our data, we randomly sampled ξ_1 and ξ_2 with a range of non-negative standard deviations. These values were used to predict *T2* from *T0*, a and b, looking for combinations of σ_1 and σ_2 that minimized the difference between variances of observed and estimated *T2*. This analysis yielded a range of values from $\sigma_1 = 0.07$, $\sigma_2 = 0$ to $\sigma_1 = 0$, $\sigma_2 = 1.62$, same output as mathematically predicted above.

1.5.9 Data availability

The data supporting the findings of this study are available within the article and supplementary information.

1.6 Acknowledgments

We thank M. Vergassola for assistance with the analysis of stability and stochasticity, and the reviewers for greatly improving this work with their suggestions. We thank R. Johnson and G. Graham for assistance with experimental setup, and S. Cheung, J. Chen and A. Qiu for data assistance. Work was supported by grants to L.C. from the National Science Foundation (DEB-1354253). A.M.P. is supported by the Science Without Borders Fellowship / CAPES – Brazil, and by the Chris Wills Graduate Student Research Award.

Chapter 1, in full, is a reprint of the material as it appears in Proenca AM, Rang CU, Buetz C, Shi C, Chao L (2018). Age structure landscapes emerge from the equilibrium between aging and rejuvenation in bacterial populations. *Nature Communications* 9:3722. The dissertation author was the primary investigator and author of this paper.

1.A Appendix

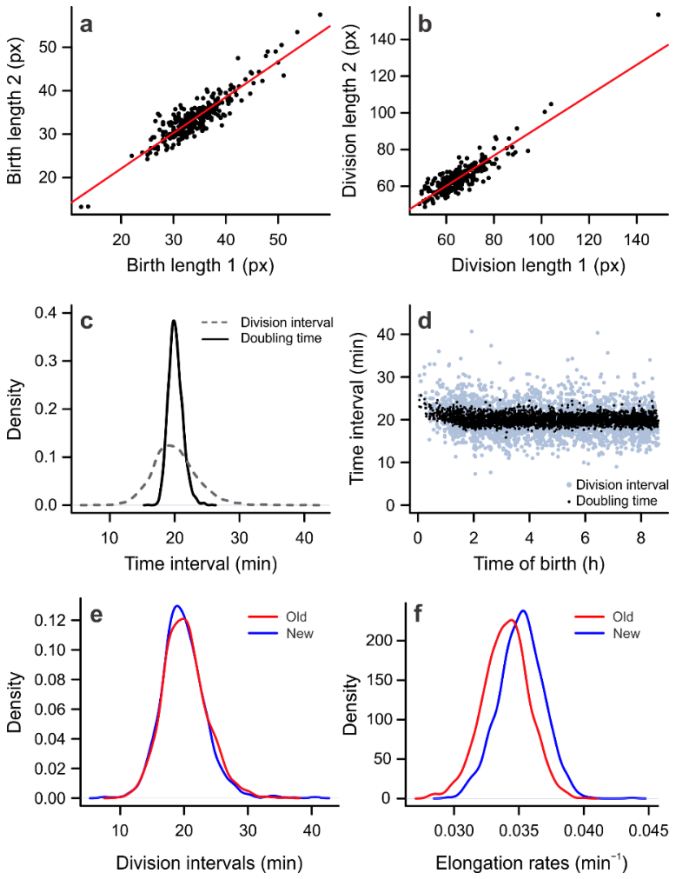

Figure 1.A.1 - Comparison of different growth parameters and control measurements.
To ensure that our measurements of bacterial length were not introducing unreasonable variability in our sample, we compared measurements acquired from mother machine cells by different individuals in separate occasions (A and B). These measurements were highly correlated for both birth lengths (A) (linear regression, $r = 0.904$, $\beta = 0.822$, $p < 0.001$) and division lengths (B) (linear regression, $r = 0.895$, $\beta = 0.825$, $p < 0.001$), thus pointing at little artificially introduced variability. Measurement errors will be part of unaccounted variability along with stochastic sources reported in this study. (C) We measured division intervals (time elapsed between birth and division) and doubling times (converted from elongation rates) for all cells in the daughter device. Division intervals displayed much larger variance than doubling times (Bartlett test, $K^2 = 3146.9$, $p < 0.001$), despite exhibiting the same mean values (paired two-tailed t test, $t = 1.212$, $df = 2887$, $p = 0.225$). (D) Both doubling times and division intervals remained constant over time for our bacterial populations. (E) New and old daughters exhibited a significant, albeit very small, division interval difference (one-tailed t test, $t = 1.944$, $df = 2851.7$, $p = 0.026$). (F) The distinction between daughters becomes evident when comparing elongation rates, which combine the information of cell length and division intervals as a physiologically meaningful parameter. New daughters displayed faster growth (one-tailed t test, 17.842, $df = 2859.9$, $p < 0.001$), indicating that the physiological asymmetry arises due to faster elongation more than due to shorter division intervals. Thus, we performed the following analyses in this study using the more intuitive conversion of elongation rates into doubling times.

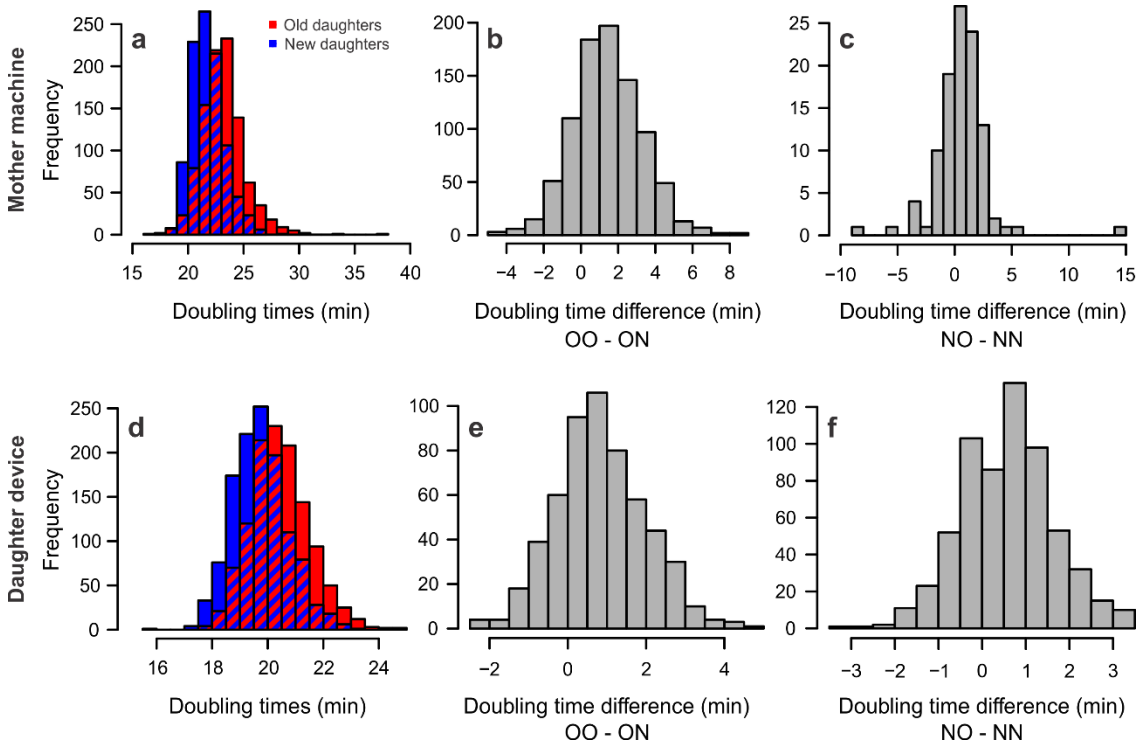

Figure 1.A.2 - Old daughters display longer doubling times in all age categories.
(A, B and C) Mother machine data corresponding to Fig. 2A. (A) Comparing all sibling pairs, old daughters displayed a significantly longer doubling time (paired one-tailed t test, $t = 21.884$, $df = 986$, $p < 0.001$). (B) Analyzing the sibling pairs at the closed edge of growth wells, we observed that the difference between OO and ON doubling times was significantly higher than zero (one-tailed t test, $t = 23.152$, $df = 881$, $p < 0.001$). (C) The same was verified for sibling pairs NO and NN, closer to the open end of the growth wells (one-tailed t test, $t = 2.308$, $df = 1.4$, $p = 0.011$). (D, E and F) Daughter device data corresponding to the same age categories. (D) Overall, old daughters displayed longer doubling times than new daughters (paired one-tailed t test, $t = 21.805$, $df = 1199$, $p < 0.001$). As in the mother machine, the difference between doubling times was significantly higher than zero for both OO-ON pairs (E) (one-tailed t test, $t = 19.219$, $df = 555$, $p < 0.001$) and NO-NN pairs (F) (one-tailed t test, $t = 13.564$, $df = 619$, $p < 0.001$).

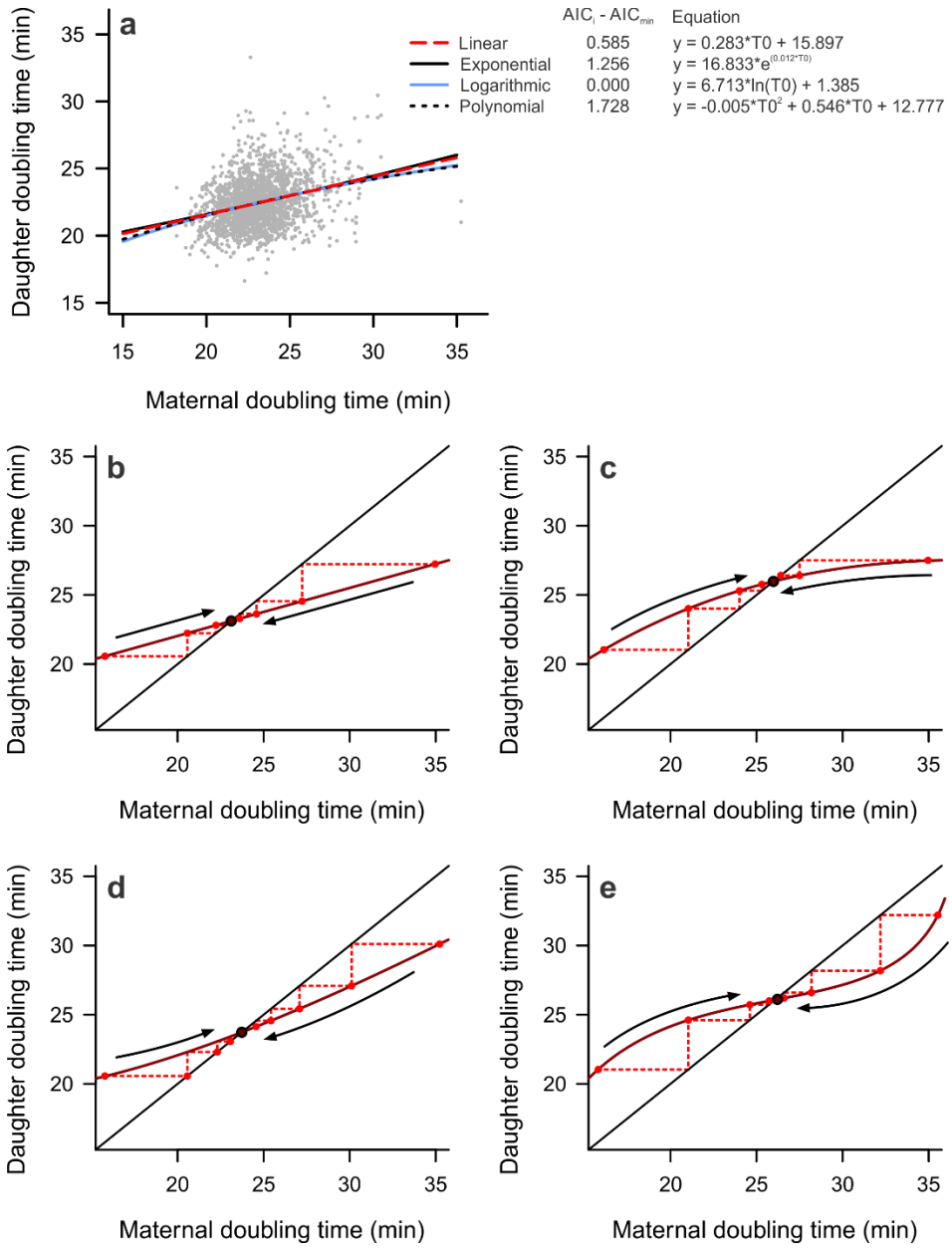

Figure 1.A.3 - Linear and non-linear models predict stable equilibrium points.
(A) Linear, exponential, logarithmic, and polynomial models showed the same positive relationship between T0 and daughter doubling times. Comparing these models through the Akaike information criterion (AIC), we observed little improvement of the fit by choosing a non-linear model. (B to E) Graphical representations of linear and non-linear models on the phase plane. The intersection between the model and identity behaves as a stable point whenever the model slope is shallower than 1 at the intersection. Thus, the existence of an equilibrium is predicted by both linear and non-linear models.

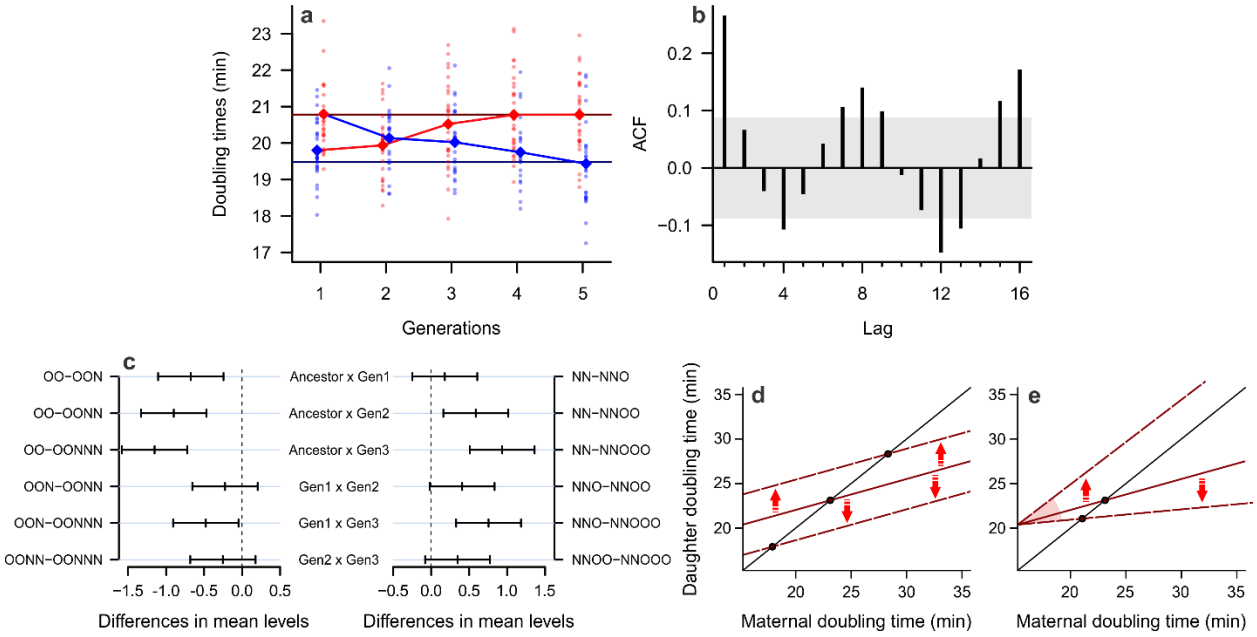

Figure 1.A.4 - Stability of attractors for lineages away from equilibrium and in the presence of stochasticity.
(A) Convergence of displaced lineages towards the correct equilibrium, expanding the visualization from Fig. 4D for one more generation. Because only complete lineages are considered, the sample size is reduced to 24 new and 30 old lineages (120 and 150 cells, respectively). (B) Autocorrelation performed for lineages from Fig. 4E cycling between equilibria through aging and rejuvenation. Lineages transition between equilibria in four generations. (C) Tukey's range test for differences of doubling time distributions for lineages transitioning from the T2 to T1 (left) or T1 to T2 (right) equilibrium (original distributions presented in Fig. 5A and 5B). (D and E) Graphical representation of the effects of stochasticity on the stability of attractors. While additive noise (represented by $b + \sigma_2$) is not disruptive (D), multiplicative noise on the slope ($a + \sigma_1$) can destabilize the attractor (E).

Table 1.A.1 - Data summary for boxplots in Figure 1.2A and 1.2B.

Device	Cell	Mean ± SD (min)	Lower whisker (min)	Lower hinge (min)	Median (min)	Upper hinge (min)	Upper whisker (min)
mother machine	OO	23.294 ± 1.783	19.104	22.084	23.173	24.230	27.404
mother machine	ON	21.849 ± 1.475	18.242	20.822	21.714	22.670	25.423
mother machine	NN	21.187 ± 1.729	18.414	20.258	20.912	21.872	24.0980
mother machine	NO	21.724 ± 2.274	18.414	20.334	21.565	22.761	25.920
daughter device	OO	20.652 ± 1.072	17.890	19.881	20.588	21.305	23.347
daughter device	ON	19.811 ± 0.988	17.671	19.157	19.772	20.427	22.316
daughter device	NN	19.604 ± 0.944	17.254	18.950	19.528	20.189	22.036
daughter device	NO	20.180 ± 0.971	17.882	19.534	20.096	20.831	22.746

Table 1.A.2 - Data summary for phase planes, Figure 1.3A and 1.4B.

Device	Daughter	Mean ± SD (min)	Equilibrium[1] (min)
mother machine	Old	23.127 ± 1.903	23.110
mother machine	New	21.778 ± 1.517	21.387
daughter device	Old	20.429 ± 1.064	20.579
daughter device	New	19.728 ± 0.986	19.525

[1]Calculated according to linear regression intersect with identity line.

Table 1.A.3 - Variance partitioning for mother machine and daughter device.

	Mother machine		**Daughter device**	
	SS[1]	**Fraction**	**SS[1]**	**Fraction**
Maternal inheritance	557.7613	0.083	406.313	0.144
Asymmetry	926.3173	0.137	295.917	0.105
Stochasticity	5253.58	0.780	2115.006	0.751
Total	6737.658		2817.236	

[1]SS = sum of squared deviations.

Table 1.A.4 - Data summary for Figure 1.4E.

Device	Daughter	Generation	Mean ± SD (min)
daughter device	Old	1	20.092 ± 0.051
daughter device	Old	2	20.418 ± 0.072
daughter device	Old	3	20.740 ± 0.121
daughter device	Old	4	20.779 ± 0.187
daughter device	New	1	19.946 ± 0.058
daughter device	New	2	19.831 ± 0.072
daughter device	New	3	19.574 ± 0.108
daughter device	New	4	19.435 ± 0.254

Table 1.A.5 - Data summary and statistics for distributions transitioning between equilibria. One-sample t tests verify whether the equilibrium attractors (Table 1.A.2) represent the mean value of the doubling time distribution of each generation.

Device	Daughter	Generation	Mean ± SD	t	df	p
daughter device	OON	1	20.051 ± 0.924	4.540	61	<0.001***
daughter device	OONN	2	19.826 ± 0.871	2.783	61	0.0071**
daughter device	OONNN	3	19.573 ± 0.854	0.512	61	0.610
daughter device	NNO	1	19.985 ± 0.877	-5.845	69	<0.001***
daughter device	NNOO	2	20.393 ± 0.997	-1.717	69	0.090
daughter device	NNOOO	3	20.74 ± 1.014	1.175	69	0.244

Note 1.A.1. Analyzing the stochasticity and stability of the doubling time equilibrium in bacterial lineages. Reproduced with permission from Dr. Massimo Vergassola, Department of Physics, University of California, San Diego, La Jolla, CA 92093

We consider the equation

$$X(n+1) = X(n)[a + \xi_1 n] + b + \xi_2(n) \quad \text{(Supplementary Equation 1)}$$

where a and b are fixed constants and the ξ's are Gaussian independent random variables, drawn independently for each time interval, i.e. $\langle \xi_1(n)\xi_1(m)\rangle = 0$ if $n \neq m$ and $\langle \xi_1(n)\xi_1(n)\rangle = \sigma_1^2$.

We first consider the deterministic case $\sigma_1 = \sigma_2 = 0$. The iteration (1) has then the fixed point $X^* = \frac{b}{1-a}$ for $a < 1$. For $a \geq 1$, the system is unstable and X keeps growing under the iterations. For $|a| < 1$, initial deviations from the fixed point X^* relax exponentially: $\delta X(n) = \delta X(0)a^n$, where $X(n) = X^* + \delta X(n)$.

For $|a| < 1$, we next consider the additive noise case $\sigma_1 = 0$, $\sigma_2 \neq 0$. By the linearity of the iteration and the Gaussianity of ξ_2, we obtain that X will also be Gaussian. Its mean is X^* and the correlation function of its fluctuations decay exponentially with the time delay:

$$\langle \delta X(n)\delta X(m)\rangle = \frac{a^{|n-m|}}{1-a^2}\sigma_2^2 \quad \text{(Supplementary Equation 2)}$$

In other words, the process is a discrete version of the Ornstein-Uhlenbeck process in the (time) continuum.

For $|a| < 1$, we finally consider the multiplicative noise case $\sigma_1 \neq 0$ (and for simplicity $\sigma_2 = 0$). The recurrence equation is now

$$\delta X(n+1) = \delta X(n)\big(a + \xi_1(n)\big) + \xi_1(n) \quad \text{(Supplementary Equation 3)}$$

The noise is now multiplying δX, which generates the non-Gaussianity of the fluctuations shown hereafter.

Multiplicative noise can lead to indefinite growth along some trajectories. Indeed, if $|a + \xi_1| > 1$ the amplitude of the fluctuations increases with the iteration, as it was shown above. The probability of $|a + \xi_1| > 1$ is unlikely if $a + \sigma_1 << 1$. However, a stretch of growing events is of course possible, with a probability that decays exponentially with the length of the stretch (this can be generally formalized using large-deviations theory). We qualitatively conclude that the far tails of the probability distribution for the fluctuations do not stabilize as they are affected by those extreme events.

More quantitatively, we can write down the equations for the moments of the fluctuations $\langle \delta X^p \rangle$ and investigate their convergence. Let us start with the variance

$$\langle \delta X(n+1)^2 \rangle = \langle \delta X(n)^2 \rangle (a^2 + \sigma_1^2) + \sigma_1^2 \quad \text{(Supplementary Equation 4)}$$

which has the fixed point

$$\langle \delta X^2 \rangle = \frac{\sigma_1^2 X^{*2}}{1 - a^2 - \sigma_1^2} \quad \text{(Supplementary Equation 5)}$$

Note that the condition for stabilization of the variance is $a^2 + \sigma_1^2 < 1$, i.e. it is not guaranteed to hold by the condition for the stabilization of the mean $|a| < 1$.

A similar equation can be written for the third-order moment

$$\langle \delta X(n+1)^3 \rangle = \langle \delta X(n)^3 \rangle (a^3 + 3a\sigma_1^2) + 6aX^* \sigma_1^2 \langle \delta X(n)^2 \rangle \quad \text{(Supplementary Equation 6)}$$

Note that the third-order moment is generally non-vanishing, which illustrates the non-Gaussianity of the fluctuations. The condition for stabilization of the third-order moment is $a^3 + 3a\sigma_1^2 < 1$, i.e. $\langle (a + \xi_1)^3 \rangle < 1$.

The fourth-order moment obeys

$$\langle \delta X(n+1)^4 \rangle = \langle \delta X(n)^4 \rangle (a^4 + 6a^2\sigma_1^2 + 3\sigma_1^4) + 4X^* \langle \delta X(n)^3 \rangle (3a^2\sigma_1^2 + 3\sigma_1^4) + 6X^{*2} \langle \delta X(n)^2 \rangle (a^2\sigma_1^2 + 3\sigma_1^4) + 3X^{*4}\sigma_1^4 \quad \text{(Supplementary Equation 7)}$$

Provided lower-order moments stabilize, the additional condition of stabilization for the fourth-order is $\langle (a + \xi_1)^4 \rangle < 1$.

The pattern for a generic order is clear: if lower-order moments stabilize, the additional condition for the stabilization of the *p*-th moment is $\langle (a + \xi_1)^p \rangle < 1$. These conditions are eventually going to be violated. Indeed, even for $\sigma_1 << 1$, if we consider large even orders $p = 2q$, the equality $\langle {\xi_1}^{2q} \rangle = \sigma_1^{2q}(2q-1)!!$ holds and the exponentially decaying (in q) factor σ_1^{2q} cannot compensate for the-faster-than-exponential growth of the skip factorial $(2q-1)!!$.

In practice, for the concrete numbers $a = 0.3472$ and $\sigma_1 = 0.07$, the conditions for stabilization of the first moments $a^2 + \sigma_1^2 = 0.125$, $\langle (a + \xi_1)^3 \rangle = 0.047$, $\langle (a + \xi_1)^4 \rangle = 0.018$ are all largely satisfied. The transition to moments that do not stabilize takes place for orders in the hundreds, which are unreachable and irrelevant for any realistic measurement.

1.7 References

Ackermann, Martin, Lin Chao, Carl T Bergstrom, and Michael Doebeli. 2007. "On the Evolutionary Origin of Aging." *Aging Cell* 6 (2): 235–44. doi:10.1111/j.1474-9726.2007.00281.x.

Ackermann, Martin, Alexandra Schauerte, Stephen C Stearns, and Urs Jenal. 2007. "Experimental Evolution of Aging in a Bacterium." *BMC Evolutionary Biology* 7 (January): 126. doi:10.1186/1471-2148-7-126.

Ackermann, Martin, Stephen C. Stearns, and Urs Jenal. 2003. "Senescence in a Bacterium with Asymmetric Division." *Science* 300: 1920.

Bufalino, Mary Rose, Brian DeVeale, and Derek van der Kooy. 2013. "The Asymmetric Segregation of Damaged Proteins Is Stem Cell-Type Dependent." *Journal of Cell Biology* 201 (4): 523–30. doi:10.1083/jcb.201207052.

Chao, Lin. 2010. "A Model for Damage Load and Its Implications for the Evolution of Bacterial Aging." *PLoS Genetics* 6 (8): e1001076. doi:10.1371/journal.pgen.1001076.

Chao, Lin, Camilla Ulla Rang, Audrey Menegaz Proenca, and Jasper Ubirajara Chao. 2016. "Asymmetrical Damage Partitioning in Bacteria: A Model for the Evolution of Stochasticity, Determinism, and Genetic Assimilation." *PLoS Computational Biology* 12 (1): e1004700. doi:10.1371/journal.pcbi.1004700.

Coelho, Miguel, Aygül Dereli, Anett Haese, Sebastian Kühn, Liliana Malinovska, Morgan E. Desantis, James Shorter, Simon Alberti, Thilo Gross, and Iva M. Tolić-Nørrelykke. 2013. "Fission Yeast Does Not Age under Favorable Conditions, but Does so after Stress." *Current Biology* 23 (19): 1844–52. doi:10.1016/j.cub.2013.07.084.

Coelho, Miguel, Steven J. Lade, Simon Alberti, Thilo Gross, and Iva M. Tolic. 2014. "Fusion of Protein Aggregates Facilitates Asymmetric Damage Segregation." *PLoS Biology* 12 (6): e1001886. doi:10.1371/journal.pbio.1001886.

Coquel, Anne Sophie, Jean Pascal Jacob, Mael Primet, Alice Demarez, Mariella Dimiccoli, Thomas Julou, Lionel Moisan, Ariel B. Lindner, and Hugues Berry. 2013. "Localization of Protein Aggregation in Escherichia Coli Is Governed by Diffusion and Nucleoid Macromolecular Crowding Effect." *PLoS Computational Biology* 9 (4). doi:10.1371/journal.pcbi.1003038.

Fuentealba, Luis C, Edward Eivers, Douglas Geissert, Vincent Taelman, and E M De Robertis. 2008. "Asymmetric Mitosis: Unequal Segregation of Proteins Destined for Degradation." *Proceedings of the National Academy of Sciences of the United States of America* 105 (22): 7732–37. doi:10.1073/pnas.0803027105.

Higuchi-Sanabria, Ryo, Wolfgang M.A. Pernice, Jason D. Vevea, Dana M. Alessi Wolken, Istvan R. Boldogh, and Liza A. Pon. 2014. "Role of Asymmetric Cell Division in Lifespan Control in Saccharomyces Cerevisiae." *FEMS Yeast Research* 14 (8): 1133–46. doi:10.1111/1567-

1364.12216.

Kirkwood, T. B. L. 2008. “Understanding Ageing from an Evolutionary Perspective.” *Journal of Internal Medicine* 263 (2): 117–27. doi:10.1111/j.1365-2796.2007.01901.x.

Laney, Samuel R., Robert J. Olson, and Heidi M. Sosik. 2012. “Diatoms Favor Their Younger Daughters.” *Limnology and Oceanography* 57 (5): 1572–78. doi:10.4319/lo.2012.57.5.1572.

Lansing, A. I. 1948. “Evidence for Aging as a Consequence of Growth Cessation.” *Proceedings of the National Academy of Sciences of the United States of America* 34 (6): 304–10. doi:10.1073/pnas.34.6.304.

Lansing, Albert I. 1947. “A Transmissible, Cumulative, and Reversible Factor in Aging.” *Journal of Gerontology* 2 (3): 228–39. doi:https://doi.org/10.1093/geronj/2.3.228.

Lindner, Ariel B., and Alice Demarez. 2009. “Protein Aggregation as a Paradigm of Aging.” *Biochimica et Biophysica Acta - General Subjects* 1790 (10). Elsevier B.V.: 980–96. doi:10.1016/j.bbagen.2009.06.005.

Lindner, Ariel B, Richard Madden, Alice Demarez, Eric J Stewart, and François Taddei. 2008. “Asymmetric Segregation of Protein Aggregates Is Associated with Cellular Aging and Rejuvenation.” *Proceedings of the National Academy of Sciences of the United States of America* 105 (8): 3076–81. doi:10.1073/pnas.0708931105.

López-Otín, Carlos, Maria A. Blasco, Linda Partridge, Manuel Serrano, and Guido Kroemer. 2013. “The Hallmarks of Aging.” *Cell* 153: 1194–1217. doi:10.1016/j.cell.2013.05.039.

May, Robert M. 1976. “Simple Mathematical Models with Very Complicated Dynamics.” *Nature* 261: 459–67.

Mondragón-Palomino, Octavio, Tal Danino, Jangir Selimkhanov, Lev Tsimring, and Jeff Hasty. 2011. “Entrainment of a Population of Synthetic Genetic Oscillators.” *Science* 333 (6047): 1315–19. doi:10.1126/science.1205369.

Moore, D. L., G. A. Pilz, M. J. Arauzo-Bravo, Y. Barral, and S. Jessberger. 2015. “A Mechanism for the Segregation of Age in Mammalian Neural Stem Cells.” *Science* 349 (6254): 1334–38. doi:10.1126/science.aac9868.

Nakaoka, Hidenori, and Yuichi Wakamoto. 2017. “Aging, Mortality, and the Fast Growth Trade-off of Schizosaccharomyces Pombe.” *PLOS Biology* 15 (6): e2001109. doi:10.1101/128298.

Ogrodnik, Mikołaj, Hanna Salmonowicz, Rachel Brown, Joanna Turkowska, Władysław Średniawa, Sundararaghavan Pattabiraman, Triana Amen, Ayelet-chen Abraham, Noam Eichler, Roman Lyakhovetsky, and Daniel Kaganovich. 2014. “Dynamic JUNQ Inclusion Bodies Are Asymmetrically Inherited in Mammalian Cell Lines through the Asymmetric Partitioning of Vimentin.” *Proceedings of the National Academy of Sciences of the United*

States of America 111 (22): 8049–54. doi:10.1073/pnas.1324035111.

R Core Team. 2017. “R: A Language and Environment for Statistical Computing.” Vienna, Austria: R Foundation for Statistical Computing. https://www.r-project.org/.

Rang, Camilla U, Annie Y Peng, and Lin Chao. 2011. “Temporal Dynamics of Bacterial Aging and Rejuvenation.” *Current Biology* 21 (21): 1813–16. doi:10.1016/j.cub.2011.09.018.

Rang, Camilla U, Annie Y Peng, Art F Poon, and Lin Chao. 2012. “Ageing in Escherichia Coli Requires Damage by an Extrinsic Agent.” *Microbiology* 158 (Pt 6): 1553–59. doi:10.1099/mic.0.057240-0.

Rokney, Assaf, Merav Shagan, Martin Kessel, Yoav Smith, Ilan Rosenshine, and Amos B. Oppenheim. 2009. “E. Coli Transports Aggregated Proteins to the Poles by a Specific and Energy-Dependent Process.” *Journal of Molecular Biology* 392 (3). Elsevier Ltd: 589–601. doi:10.1016/j.jmb.2009.07.009.

Rose, Michael R. 1991. *Evolutionary Biology of Aging*. New York: Oxford University Press.

Stewart, Eric J, Richard Madden, Gregory Paul, and François Taddei. 2005. “Aging and Death in an Organism That Reproduces by Morphologically Symmetric Division.” *PLoS Biology* 3 (2): e45. doi:10.1371/journal.pbio.0030045.

Taheri-Araghi, Sattar, Serena Bradde, John T. Sauls, Norbert S. Hill, Petra Anne Levin, Johan Paulsson, Massimo Vergassola, and Suckjoon Jun. 2015. “Cell-Size Control and Homeostasis in Bacteria.” *Current Biology* 25 (December). Elsevier Ltd: 385–91. doi:10.1016/j.cub.2014.12.009.

Tsokos, Christos G, and Michael T Laub. 2012. “Polarity and Cell Fate Asymmetry in Caulobacter Crescentus.” *Current Opinion in Microbiology* 15 (6). Elsevier Ltd: 744–50. doi:10.1016/j.mib.2012.10.011.

Ullman, G., M. Wallden, E. G. Marklund, A. Mahmutovic, I. Razinkov, and J. Elf. 2012. “High-Throughput Gene Expression Analysis at the Level of Single Proteins Using a Microfluidic Turbidostat and Automated Cell Tracking.” *Philosophical Transactions of the Royal Society B: Biological Sciences* 368 (1611): 20120025. doi:10.1098/rstb.2012.0025.

Valfort, Aurore-Cécile, Caroline Launay, Marie Sémon, and Marie Delattre. 2018. “Evolution of Mitotic Spindle Behavior during the First Asymmetric Embryonic Division of Nematodes.” *PLoS Biology* 16 (1): e2005099. doi:10.1371/journal.pbio.2005099.

Wang, Ping, Lydia Robert, James Pelletier, Wei Lien Dang, Francois Taddei, Andrew Wright, and Suckjoon Jun. 2010. “Robust Growth of *Escherichia coli*.” *Current Biology* 20 (12). Elsevier Ltd: 1099–1103. doi:10.1016/j.cub.2010.04.045.

Watve, Milind, Sweta Parab, Prajakta Jogdand, and Sarita Keni. 2006. “Aging May Be a Conditional Strategic Choice and Not an Inevitable Outcome for Bacteria.” *Proceedings of the National Academy of Sciences of the United States of America* 103 (40): 14831–35.

doi:10.1073/pnas.0606499103.

Winkler, Juliane, Anja Seybert, Lars König, Sabine Pruggnaller, Uta Haselmann, Victor Sourjik, Matthias Weiss, Achilleas S Frangakis, Axel Mogk, and Bernd Bukau. 2010. “Quantitative and Spatio-Temporal Features of Protein Aggregation in *Escherichia coli* and Consequences on Protein Quality Control and Cellular Ageing.” *The EMBO Journal* 29 (5): 910–23. doi:10.1038/emboj.2009.412.

CHAPTER 2

Cell aging preserves cellular immortality in the presence of lethal levels of damage

2.1 Abstract

Cellular aging, a progressive functional decline driven by damage accumulation, often culminates in the mortality of a cell lineage. Certain lineages, however, are able to sustain long-lasting immortality, as prominently exemplified by stem cells. Here we show that *Escherichia coli* cell lineages exhibit comparable patterns of mortality and immortality. Through single-cell microscopy and microfluidic techniques, we find that these patterns are explained by the dynamics of damage accumulation and asymmetric partitioning between daughter cells. At low damage accumulation rates, both aging and rejuvenating lineages retain immortality by reaching their respective states of physiological equilibrium. We show that both asymmetry and equilibrium are present in repair mutants lacking certain repair chaperones, suggesting that intact repair capacity is not essential for immortal proliferation. We show that this growth equilibrium, however, is displaced by extrinsic damage in a dosage-dependent response. Moreover, we demonstrate that aging lineages become mortal when damage accumulation rates surpass a threshold, while rejuvenating lineages within the same population remain immortal. Thus, the processes of damage accumulation and partitioning through asymmetric cell division are essential in the determination of proliferative mortality and immortality in bacterial populations. This study provides further evidence for the characterization of cellular aging as a general process, affecting prokaryotes and eukaryotes alike and according to similar evolutionary constraints.

2.2 Introduction

Aging, or the progressive loss of function at the macromolecule, tissue, organ or individual level, is largely driven by the deterioration of intracellular processes. Accordingly, the hallmarks of the aging phenotype — such as telomeric attrition, mitochondrial dysfunction, loss of proteostasis, and genomic instability —, which have been well characterized by previous studies (López-Otín et al. 2013), reveal conserved genetic and biochemical pathways at the cellular level. Considering cellular aging as a baseline for the study of aging as a general process, we can summarize its mechanisms as the gradual intracellular accumulation of damage from various sources, along with a decreasing repair capacity. Furthermore, excessive damage accumulation within a cell lineage may lead to cellular senescence, when individual cells cease replicating and the lineage transitions to a mortal state (Aravinthan 2015; Campisi and d'Adda di Fagagna 2007; Jeyapalan and Sedivy 2008).

The cellular aging process encompasses both multi and unicellular organisms, such as yeast, diatoms, and even bacteria (Erjavec et al. 2008; Laney, Olson, and Sosik 2012; Rang, Peng, and Chao 2011; Stewart et al. 2005). Due to the traditional view of unicellular prokaryotes as being functionally immortal, these organisms are often overlooked in the discussion of cellular aging. However, research in bacterial aging stands out for offering quantitative approaches to data collection and analysis, coupled with technical improvements on single-cell microscopy, which have detailed the aging phenotype and its progression. Although bacteria do not possess some of the eukaryotic aging targets, like telomeres and mitochondria, they are sensitive to stresses that induce non-genetic damage accumulation, such as oxidation and disruptions in protein folding (Książek 2010; Sabate, De Groot, and Ventura 2010). Stressed bacteria accumulate misfolded proteins in the form of polar-localized aggregates (Lindner et al. 2008; Winkler et al. 2010; Rokney

et al. 2009; Coquel et al. 2013), therefore displaying loss of proteostasis. Repair occurs in a slow and energy-consuming fashion, where chaperones such as DnaK and ClpB mediate the disaggregation and unfolding of damaged proteins (Sabate, De Groot, and Ventura 2010; Winkler et al. 2010). Additionally, the potential prokaryotic origin of mitochondria raises the possibility of regarding bacterial aging as a model for mitochondrial dysfunction, a noted hallmark of aging (López-Otín et al. 2013).

Besides aggregating and repairing damaged components, bacterial populations have developed another remarkable strategy to handle non-genetic damage. Experimental data from long term microscopy of bacterial lineages revealed that, in the presence of intracellular damage, each cellular division produces two physiologically asymmetric daughters (Ackermann, Stearns, and Jenal 2003; Stewart et al. 2005; Lindner et al. 2008; Rang et al. 2012; Proenca et al. 2018). This asymmetry is generated because the damage harbored by the mother is biased towards the old cell pole (Lindner et al. 2008; Winkler et al. 2010), causing the daughter that inherits this pole — termed the old daughter — to age. Its sibling, on the other hand, rejuvenates through the inheritance of a lower damage load, being called the new daughter. Therefore, by partitioning damage with asymmetry, bacterial populations engage in a trade-off where the fast-growth of new daughters is sustained at the expense of the declining cellular function of old daughters. Mathematical models and computational simulations were developed to estimate the advantage of asymmetry, in contrast with a symmetric control population — a hypothetical scenario where both daughters display equal physiology (Chao et al. 2016). The models have shown that asymmetry is evolutionarily advantageous because it increases the variance of elongation rates, which in turn increases the efficiency of natural selection and the mean fitness of the lineage. Diverse studies are beginning to show that asymmetric partitioning is not unique to bacteria, but an advantageous mechanism for

the progression of cell lineages. In fact, this process was recently observed in neural, embryonic and germline stem cells (Fuentealba et al. 2008; Moore et al. 2015; Bufalino, DeVeale, and van der Kooy 2013), where damage allocation plays a central role in self-renewal capacity, fate determination, and somatic sequestration of damage.

A better understanding on how the key features of aging are interconnected requires the eventual development of conceptual and mathematical models that can integrate with experimental studies the growth and aging of individual organisms or cells. Unicellular systems, such as bacteria, satisfy all these requirements. Here we show that the maintenance of proliferative immortality in *E. coli* lineages depends on the physiological equilibrium produced by contrasting damage accumulation and asymmetric partitioning. We demonstrate that unstressed lineages accumulate damage produced by standard respiration levels, subsequently partitioning this load with a level of asymmetry that allows for the dilution of damage within both new and old daughters. We show that E. coli mutants with decreased repair capacity also exhibit asymmetric new and old daughters, reaching distinct states of growth equilibrium. Furthermore, bacterial aging responds with a positive dosage relationship to an external damaging agent, which progressively disrupts proteostasis by increasing damage accumulation rates and disrupting asymmetry. With a sufficiently elevated stress level, the damage accumulation within old lineages surpasses their immortality threshold, leading these lineages to arrest division and become mortal. However, due to asymmetric partitioning, new lineages within the same population retain proliferative immortality. Our results show that the appropriate model and system can contribute to identifying the dynamics of mortality and immortality in the context of cellular aging.

2.3 Results

2.3.1 Functionally immortal bacterial lineages display damage accumulation and asymmetry

To determine whether bacterial lineages undergoing immortal proliferation displayed damage accumulation and partitioning dynamics, we cultured unstressed *Escherichia coli* cells using microfluidic devices. We employed the "mother machine" design (Wang et al. 2010) containing series of 1.2 µm wide growth wells at the bottom of which an old daughter remains trapped for the length of the experiment. Each well was connected in one end to large flow channels, constantly supplying fresh culture medium to maintain a healthy state for an extended time. Bacteria were loaded and tracked through time-lapse microscopy for 24 h in the absence of extrinsic damage. As an estimate of fitness, elongation rates and corresponding doubling time conversions were determined for each individual, along with its age according to cell pole inheritance following division.

Under such conditions, our previous studies have shown that new and old daughters display physiological asymmetry and long-term growth stability (Proenca et al. 2018). We confirmed these results in the present experiments, observing that new daughters displayed significantly faster elongation rates when compared to old daughters (Figure 2.1A), a distinction that remained constant over time. Moreover, comparing the maternal doubling time (hereby called T_0) to that of its daughters (new = T_1; old = T_2) in a phase plane, a clear separation between new (21.79 ± 1.60 min) and old (23.23 ± 2.12 min; mean ± SD) daughter subpopulations emerged (Figure 2.1B, Figure 2.A.1). In these conditions, the difference between T_1 and T_2 (n = 1,384 pairs) was significantly larger than zero (one sample t test, $t = 24.716$, $df = 1383$, $p < 0.001$). These results

suggest that old daughters in our populations are inheriting a larger damage load upon division, despite the absence of extrinsic damage in our growth conditions.

To quantify the possible damage accumulation and partitioning in these populations, we applied these results to a population genetics model on unicellular aging (Chao 2010). Because the accumulation of intrinsic damage positively correlates with increased doubling times, we can estimate maternal damage levels, the fraction inherited by each daughter upon division, and the resulting T_1 and T_2, reconstructing the progression of aging within a lineage. For this goal, we described cell lineage dynamics though three key parameters: Π, the doubling time of a damage-free cell; λ, the rate of damage accumulation within a single cell (0 to ~0.01 min^{-1}); and *a*, the partitioning asymmetry, ranging from 0 (complete asymmetry) to 0.5 (symmetric division).

Our growth parameters revealed the presence of intrinsic damage and asymmetry in physiologically stable *E. coli* (Table 2.A.1). Despite the ideal growth conditions provided by our microfluidic device, we found that bacterial populations displayed longer doubling times (22.34 ± 2.12 min, mean ± SD) than predicted for damage-free cells (Π = 19.66 min; one sample t test, $t = 75.04$, $df = 3482$, $p < 0.001$). These longer doubling times were driven by damage accumulation — which occurred at an average rate $\lambda = 0.0028\ min^{-1}$ —, thus suggesting that metabolic processes in healthy cells may induce the retention of intrinsic damage. Finally, as suggested by the separation between T_1 and T_2 subpopulations, we verified that these damage loads were partitioned asymmetrically at division, with old daughters inheriting 63% of the maternal damage ($a = 0.37$).

2.3.2 Damage accumulation and partitioning in stable growth equilibrium

The growth parameters Π, λ and a can be used to predict doubling times T_1 and T_2. In Figure 2.1B, the solid lines show predicted doubling times for our average population parameters, thus

showing the trend of new and old subpopulations. The crossing between these model lines and the identity line represents points of growth equilibrium where $T_0 = T_1$ or $T_0 = T_2$ (Figure 2.1C). Asymmetric populations thus stabilize around two points simultaneously — one for new lineages and other for the old, with cells continuously inheriting either pole remaining at equilibrium over generations (Rang, Peng, and Chao 2011; Chao 2010; Proenca et al. 2018). Cell lineages in physiological equilibrium replicate indefinitely, therefore remaining functionally immortal.

To confirm the long-term stability of new and old lineages in our experiments, we analyzed linear regressions between T_0 and T_1 or T_2 as previously described (Proenca et al. 2018) (Figure 2.A.1). Bacterial lineages remain stable provided the existence of equilibrium points, which is satisfied by the intersection between each linear regression and the identity line (Figure 2.1C and Figure 2.A.1). This intersection occurs when the slope of T_1 or T_2 lines is less than 1, which our data satisfies for both T_1 ($a = 0.246$, $p < 0.001$) and T_2 ($a = 0.309$, $p < 0.001$). In the stable environment of microfluidic devices, this equilibrium can still be disrupted by the stochasticity present in doubling times. This stochasticity can be described as random variables ξ_1 acting on the slopes in $T_i = T0*(a + \xi_1) + b$, obtained each generation from a Gaussian distribution with standard deviation of σ_1. Loss of equilibrium occurs when $a^2 + \sigma_1^2 \geq 1$ (see Methods for details). We estimated σ_1 for T_1 and T_2 lines by obtaining the deviations from slopes in $(T_i - b)/T0 = a + \sigma_1$. Both new ($\sigma_1 = 0.0657$) and old ($\sigma_1 = 0.0876$) lineages satisfied the stability requirement $a^2 + \sigma_1^2 < 1$, with $a^2 + \sigma_1^2 = 0.0649$ for T_1 and $a^2 + \sigma_1^2 = 0.1032$ for T_2.

Besides the possibility of being disrupted by stochasticity, our aging model predicts that stable equilibrium can be disrupted by the accumulation of intrinsic damage (Chao 2010). Our parameters estimate that an increase in damage accumulation rates, from $\lambda = 0.002$ to $0.008\ min^{-1}$, would progressively drive the equilibrium points towards longer doubling times. Because

asymmetric partitioning produces higher doubling times in old daughters, a sufficiently intense λ would act as a differential mortality threshold, leading to division arrest — i.e. a state of mortality — in the old lineage, while new daughters remain immortal (Figure 2.1D).

To connect our observation of immortality and growth equilibrium to the internal dynamics of damage accumulation and partitioning, we estimated damage loads using our growth parameters. From experimental doubling times, we calculated the damage loads harbored by a mother, new and old daughters at the time of birth (k_0, k_1, k_2) and division (D_0, D_1, D_2; Figure 2.1E). It is important to note that this model considers the entirety of damage loads present in each cell, be it in aggregate of diffuse form. Each cell is born with a load ki, and accumulates $\lambda * T_i$ over its lifetime, resulting in a load D_i. We verified that $k_2 > k_1$, as expected from observed doubling times and asymmetry (paired one-tailed t test, t = 27.988, df = 1244, $p < 0.001$). More, interestingly, we compared each mother to its old daughter and verified that $k_2 = k_0$ (paired two-tailed t test, t = 0.373, df = 1244, p = 0.709). This indicates that old lineages in a state of equilibrium, as observed in the mother machine, are born with a constant level of intrinsic damage. Consequently, the damage accumulated by a mother over its lifetime is equivalent to the load inherited by new daughters upon division, or $\lambda * T_0 = k_1$ (t = 0.367, df = 1244, p = 0.714).

Taken together, our results suggest that unstressed bacterial populations accumulate intrinsic non-genetic damage. Every generation, new daughters inherit the damage a mother accumulated over its lifetime ($k_1 = D_0 * a = \lambda * T_0$), while old daughters inherit the same amount the mother had at birth ($k_2 = D_0 * (1 - a) = k_0$). These dynamics of damage accumulation and partitioning allow for a state of physiological equilibrium, where old lineages display stable growth over time and retain proliferative immortality.

2.3.3 Large protein aggregates become anchored at old cell poles

To visualize the biasing of damage loads towards old daughters in our microfluidic device, we cultured *E. coli* expressing the small chaperone IbpA fusioned to yellow fluorescent protein (YFP). IbpA-YFP was shown to co-localize with protein aggregates in bacterial cells (Lindner et al. 2008), thus serving as a marker for the presence and position of non-genetic damage (Rang et al. 2018). By culturing this strain in our microfluidic device, we observed the progressive accumulation of damage in the old poles of lineages in a state of equilibrium (Figure 2.1F-M). We quantified the inheritance of IbpA-YFP fluorescent foci by following lineages over time, determining the subcellular localization of the aggregate and its partitioning upon division (Coelho et al. 2013). Over 194 cell divisions, we observed the appearance of 43 new fluorescent foci. Small foci first appeared in the center of a cell 37.2% of the observations, diffusing freely throughout the bacteria (Figure 2.A.1). However, as these aggregates accumulated more misfolded proteins, they quickly became anchored at the old poles (Figure 2.1L-M), resulting in the inheritance of fluorescent foci by old daughters in 80.4% of observed division events (Figure 2.A.1). It is important to note, however, that the YFP fusion might increase aggregation rates of the small chaperone IbpA (Govers et al. 2018), and unstressed cells likely harbor diffuse fluorescence and smaller foci rather than large aggregates. Nonetheless, the IbpA-YFP marker demonstrates the potential for asymmetric damage partitioning arising from the anchoring of protein aggregates at the old poles of old daughters over several generations.

2.3.4 Asymmetry and immortal proliferation in protein repair mutants

Given the asymmetric damage partitioning in equilibrium lineages, we investigated the relevance of the protein repair machinery for the maintenance of proliferative immortality. For this,

we employed *E. coli* single-gene knockout mutants lacking the chaperones ClpB or DnaK (Keio collection), which play a prominent role in the solubilization of protein aggregates (Doyle and Wickner 2009; Winkler et al. 2010; Sabate, De Groot, and Ventura 2010). We cultured these cells in mother machine devices as described above, screening bacterial lineages for asymmetric damage partitioning and physiological equilibrium. By following old lineages over time, we verified that both new and old Δ*clpB* daughters displayed constant elongation rates throughout the experiment (Figure 2.2A). We observed that Δ*clpB* mutants also displayed asymmetric doubling times, with new (24.81 ± 1.64, mean ± SD) daughters growing faster than their old (25.97 ± 1.87, mean ± SD) siblings (Figure 2.2B; paired one-tailed t test, $t = 16.846$, $df = 770$, $p < 0.001$). A distinct pattern emerged from the analysis of Δ*dnaK* mutants, with several mortality events occurring over time (Figure 2.2C). Nonetheless, a significant distinction between new (28.06 ± 2.49, mean ± SD) and old (30.20 ± 8.27, mean ± SD) daughter doubling times was observed in these cells (Figure 2.2D; paired one-tailed t test, $t = 4.262$, $df = 266$, $p < 0.001$).

To verify the stability of growth equilibrium in asymmetric Δ*clpB* and Δ*dnaK* populations, we analyzed the linear models presented in Figure 2.2B and D. To include mortality events in the analysis, doubling times were converted to elongation rates. We investigated whether the stochasticity present in the data could disrupt equilibrium stability in our populations, determining the noise acting on regression slopes as σ_1 in $(T_i - b)/T_0 = a + \sigma_1$. To generate 95% confidence intervals (CI), we performed a 10,000-fold bootstrap on T_0, T_1, T_2 trios. We verified that Δ*clpB* mutants satisfied the stability requirement $a^2 + \sigma_1^2 < 1$ (Figure 2.2E), therefore remaining proliferatively immortal, for both new ($a^2 + \sigma_1^2 = 0.035$ [0.016-0.064], mean [95% CI]) and old lineages ($a^2 + \sigma_1^2 = 0.107$ [0.051-0.206]). For Δ*dnaK*, while new ($a^2 + \sigma_1^2 = 0.241$ [0.020-0.624]) and old lineages ($a^2 + \sigma_1^2 = 0.473$ [0.113-0.956]) satisfied the stability requirement, several

mortality events were observed, with our bootstrap analysis suggesting a 1.45% probability of equilibrium loss (binomial test, $p < 0.001$) in Δ*dnaK* old lineages.

Taken together, these results suggest that repair chaperones ClpB and DnaK might have distinct roles in the maintenance of equilibrium stability. While the decreased protein repair capacity in Δ*clpB* mutants still allowed for the stable proliferation of new and old daughters, old lineages in Δ*dnaK* mutants begin to show signs of stability loss. We thus hypothesize that dynamics of damage accumulation may greatly impact proliferative immortality, with asymmetry determining a differential fate for new and old lineages.

2.3.5 The transition from immortality to mortality is determined by damage accumulation and asymmetric partitioning

To investigate whether aging cell lineages would retain physiological equilibrium — therefore, proliferative immortality — under increasing levels of damage accumulation, we cultured bacteria in the presence of extrinsic damage. We employed light excitation (490 nm wavelength), commonly used for green-fluorescent protein imaging, as a damaging agent known for inducing the production of reactive oxygen species and mitochondrial damage (Camilla U Rang et al. 2012; Dixit and Cyr 2003; Gourmelon, Cillard, and Pommepuy 1994; Godley et al. 2005). Bacteria were cultured in microfluidic devices and treated with variable lengths of light exposure, ranging from 70 ms to 3 s, administered every 2 min for up to 24 h. Each experiment was preceded by 24 h of control imaging in the absence of extrinsic damage.

Analyzing cell lineages over time, we observed a significant decrease in elongation rates on each exposure treatment relative to its control (Figure 2.3A and Table 2.A.2; unpaired two-sample t tests; $p < 0.001$). The treatments revealed a significant effect of both age and light

exposure on individual elongation rates, with new daughters maintaining significantly faster growth than their old siblings in all cases (Figure 2.3B). A similar effect was observed for the impact of light exposure and age on damage inherited at birth (Figure 2.A.2), showing that the overall damage inheritance increased with treatment. We determined the growth parameters of each treatment (Table 2.A.3), verifying that λ increased linearly with the length of exposure to light excitation (Figure 2.3C). This demonstrates that the rates of extrinsic damage infliction correlate linearly with the rate of intracellular damage accumulation for our experimental design. From the growth parameters Π, λ and *a*, we calculated the estimated doubling times of new and old lineages, as well as the predicted doubling time equilibria for each treatment level (Figure 2.3D to H). Our results showed a separation between new and old daughter subpopulations in all cases (Table 2.A.4).

The increasing induction of damage accumulation led to the stabilization of new and old lineages at equilibria with progressively longer doubling times. Extreme damage levels caused the old lineage equilibrium to approach infinite doubling times (Figure 2.4A-B) with 3 s of exposure, meaning that old daughters undergo division arrest, suggesting a damage accumulation rate of 0.009 min^{-1} as the threshold at which aging lineages transition to mortality. Fewer mortality events were observed in new daughters, indicating that new lineages might remain proliferative under the same conditions. Interestingly, we observed that the difference between damage loads at birth (k_2 and k_1) was significantly reduced at 3 s of exposure, when compared to control conditions (Figure 2.A.2; two-tailed t test, t = 2.805, df = 80.995, p = 0.0063). This outcome was surprising, since one of the advantages of asymmetric damage partitioning in bacterial populations is the ability to endure higher levels of damage (Chao et al. 2016). Therefore, we expected to find that populations exhibiting large damage accumulation rates should display greater asymmetry.

Our experiments, nonetheless, revealed a consistent pattern of diminishing asymmetry with the infliction of light excitation. Although all populations remained asymmetrical, with a maximum $a = 0.47$, the asymmetry coefficient approached 0.5 as λ increased Figure 2.4C). A possible driver of increasing symmetry would be the fast accumulation of new damaged components, as expressed by increasing λ, surpassing the rate at which such components aggregate. As a result, more damage would be partitioned as diffused rather than polar anchored molecules at the time of division (Chao et al. 2016), leading to an increase in stochastically partitioned damage. To investigate this hypothesis, we tested whether the doubling time variance produced by stochasticity increased with light exposure. We first normalized the doubling times of each sibling pair around the expected values for symmetric cells (Figure 2.4D-H) for each treatment level. This normalization removes the variance produced by noise in maternal growth. Since new and old daughters in our populations are physiologically distinct, two distributions arise from the normalized data. The distance (D) between these distributions is produced by asymmetry, which defines the variance explained by deterministic factors as $D^2/4$ (see Methods and Chao et al. 2016 for details). The average variance of new and old distributions $(V_N + V_O)/ 2$, on the other hand, represents the doubling time variance explained by stochasticity. The estimates of deterministic and stochastic variance were summarized in Figure 2.4I and Table 2.A.5. With higher levels of light excitation, we observed an increase in the variance explained by stochasticity, whereas the deterministic variance remained nearly constant. These results indicate that, while the deterministic physiological distinction between new and old daughters remains present, the perceived asymmetry between these lineages is attenuated by stochasticity as extrinsic damage levels increase. It is important to observe that, while our results depict the effect of constant damage exposure, other interesting outcomes could arise from transient damage pulses.

To determine whether new and old lineages remained in equilibrium despite the presence of large stochasticity, we performed a stability analysis on elongation rates. We followed the same principles described in Figure 2.2 and Figure 2.A.1, where a linear regression between T_0 and T_1 or T_0 and T_2 is evaluated for its stability in crossing the identity lines. The maintenance of this crossing, which acts as an equilibrium attractor, determines that these lineages display stable growth over time, thus retaining immortal proliferation. In the presence of stochasticity acting on the regression slope, the condition $a^2 + \sigma_1^2 < 1$ must be satisfied for the retention of equilibrium. We estimated the slopes and σ_1 values for each light exposure treatment (Figure 2.4J), performing a bootstrap analysis to obtain confidence intervals. The stability condition in our experiments was reached by all lineages until 3 s of light exposure. At 3 s of exposure, or $\lambda = 0.009$ min^{-1}, old lineages reached their mortality threshold and became unstable, resulting in the mortality events observed in Figure 2.4A-B. All new lineages in our experiments remained stable. However, because the confidence intervals in Figure 2.4J indicated a chance of new lineages also losing stability at 3 s, we investigated the probability of retaining immortal proliferation in Figure 2.4K. Our analysis revealed that old lineages exhibited a significantly higher probability of losing equilibrium (50.24%) than new lineages (28.10%, $x^2 = 1027.7$, df = 1, $p < 0.001$), therefore indicating that asymmetric damage partitioning leads to differential maintenance of immortality in new and old lineages within the same population. These results suggest that, despite the decrease in asymmetric partitioning, new daughters are able to endure higher levels of damage while remaining functionally immortal.

2.3.6 Old lineages transition from immortality to mortality under extrinsic stress

To determine whether the differential mortality of new and old daughters could be translated to other damage sources, we repeated our experiments replacing light exposure with heat stress (Figure 2.5A-C) or streptomycin (Figure 2.5D-F) as damaging agents. We exposed cells growing in the mother machine to 38, 40 and 43°C, as heat exposure can lead to the accumulation of misfolded proteins and senescence (Winkler et al. 2010; Steiner et al. 2017). We observed an increase in mortality events at 38 and 40°C, although elongation rates remained constant over time (Figure 2.5A-B, Table 2.A.4). At 43°C, however, elongation rates declined and old lineages lost stability ($a^2 + \sigma_1^2 = 1.144$), while new lineages remained in equilibrium ($a^2 + \sigma_1^2 = 0.965$). Our bootstrap analysis suggested that old lineages had a higher probability of transitioning to mortality (67.1%) than new lineages (43.4%, $x^2 = 1136$, df = 1, $p < 0.001$) (Figure 2.5C). We verified a similar outcome for populations exposed to 2, 4 or 5 $\mu g.ml^{-1}$ of streptomycin, which has been shown to induce protein misfolding in *E. coli* (Ni et al. 2012; Coquel et al. 2013; Rang et al. 2012). While new and old lineages remained stable at 2 and 4 $\mu g.ml^{-1}$ (Figure 2.5D-E, Table 2.A.4), both lineages lost stability at 5 $\mu g.ml^{-1}$. Still, our analysis detected a differential probability of crossing the mortality threshold, with new lineages displaying a lower chance (81.2%) of becoming mortal than old lineages (88.0%, $x^2 = 177.13$, df = 1, $p < 0.001$) (Figure 2.5F). Taken together, these results suggest that the asymmetric partitioning of damage leads to a differential transitioning from immortality to mortality in stressed bacterial populations. The asymmetric allocation of non-genetic damage, whether inflicted by light exposure, heat or streptomycin, leads to higher mortality in old lineages while allowing the immortality of new lineages within the same population. Therefore, these observations offer cellular aging as a model for both the maintenance of continuous replication, as in stem cells, and the loss of proliferative capacity due to cellular aging.

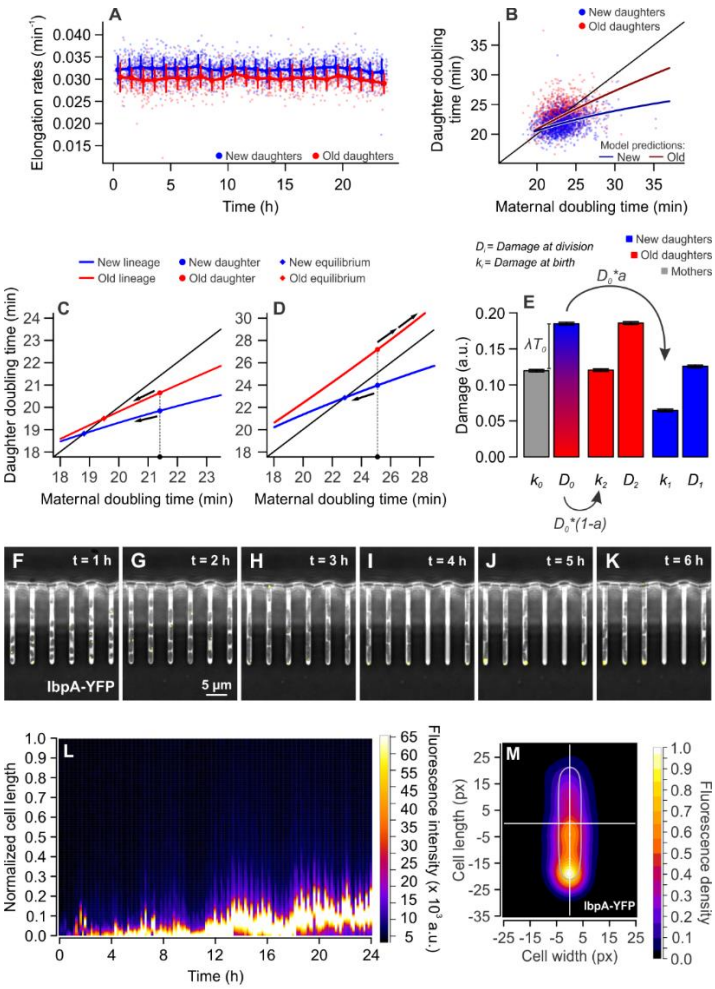

Figure 2.1 - Maintenance of growth equilibrium and immortality through asymmetric damage partitioning.
(A) New daughters (n = 1782; 0.032 ± 0.0023 min^{-1}, mean ± SD) elongated at significantly higher rates than old daughters (n = 1285; 0.030 ± 0.0025 min^{-1}, mean ± SD), a distinction that remained stable over several hours (one-tailed t test, t = 24.747, df = 2612.5, $p < 0.001$). Binned data comprises mean ± SD. (B) The distinction between new and old daughters was also verified for the doubling times of sibling pairs (paired one-tailed t test, t = 24.716, df = 1383, $p < 0.001$). The separation of new and old subpopulations, according to the estimation of growth parameters (see Methods), was produced by the accumulation of damage at a rate $\lambda = 0.0028$ min^{-1}, and the partitioning such load with asymmetry $a = 0.375$. (C and D) Model predictions on cellular aging with $\Pi = 18$ min, a = 0.4. (C) With $\lambda = 0.002$ min^{-1}, asymmetry produces a separation between new (blue) and old (red) subpopulations. The intersection of model predictions and the identity line creates equilibrium points where $T_0 = T_1$ or $T_0 = T_2$, to which new or old daughters converge over generations (arrows). (D) With $\lambda = 0.008$ min^{-1}, the old lineages are predicted to lose equilibrium and arrest division. New daughters, through constant rejuvenation, would retain replicative immortality at the same damage levels. (E) Damage load harbored by a mother and its daughters at the time of birth (k_0, k_1, k_2) and division (D_0, D_1, D_2). Applying the average growth parameters Π and λ to calculate k_1 and k_2, we verified that old daughters inherit larger damage loads than new daughters (paired one-tailed t test, t = 27.988, df = 1244, $p < 0.001$) and also bear more damage at the time of division (paired one-tailed t test, t = 27.914, df = 1244, $p < 0.001$). Bars represent mean ± standard error. (F to K) Time lapse microscopy images showing the accumulation of misfolded proteins at the old cell poles over time. The small chaperone IbpA (yellow dots) co-localizes with damaged proteins, allowing the visualization of protein aggregates. (L) The fluorescence profile of an old lineage expressing IbpA-YFP shows that a protein aggregate develops over time, remaining trapped in the old pole over generations. Fluorescence profiles were measured every 10 min. See also Figure 2.A.1. for non-normalized length. (M) Combined IbpA-YFP fluorescence heatmap of 428 old daughters at the bottom of mother machine wells, imaged over 6h.

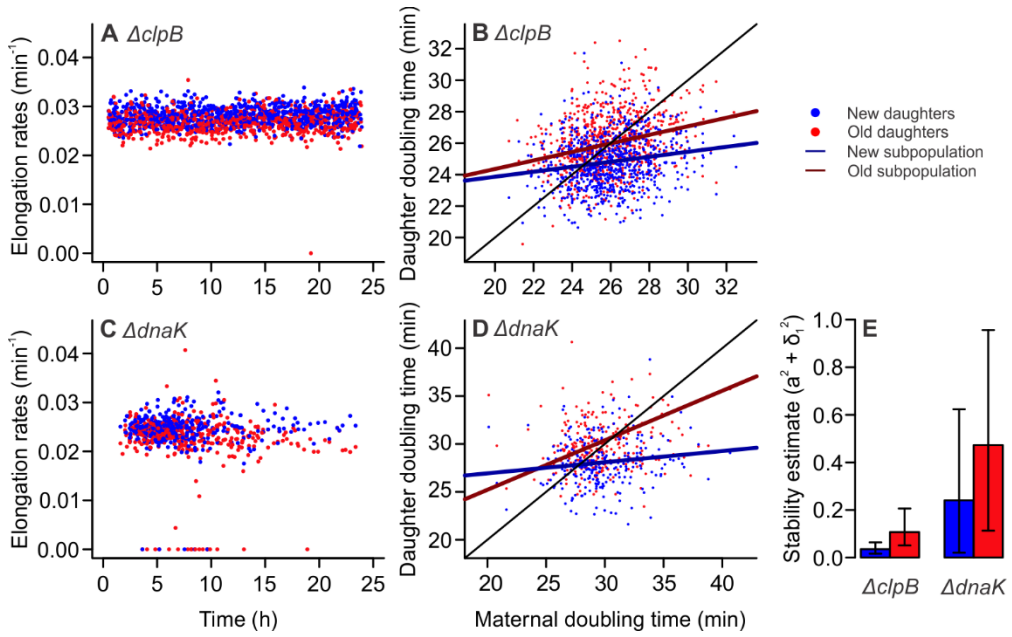

Figure 2.2 - Equilibrium and asymmetry are present in repair mutants lacking ClpB or DnaK chaperones.
(A) Δ*clpB* cells (n = 1642; 0.027 ± 0.002, mean ± SD) exhibited stable elongation rates over time, suggesting these mutants might be in growth equilibrium. A single mortality event was observed. (B) Δ*clpB* mutants retained asymmetric doubling times. A two-way ANOVA indicated a significant effect of both T_0 ($F = 82.32$, $p < 0.001$) and age ($F = 178.07$, $p < 0.001$) on doubling times, with interaction between factors ($F = 5.66$, $p = 0.017$). (C) Δ*dnaK* mutants (n = 786, 0.0236 ± 0.004) exhibited signs of stability loss, with several mortality events occurring throughout the experiment. (D) Similarly to Δ*clpB*, Δ*dnaK* mutants exhibited a separation between new and old subpopulations, with a two-way ANCOVA indicating a significant effect of T_0 ($F = 12.78$, $p < 0.001$) and age ($F = 16.89$, $p < 0.001$) on doubling times, with interaction between factors ($F = 5.11$, $p = 0.024$). (E) A stability analysis performed on linear models from (B) and (D) revealed that both strains satisfy the stability requirement $a^2+\sigma_1^2 < 1$. Although mortality events were observed for Δ*dnaK* mutants, the strain remains mostly stable. Our bootstrap analysis revealed a 1.45% probability of losing equilibrium for old lineages, and complete stability for new lineages ($x^2 = 129.86$, df = 1, $p < 0.001$). Error bars: 95% confidence intervals.

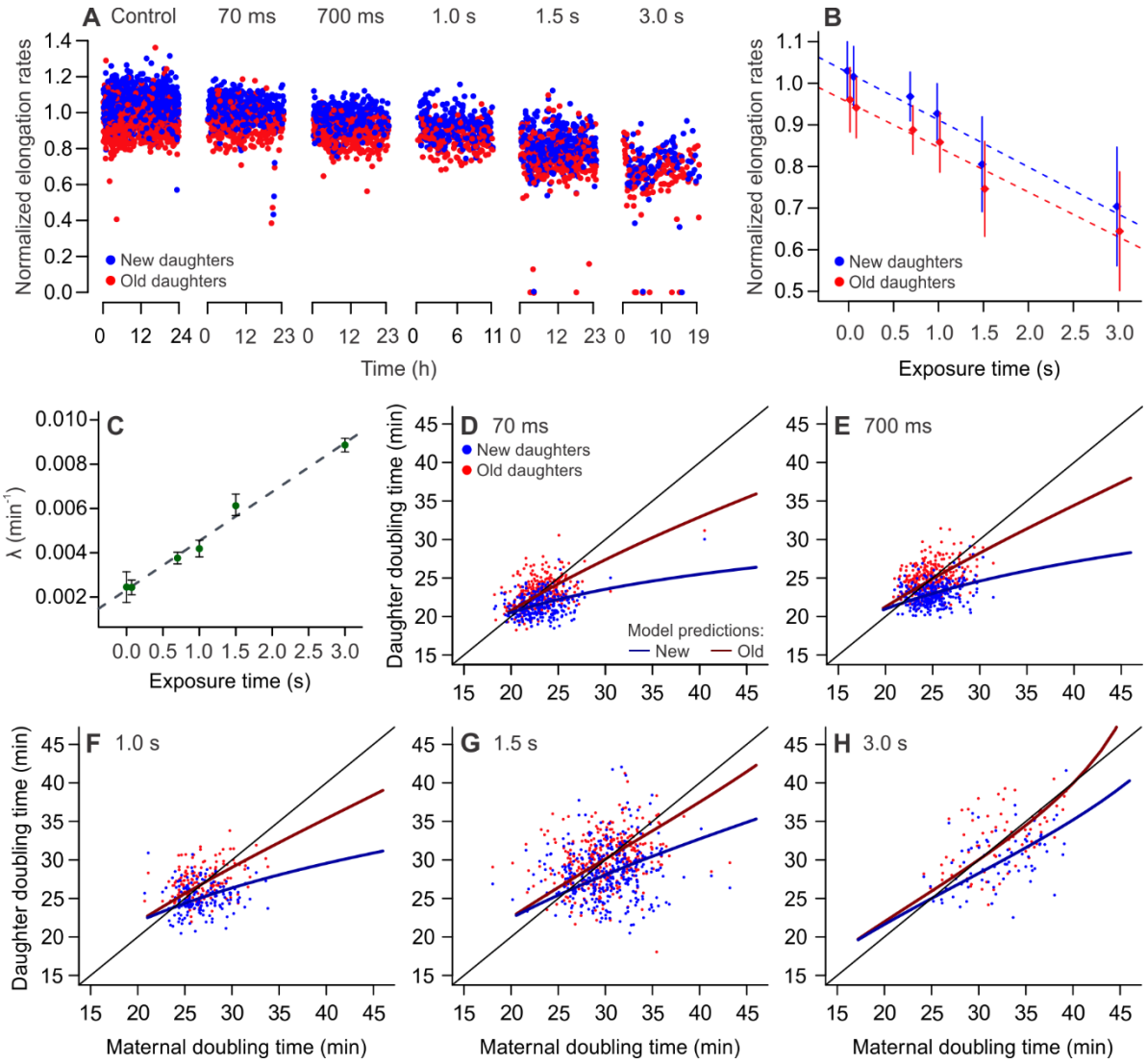

Figure 2.3 - Damage accumulation decreases elongation rates and displaces growth equilibrium.
All panels depict MG1655 wild-type *E. coli*. (A) Exposure to phototoxic damage led to decreasing elongation rates in all treatment levels (length of exposure, every 2 min: 70 ms, 700 ms, 1 s, 1.5 s, 3 s). (B) Both new and old daughters displayed slower growth in response to phototoxic damage ($F = 9272$, $p < 0.001$), with new daughters growing faster than their old siblings in all cases ($F = 1505$, $p < 0.001$). There was significant interaction between age and damage level in determining elongation rates ($F = 2384$, $p < 0.001$; two-way ANCOVA). Data are represented as mean ± SD. (C) Linear correlation between length of phototoxic damage exposure and damage accumulation rates estimated for each treatment ($p < 0.001$, $R^2 = 0.98$). Data are represented as mean ± 95% CI. (D to H) Distinct subpopulations of young and old daughters were observed in all treatment levels, with increasingly longer doubling time equilibria. At 3 s of exposure ($\lambda = 0.009$ min^{-1}), the old lineages lie at the threshold of arresting proliferation.

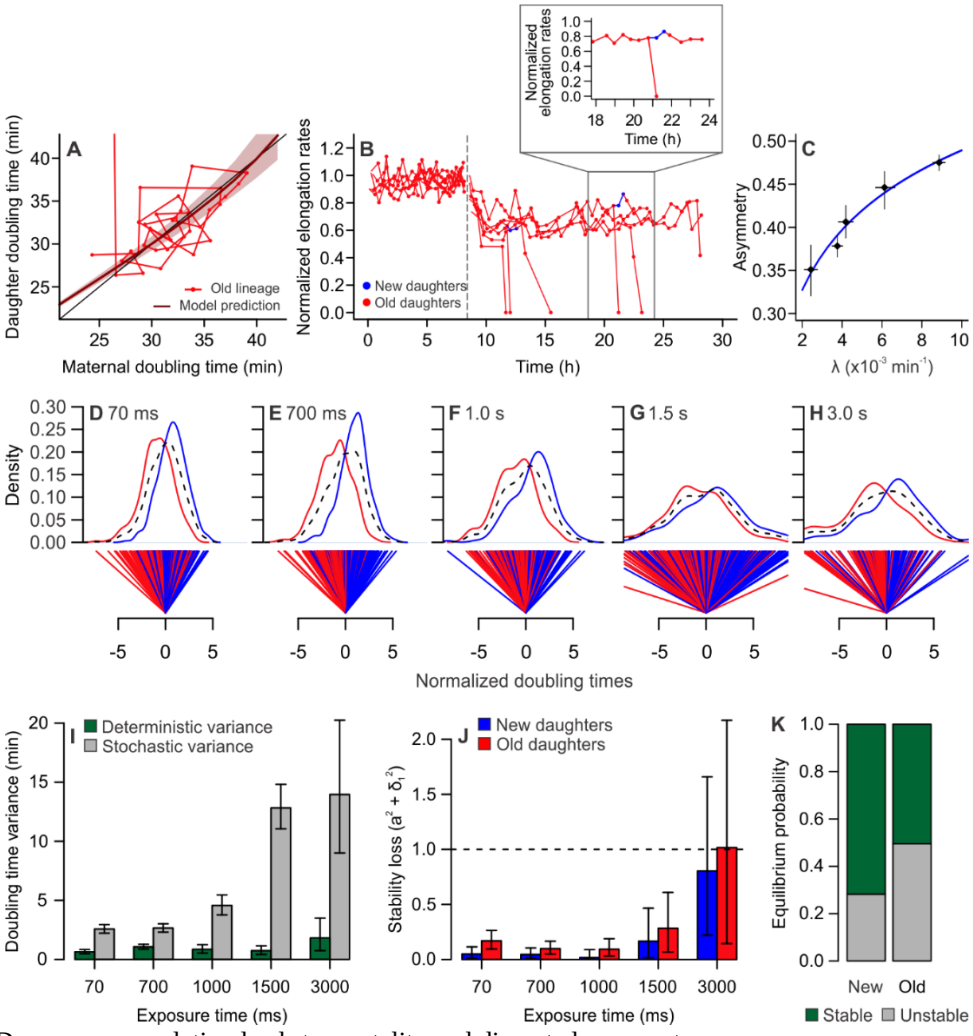

Figure 2.4 - Damage accumulation leads to mortality and disrupted asymmetry.
All panels depict MG1655 wild-type *E. coli*. (A) Doubling times of an old lineage as it accumulates damage at λ = 0.009 min^{-1}, induced by 3 s of light exposure. The line representing model predictions (dark red) approaches identity (black), indicating that these cells do not reach equilibrium. After a few generations the last daughter in the lineage arrests growth, which equals an infinite doubling time, which represents the crossing of a mortality threshold for the lineage. (B) Elongation rates of old lineages, showing the transition from control imaging (0 – 8.6 h) to the infliction of 3 s of light exposure every 2 min. All cells exhibited lower growth rates, culminating in division arrest for old daughters. New daughters outlived their old siblings by at least one generation, and were sometimes able to generate a new lineage in the growth wells (shown in blue and expanded in the detail). All values were normalized by the average control elongation rates. (C) Increasing damage accumulation rates disrupted asymmetric partitioning, as shown by the asymmetry coefficient approaching 0.5 ($a = 0.1007*\ln(\lambda) + 0.95$, $p < 0.001$). Points represent average growth parameters and 95% confidence intervals. (D-H) Distributions of new (blue) and old (red) daughter doubling times were normalized around a symmetric midpoint. While the combined population has a distribution centered at zero (dashed black lines), new and old subpopulations split into two separate distributions. The distance between the averages of these distributions expresses the doubling time variance produced by deterministic physiological asymmetry. The average variance of new and old distributions around their own means, on the other hand, represents the variance produced by stochasticity. (I) Deterministic and stochastic portions of the variance from (D-H) were summarized for increasing light exposure, showing an increase in stochasticity. Error bars represent 95% confidence intervals. (J) Our stability analysis indicated that new and old daughters remained in stable equilibrium until exposed to 3 s of phototoxic stress. At 3 s, old daughters no longer satisfy the stability requirement ($a^2 + \sigma_1^2 = 1.016$), thus transitioning to a mortal state. Error bars represent 95% confidence intervals. (K) At 3 s of exposure, old lineages displayed a 49.53% probability of losing equilibrium, while new lineages exhibited only a 28.10% probability of mortality (test for equality of proportions, $x^2 = 1027.7$, df = 1, $p < 0.001$).

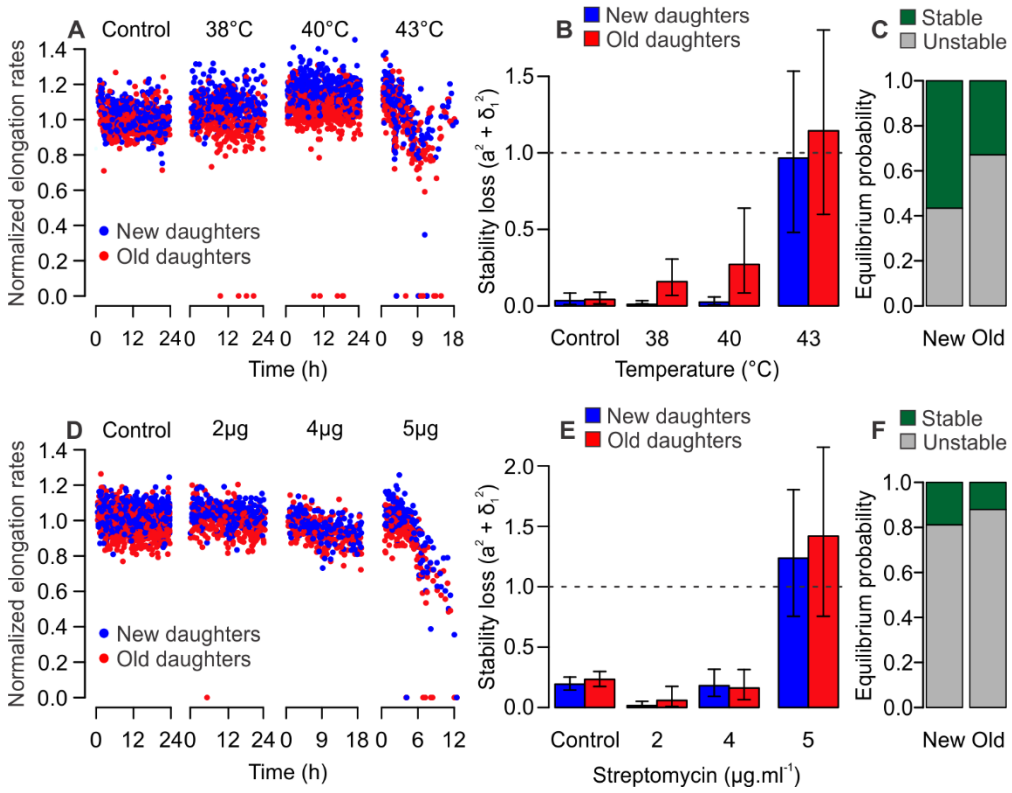

Figure 2.5 - Old lineages are more likely to reach mortality when exposed to heat or streptomycin.
All panels depict MG1655 wild-type *E. coli*. (A) Elongation rates over time for populations exposed to control temperatures, 38, 40 or 43°C heat stress (n = 875, 535, 782, and 380 cells). A few mortality events were observed for 38 and 40°C, with elongation rates declining at 43°C. (B) At 38 and 40°C both new and old lineages satisfied the stability requirement $a^2 + \sigma_1^2 < 1$. At 43°C, new lineages in our experiment remained stable, while old lineages lost equilibrium. (C) At 43°C, Old lineages displayed a significantly higher probability (67.1%) of losing equilibrium than new lineages (43.4%, $x^2 = 1136$, df = 1, $p < 0.001$). (D) Populations exposed to 0, 2, 4 or 5 µg.ml^{-1} streptomycin (n = 1,322, 453, 337, and 292 cells) showed declining elongation rates over time. (E) Both lineages remained in stable equilibrium for 2 and 4 µg.ml^{-1} streptomycin, however new ($a^2 + \sigma_1^2 = 1.236$) and old ($a^2 + \sigma_1^2 = 1.420$) lineages lost stability at 5 µg.ml^{-1}. (F) Although both lineages displayed a large probability of transitioning to mortality, old lineages (88.0%) had a higher chance of losing equilibrium than new lineages (81.2%, $x^2 = 177.13$, df = 1, $p < 0.001$) at 5 µg.ml^{-1} streptomycin. (B and E) Error bars represent 95% confidence intervals.

2.4 Discussion

Individuals age by progressively accumulating damage over their lifespan, leading to loss of function late in life (Rose 1991; Kirkwood 2008). Because biological organisms are composed of individual cells, the process of cellular aging represents a baseline for understanding the general principles of aging and its phenotypic manifestations. Cellular aging comprises the dynamics of intracellular damage accumulation and partitioning, whose manipulation and quantification becomes possible in unicellular systems, such as bacteria. Bacterial populations display phenotypic variation arising from asymmetric cell divisions, an evolutionarily advantageous strategy for increasing the efficiency of natural selection (Chao et al. 2016). Previous studies have shown that, as a consequence of asymmetric cellular divisions, aging and rejuvenating bacterial lineages stabilize at distinct states of physiological equilibrium (Chao 2010; Camilla U Rang, Peng, and Chao 2011; Proenca et al. 2018). While in equilibrium, these lineages remain functionally immortal. Here we showed that this state of equilibrium is maintained by the balance between damage accumulation and asymmetric partitioning. Unstressed bacterial lineages, despite their immortal proliferation and constant environment, accumulated damage derived from standard metabolic rates, and partitioned around 63% of their damage load towards old daughters. Repair mutants lacking the repair chaperones still retained asymmetric partitioning and the ability to reach equilibrium, supporting the notion that asymmetry contributes towards proliferative immortality in lineages that must rejuvenate constantly. This is the case of stem cells, which were recently shown to asymmetrically segregate damaged components and proteins targeted for degradation (Bufalino, DeVeale, and van der Kooy 2013; Moore et al. 2015; Fuentealba et al. 2008).

Although stem cell lineages rejuvenate at every division, their proliferation reaches exhaustion in old individuals (López-Otín et al. 2013). Interestingly, stem cells from old mice were

also shown to have a disrupted diffusion barrier (Moore et al. 2015), which renders division more symmetric by causing the stem sibling to inherit damaged components. Our results suggest that a similar phenomenon takes place in bacterial lineages. We expected to find a larger asymmetry between daughter cells produced under high levels of extrinsic damage, but instead the treatments caused a disruption in efficient asymmetric partitioning and increased stochasticity. Because bacterial asymmetry depends on the allocation of misfolded proteins to old cell poles, cells exposed to high levels of stress might be failing to sequester their damaged components. It is possible that old poles become saturated with damage, causing aggregates of misfolded proteins to be randomly deposited in the new pole or along the cell. Another possibility is that high damage accumulation rates interfere with the repair machinery, composed of chaperones that co-localize with damage and are responsible for maintaining proteostasis (Doyle and Wickner 2009; Winkler et al. 2010; Sabate, De Groot, and Ventura 2010).

The fact that asymmetry was disrupted by damage accumulation did not prevent new and old lineages to undergo strikingly distinct paths under intense levels of extrinsic damage. When extreme damage accumulation rates are induced, new lineages display increased doubling times but remain in equilibrium. Old lineages, however, undergo division arrest as a consequence of inheriting larger damage loads, satisfying the classical pattern of cellular aging. In this scenario, old daughters have reached the mortality threshold, while new daughters remain functionally immortal. Asymmetry therefore allows for the coexistence of two distinct physiological states in a clonal cell population. If this mechanism can be extrapolated to cells within somatic tissues, asymmetric damage segregation could offer an explanation for the simultaneous occurrence of senescent and proliferative cells in aging tissues (Aravinthan 2015; Jeyapalan and Sedivy 2008).

Since asymmetry dictates mortality or immortality in sibling cells, it may also relate to the processes of cellular differentiation and fate determination.

Addressing the study of aging from a cellular perspective, our findings showed that bacterial systems can provide an integrative view of the general principles driving the aging phenotype. From a simple cellular system, we can quantify the dynamics of damage accumulation and partitioning along generations. Asymmetric partitioning of damage drives cell populations to reach a stable equilibrium, where the aging of a lineage enables the continued rejuvenation of another. Moreover, even when old lineages cross the threshold and become mortal, asymmetry allows the survival of new daughters and ensures the continuity of the population. Applying this framework to the aging research may largely contribute to the understanding of an evolutionarily conserved basis for the progressive functional decline experienced by prokaryotes and eukaryotes alike.

2.5 Materials and methods

2.5.1 Bacterial strains and growth conditions

Experiments were performed with K-12 *E. coli* wild-type strain MG1655 for the determination of damage accumulation in immortally proliferating bacteria, and for experiments on the disruption of growth equilibrium. The visualization of protein aggregates was performed with MG1655 *E. coli* expressing YFP bound to the small heat-shock protein IbpA, constructed according to Rang et al. (2018) from the construct *IbpA-yfp-Cm*^{r} kindly provided by Ariel B. Lindner (INSERM, France) (Lindner et al. 2008). Repair mutants were screened for asymmetry and equilibrium using *E. coli* BW25113 Δ*clpB* (CGSC #11763) and Δ*dnaK* (CGSC #8342) from the Keio knockout collection (Baba et al. 2006). The antibiotic resistance marker was not removed

from these strains. For all experiments, cultures were inoculated in lysogeny broth (LB broth; per liter: 10 g tryptone, 5 g yeast extract, 5 g NaCl) and grown overnight at 37°C with agitation. The culture medium was supplemented with 0.075% Tween 20 upon inoculation within microfluidic devices, which prevents the formation of biofilms in the flow channels.

2.5.2 Microfluidic device design and fabrication

The device used in this study was based on the mother machine design by Wang et al. (2010), subsequently modified by Ryan Johnson (University of California, San Diego) for the addition of more growth wells. This device included 16 parallel flow channels containing 2000 growth wells (1.25 x 30 x 1 μm) each. Polydimethylsiloxane (PDMS) microfluidic chips were fabricated from master silicon wafers used as negative molds, provided by the Ryan Johnson and the Jeff Hasty Lab (University of California, San Diego). PDMS chips fabricated through soft lithography yielded 12 devices per process and were attached to 24 x 40 mm coverslips through a covalent bond. Previous control experiments have shown that the asymmetry observed in mother machine devices is not produced by starvation (Wang et al. 2010; Proenca et al. 2018) and that wide (> 1.0 μm) growth channels can produce cells with faster growth rates than liquid cultures (Yang et al. 2018).

2.5.3 Cell loading and experimental conditions

Cultures were grown overnight in LB medium and centrifuged for 2 min at 5300 g. The supernatant medium was subsequently discarded, and the pellet was resuspended in 50 μL of medium supplemented with Tween 20. Prior to loading, microfluidic devices were placed in a vacuum chamber for 10 to 15 min. Bacteria were loaded by placing a droplet of concentrated

culture over the loading port, posteriorly used as an outlet during the experiment, and a droplet of sterile medium over the opposite port. Once all channels were properly filled, bacteria were pushed into the growth traps by centrifuging the device at 1410 g for 7 min. Input and output 60 ml syringes were connected to the ports for a continuous supply of growth medium throughout the experiment. The device was incubated at 37º C during imaging. When required, extrinsic damage was induced by fluorescent light exposure (490 nm wavelength) using a FITC filter, set at 25% strength. The length of exposure to light excitation ranged from 70 ms to 3 s, applied in 2 min intervals. Damage induced by heat stress was produced by increasing the incubation temperature in the microscope chamber to 38, 40 or 43°C, which was monitored in real time. Extrinsic damage induced by sub-inhibitory streptomycin concentrations was introduced by adding 2, 4 or 5 $\mu g.ml^{-1}$ of antibiotic to the growth medium. Each of these experiments was preceded by a 24 h control imaging of the same bacterial lineages.

2.5.4 Time-lapse image acquisition

Cell movies were collected by a Nikon Eclipse Ti-S microscope, with imaging intervals controlled by NIS-Elements AR software. Phase images were collected in 2 min intervals during the entire length of mother machine experiments, immediately followed by the acquisition of FITC pictures when required. For heat or streptomycin stress experiments, no FITC imaging was used.

2.5.5 Quantification of bacterial growth

Images were analyzed with the free software ImageJ (NIH, https://imagej.nih.gov/ij), recording cell coordinates as Regions of Interest (ROI) and cell names as indicatives of lineage and cell pole inheritance. Cell lengths were determined immediately before and after each division

and time of division was recorded. Elongation rates (r) and doubling times (ln(2)/r) were calculated from the data, and the resulting tables were entered in an R program to determine maternity, sibling pairs and lineage trees. To ensure that the measurements were unbiased, we performed blind data collections where elongation rates were recorded without knowledge of pole inheritance. The ImageJ plugin MicrobeJ was used for the creation of fluorescence profiles and heatmaps (Ducret, Quardokus, and Brun 2016).

Data presented in Proenca et al. (Proenca et al. 2018) for verifying the stability of the old lineage equilibrium attractor was included in our control data from phase imaging, accompanied by new control experiments performed for this study. These experiments provided the necessary baseline for our aging model parameters.

2.5.6 Statistical analysis

Statistical analysis was performed using R version 3.4.1. p-values < 0.05 were considered statistically significant. Because distinct microfluidic devices yield small yet robust measurement differences, elongation rates and doubling times were normalized by population means when comparing data from different experiments. Data from phase imaging, our controls, were normalized by their respective averages. Normalized data for all replicates were pooled and compared by one or two sample t-tests, as reported. Data from light exposure, heat or streptomycin stress imaging were normalized by the respective control experiment mean elongation rates. Raw data corresponding to these normalizations were presented in phase planes for individual populations. Statistical parameters were reported as mean ± SD, or as mean ± 95% confidence intervals for growth parameters, as indicated in the text. Sample sizes (cells, sibling pairs or replicates, as informed) are indicated along with reports of statistical analyses.

2.5.7 Cellular aging model

This population genetics model determines the role of asymmetric partitioning of damage upon cell division as a mechanism of survival in the presence of damage (Chao 2010). It was developed for bacterial populations, assuming that cells must build-up an intracellular product to a checkpoint before dividing. Based on the rate with which a bacterium accumulates damage during its lifetime (λ) and the doubling time of fittest cell (Π), the damage load received at birth (k_0) by a mother bacterium can be determined from its doubling time (T_0) as

$$k_0 = 1 - \left(\lambda/_2\right)T_0 - \Pi/_{T_0}$$

The load received at birth (k_0), along with the amount accumulated in its lifetime ($\lambda T0$), is the damage a bacterium will segregate to its daughters according to the asymmetry coefficient (a), ranging from 0 (complete asymmetry) to 0.5 (symmetry):

$$k_1 = (k_0 + \lambda T_0)a$$

$$k_2 = (k_0 + \lambda T_0)(1 - a)$$

This asymmetric inheritance will affect the doubling times of the offspring, causing old daughters, which receive the higher load (k_2), to slow down compared to their young siblings. The doubling times of each daughter, T_1 and T_2, are given by

$$T_1 = \frac{(1 - k_1) - \sqrt{(1 - k_1)^2 - 2\Pi\lambda}}{\lambda}$$

$$T_2 = \frac{(1 - k_2) - \sqrt{(1 - k_2)^2 - 2\Pi\lambda}}{\lambda}$$

Estimates of doubling time equilibrium were determined as the points where prediction lines cross the identity, which can be calculated as

$$\alpha = \frac{a}{1 - a}$$

$$\hat{T}_1 = \frac{1 - \sqrt{1 - 4\Pi\lambda(1/_2 + \alpha)}}{2\lambda(1/_2 + \alpha)}$$

$$\hat{T}_2 = \frac{1 - \sqrt{1 - 4\Pi\lambda(1/2 + 1/\alpha)}}{2\lambda(1/2 + 1/\alpha)}$$

2.5.8 Estimation of growth parameters

The data collected for doubling times of trios composed by a mother bacterium and its two daughters was entered in the model to determine growth parameters. The doubling times of the daughters (T_1 and T_2) were estimated from a known maternal doubling time, using varying values of Π, λ and *a*, and compared to the observed doubling times. Optimal parameters were those that provided the least mean squared difference between expected and observed doubling times. An independent combination of Π, λ and *a* was estimated for each control experiment, while only λ and a were estimated for light treatment experiments (since Π is the baseline doubling time, it was provided by the respective control parameter). Non-sensical parameters were excluded based on previous knowledge of the model, such as the impossibility of a being either negative or larger than 1, or Π being larger than any observed doubling time. To obtain the 95% confidence intervals for each parameter, the average of results was entered in a bootstrapped estimate of parameter combinations, repeated 10,000 times with resampling of the observed mother and daughter trios.

2.5.9 Estimation of deterministic and stochastic variance components

Doubling time variances were analyzed for deterministic and stochastic components according to Chao et al. (Chao et al. 2016). For each T_0, T_1, T_2 trio, the doubling time of a hypothetical symmetric daughter was estimated based on Π, λ and T_0. Daughter doubling times were normalized by subtracting T_1 and T_2 from the symmetric daughter estimate, thus centering the mean distribution around zero. The distance (D) between the means of normalized T_1 and T_2

was estimated, as well as the variance of new (V_N) and old (V_O) distributions. The total variance (V_T) in the population corresponds to $V_T = (V_N + V_O)/2 + D^2/4$. In this equation, $D^2/4$ represents the variance produced by deterministic asymmetry. $(V_N + V_O)/2$ represents the unexplained variance, produced by stochastic sources.

2.5.10 Equilibrium stability analysis

T_0, T_1, T_2 trios from phase planes were used to determine the stability of growth equilibria for new and old lineages. When mortality events were common (stressed populations), elongation rates were used instead of doubling times. New and old lineages were analyzed separately according to linear regressions between *T_0* and *T_1* or *T_2*. The effective slope for each mother-daughter pair was determined as $(T_i - b)/T_0 = a + \xi_1$, where ξ_1 represents a random variable drawn from a Gaussian distribution each generation. The standard deviation of the ξ_1 distribution is given by σ_1. As described by Proenca et al. (Proenca et al. 2018), a point of equilibrium where the regression and identity lines intersect exists as long as the condition $a^2 + \sigma_1^2 < 1$ is satisfied. Values of $a^2 + \sigma_1^2$ were estimated for new and old daughters of experimental populations and reported as bar plots for all damaging conditions. This estimate was repeated as a 10,000-fold bootstrap of *T_0, T_1, T_2* trios for the determination of 95% confidence intervals and equilibrium probabilities.

2.6 Acknowledgements

We thank R. Johnson and G. Graham for assistance with experimental setup, and C. Buetz, S. Cheung, J. Chen, and X. Liu and for data assistance. We thank Ariel Lindner (INSERM, France) and Justin Meyer (UCSD) for kindly providing bacterial strains, and Donald R. Helinski and Christopher J. Wills (UCSD) for fruitful discussions.

Chapter 2, in full, is a reprint of the material as it appears in Proenca AM, Rang CU, Qiu A, Shi C, Chao L (2019). Cell aging preserves cellular immortality in the presence of lethal levels of damage. *PLoS Biology* 17(5): e3000266. The dissertation author was the primary investigator and author of this paper.

2.A Apendix

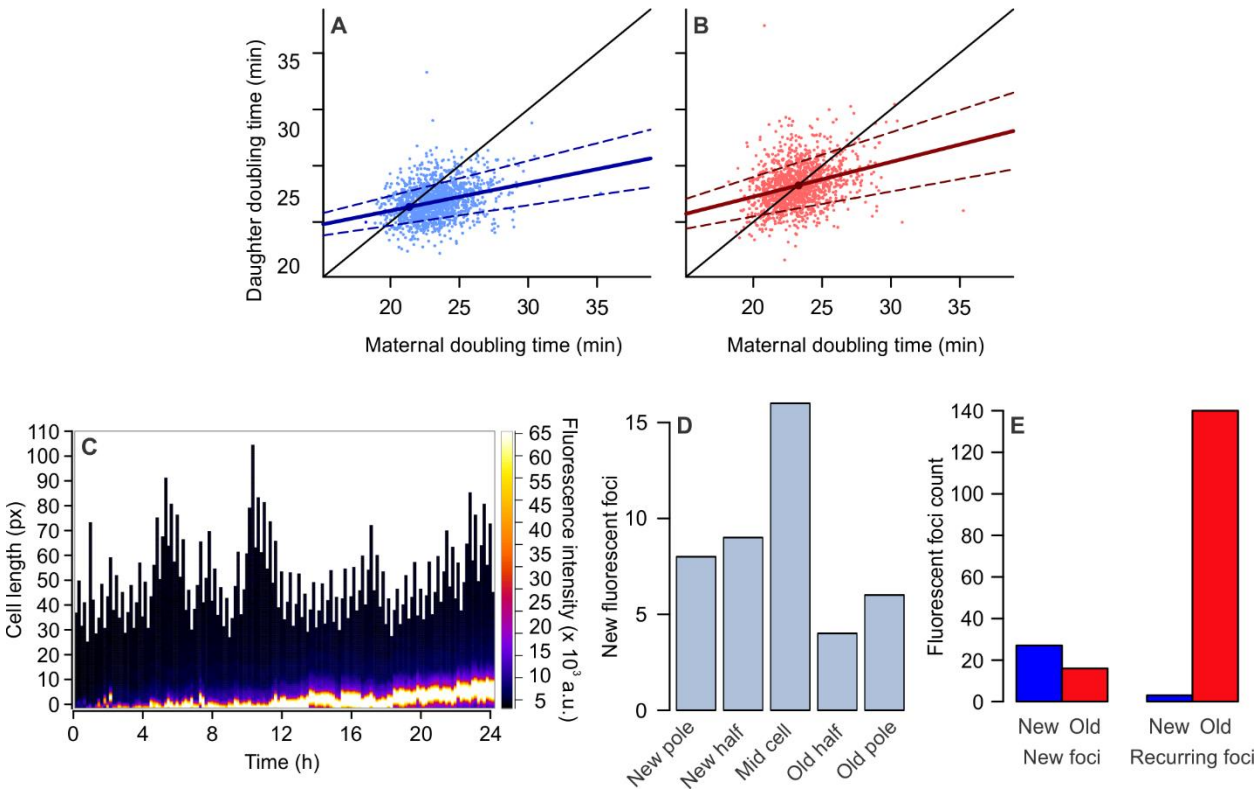

Figure 2.A.1 - Stability and protein aggregation in unstressed populations.
Growth stability in new and old lineages can be expressed by linear regressions between T_0 and T_1 (A, solid blue line) or T_2 (B, solid red line). The intersect between regression lines and the identity line represents a point of stable equilibrium to which doubling times converge. Due to the doubling time variance produced by stochasticity acting on the slopes (σ_1), given by $T_i = T_0*(a + \sigma_1) + b$, equilibria might be disrupted when $a^2 + \sigma_1^2 \geq 1$. Dashed lines in (A) and (B) represent the maximum variation in regression lines obtained by the parameter σ_1 acting on the slopes of our data, demonstrating that new and old lineages retain equilibrium in the presence of stochasticity. (C) Fluorescence profiles obtained in 10 min intervals for an old lineage, showing the anchoring of protein aggregates (IbpA-YFP) in the old pole over time. (D) Over the course of 194 cell divisions observed over 24h imaging, we verified the first appearance of 43 protein aggregates. The cellular localization of these new fluorescent foci showed no bias for old poles. (E) The partitioning of new protein aggregates upon division showed higher inheritance by new daughters (62.79% of cell divisions, n = 43, $\chi^2 = 4.651$, df = 1, p = 0.031). However, old daughters inherited the majority of recurring aggregates (97.90% of cell divisions, n = 143, $\chi^2 = 258.69$, df = 1, p < 0.001) as these became anchored to old cell poles.

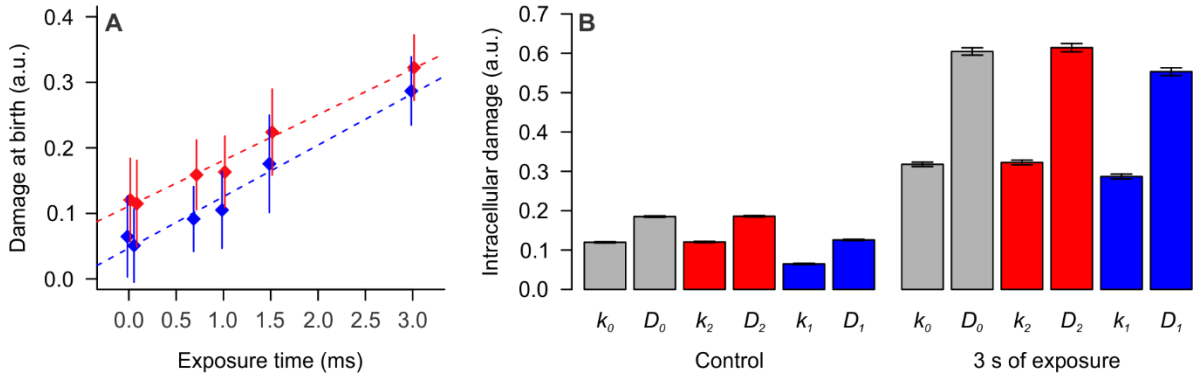

Figure 2.A.2 - Intracellular damage levels under light exposure.
Intracellular damage at birth (k_i) and division (D_i) was estimated from growth parameters extracted for each population, based on individual doubling times. (A) The levels of damage inherited by new (blue) and old (red) daughters increased with the exposure to light excitation. An ANOVA revealed a significant effect of both exposure (n = 4634 cells, F = 2792.0, $p < 0.001$) and age (F = 968.4, $p < 0.001$) on inherited damage. Data are represented as mean ± SD. (B) Intracellular damage levels of populations at control conditions (reproduced from Figure 2.1E) or 3 s of light exposure. A significant difference was observed between k_1 and k_2 (paired one-tailed t test, t = 5.175, df = 69, $p < 0.001$) and between D_1 and D_2 (paired one-tailed t test, t = 5.304, df = 69, $p < 0.001$) in the 3 s treatment. Old daughters in the treatment were born with higher damage levels than in control (two-tailed t test, t = 32.408, df = 82.118, $p < 0.001$). The difference $k_2 - k_1$ was significantly higher for control than treatment cells (two-tailed t test, t = 2.805, df = 80.995, p = 0.0063), an indication of higher symmetry in our 3 s treatment. Data are represented as mean ± SEM.

Table 2.A.1 - Growth parameters of unstressed populations. Values of growth parameters Π (min), λ (min^{-1}) and *a* obtained for wild-type populations.

Strain	**Π [95% CI]**	**λ [95% CI]**	***a* [95% CI]**
MG1655	19.735 [19.299-20.164]	0.0022 [0.0016-0.0029]	0.362 [0.330-0.385]
MG1655	19.762 [19.318-20.192]	0.0024 [0.0018-0.0031]	0.360 [0.334-0.384]
MG1655	21.031 [20.424-21.832]	0.0020 [0.0008-0.0031]	0.390 [0.359-0.421]
MG1655	20.560 [19.957-21.196]	0.0023 [0.0013-0.0032]	0.377 [0.351-0.398]
MG1655	17.211 [16.224-17.941]	0.0050 [0.0038-0.0065]	0.385 [0.353-0.414]

Table 2.A.2 - Elongation rates of MG1655 populations exposed to extrinsic damage. Means and standard deviations of normalized elongation rates (min^{-1}) measured for each level of light exposure, heat or streptomycin, compared to its respective control.

Damage type	Damage intensity	Control		Treatment		Unpaired two-tailed t test		
		n	Mean±SD	n	Mean±SD	t	df	p
Light exposure	70 ms	939	1±0.069	810	0.986±0.087	3.803	1544	0.0001
	700 ms	756	1±0.072	793	0.928±0.076	19.21	1545	<0.001
	1000 ms	580	1±0.082	445	0.901±0.080	19.345	966.18	<0.001
	1500 ms	831	1±0.098	934	0.779±0.135	39.554	1694.8	<0.001
	3000 ms	377	1±0.090	236	0.675±0.162	28.233	326.95	<0.001
Heat stress	38°C	345	1±0.081	535	1.032±0.133	4.437	876.010	<0.001
	40°C	298	1±0.086	782	1.114±0.127	16.836	787.190	<0.001
	43°C	231	1±0.093	380	0.987±0.239	0.948	536.380	0.344
Streptomycin	2 µg	513	1±0.081	453	1.013±0.088	2.391	922.260	0.017
	4 µg	340	1±0.074	337	0.946±0.075	9.383	674.680	<0.001
	5 µg	469	1±0.073	292	0.895±0.222	7.832	330.230	<0.001

Table 2.A.3 - Growth parameters of MG1655 exposed to phototoxic damage. Growth parameters λ (min^{-1}) and *a* obtained for populations exposed to phototoxic damage, using Π from each respective control population.

Exposure (ms)	**λ [95% CI]**	**a [95% CI]**
70	0.0024 [0.0021-0.0028]	0.351 [0.321-0.379]
700	0.0038 [0.0035-0.0040]	0.378 [0.366-0.391]
1000	0.0042 [0.0038-0.0046]	0.406 [0.388-0.425]
1500	0.0061 [0.0057-0.0066]	0.446 [0.421-0.465]
3000	0.0089 [0.0086-0.0092]	0.475 [0.466-0.484]

Table 2.A.4 - Doubling time asymmetry of MG1655 exposed to extrinsic damage. Means and standard deviations of new and old daughter doubling times (min), along with pairwise comparison, for populations exposed to phototoxic damage, heat stress or streptomycin. Pairs where one daughter arrested division were excluded.

Damage type	Damage level	n	Old daughter Mean±SD	New daughter Mean±SD	Paired one-tailed t test t	df	p
Light exposure	70 ms	582	23.080±1.892	21.470±1.466	14.228	290	<0.001
	700 ms	632	24.973±1.813	22.904±1.424	19.881	315	<0.001
	1000 ms	326	26.977±2.147	25.129±1.943	9.260	162	<0.001
	1500 ms	706	30.461±8.473	28.331±3.233	4.670	352	<0.001
	3000 ms	150	32.680±4.337	29.980±3.546	5.293	74	<0.001
Heat stress	38°C	242	23.033±1.94	20.999±1.618	13.486	241	<0.001
	40°C	352	21.45±1.627	19.666±1.174	18.676	351	<0.001
	43°C	155	22.881±3.424	22.122±4.45	3.292	154	<0.001
Streptomycin	2 µg	216	26.130±3.048	25.001±2.855	7.804	215	<0.001
	4 µg	162	26.628±2.243	25.751±1.902	5.686	161	<0.001
	5 µg	127	26.075±5.056	24.005±4.476	11.604	126	<0.001

Table 2.A.5 - Variance partitioning in populations exposed to phototoxic damage. Partitioning of doubling time variances into stochastic ($[V_N + V_o]/2$) and deterministic ($D^2/4$) components. Values presented as mean and 95% confidence intervals.

Exposure (ms)	D^2/4	(Vn+Vo)/2	Total Variance
70	0.649 [0.482-0.836]	2.578 [2.223-2.953]	3.226 [2.813-3.672]
700	1.070 [0.872-1.29]	2.657 [2.311-3.014]	3.727 [3.301-4.165]
1000	0.854 [0.534-1.25]	4.570 [3.769-5.456]	5.425 [4.570-6.378]
1500	0.744 [0.430-1.15]	12.829 [11.053-14.82]	13.573 [11.762-15.62]
3000	1.823 [0.747-3.496]	13.956 [9.007-20.243]	15.780 [10.301-23.17]

2.7 References

Ackermann, Martin, Stephen C. Stearns, and Urs Jenal. 2003. “Senescence in a Bacterium with Asymmetric Division.” *Science* 300: 1920.

Aravinthan, Aloysious. 2015. “Cellular Senescence: A Hitchhiker’s Guide.” *Human Cell* 28: 51–64. doi:10.1007/s13577-015-0110-x.

Baba, Tomoya, Takeshi Ara, Miki Hasegawa, Yuki Takai, Yoshiko Okumura, Miki Baba, Kirill A. Datsenko, Masaru Tomita, Barry L. Wanner, and Hirotada Mori. 2006. “Construction of *Escherichia coli* K-12 in-Frame, Single-Gene Knockout Mutants: The Keio Collection.” *Molecular Systems Biology* 2. doi:10.1038/msb4100050.

Bufalino, Mary Rose, Brian DeVeale, and Derek van der Kooy. 2013. “The Asymmetric Segregation of Damaged Proteins Is Stem Cell-Type Dependent.” *Journal of Cell Biology* 201 (4): 523–30. doi:10.1083/jcb.201207052.

Campisi, Judith, and Fabrizio d’Adda di Fagagna. 2007. “Cellular Senescence: When Bad Things Happen to Good Cells.” *Nature Reviews. Molecular Cell Biology* 8 (9): 729–40. doi:10.1038/nrm2233.

Chao, Lin. 2010. “A Model for Damage Load and Its Implications for the Evolution of Bacterial Aging.” *PLoS Genetics* 6 (8): e1001076. doi:10.1371/journal.pgen.1001076.

Chao, Lin, Camilla Ulla Rang, Audrey Menegaz Proenca, and Jasper Ubirajara Chao. 2016. “Asymmetrical Damage Partitioning in Bacteria: A Model for the Evolution of Stochasticity, Determinism, and Genetic Assimilation.” *PLoS Computational Biology* 12 (1): e1004700. doi:10.1371/journal.pcbi.1004700.

Coelho, Miguel, Aygül Dereli, Anett Haese, Sebastian Kühn, Liliana Malinovska, Morgan E. Desantis, James Shorter, Simon Alberti, Thilo Gross, and Iva M. Tolić-Nørrelykke. 2013. “Fission Yeast Does Not Age under Favorable Conditions, but Does so after Stress.” *Current Biology* 23 (19): 1844–52. doi:10.1016/j.cub.2013.07.084.

Coquel, Anne Sophie, Jean Pascal Jacob, Mael Primet, Alice Demarez, Mariella Dimiccoli, Thomas Julou, Lionel Moisan, Ariel B. Lindner, and Hugues Berry. 2013. “Localization of Protein Aggregation in *Escherichia coli* Is Governed by Diffusion and Nucleoid Macromolecular Crowding Effect.” *PLoS Computational Biology* 9 (4). doi:10.1371/journal.pcbi.1003038.

Dixit, Ram, and Richard Cyr. 2003. “Cell Damage and Reactive Oxygen Species Production Induced by Fluorescence Microscopy: Effect on Mitosis and Guidelines for Non-Invasive Fluorescence Microscopy.” *Plant Journal* 36 (2): 280–90. doi:10.1046/j.1365-313X.2003.01868.x.

Doyle, Shannon M., and Sue Wickner. 2009. “Hsp104 and ClpB: Protein Disaggregating Machines.” *Trends in Biochemical Sciences* 34 (1): 40–48. doi:10.1016/j.tibs.2008.09.010.

Ducret, Adrien, Ellen M. Quardokus, and Yves V. Brun. 2016. “MicrobeJ, a Tool for High Throughput Bacterial Cell Detection and Quantitative Analysis.” *Nature Microbiology* 1 (7). doi:10.1038/nmicrobiol.2016.77.

Erjavec, N, M Cvijovic, E Klipp, and T Nyström. 2008. “Selective Benefits of Damage Partitioning in Unicellular Systems and Its Effects on Aging.” *Proceedings of the National Academy of Sciences of the United States of America* 105 (48): 18764–69. doi:10.1073/pnas.0804550105.

Fuentealba, Luis C, Edward Eivers, Douglas Geissert, Vincent Taelman, and E M De Robertis. 2008. “Asymmetric Mitosis: Unequal Segregation of Proteins Destined for Degradation.” *Proceedings of the National Academy of Sciences of the United States of America* 105 (22): 7732–37. doi:10.1073/pnas.0803027105.

Godley, Bernard F., Farrukh A. Shamsi, Fong-Qi Liang, Stuart G. Jarrett, Sallyanne Davies, and Mike Boulton. 2005. “Blue Light Induces Mitochondrial DNA Damage and Free Radical Production in Epithelial Cells.” *Journal of Biological Chemistry* 280 (22): 21061–66. doi:10.1074/jbc.m502194200.

Gourmelon, M., J. Cillard, and M. Pommepuy. 1994. “Visible Light Damage to *Escherichia coli* in Seawater: Oxidative Stress Hypothesis.” *Journal of Applied Bacteriology* 77 (1): 105–12. doi:10.1111/j.1365-2672.1994.tb03051.x.

Govers, Sander K., Julien Mortier, Antoine Adam, and Abram Aertsen. 2018. Protein Aggregates Encode Epigenetic Memory of Stressful Encounters in Individual *Escherichia coli* Cells. *PLoS Biology*. Vol. 16. doi:10.1371/journal.pbio.2003853.

Jeyapalan, Jessie C., and John M. Sedivy. 2008. “Cellular Senescence and Organismal Aging.” *Mechanisms of Ageing and Development* 129: 467–74. doi:10.1016/j.mad.2008.04.001.

Kirkwood, T. B. L. 2008. “Understanding Ageing from an Evolutionary Perspective.” *Journal of Internal Medicine* 263 (2): 117–27. doi:10.1111/j.1365-2796.2007.01901.x.

Książek, Krzysztof. 2010. “Bacterial Aging: From Mechanistic Basis to Evolutionary Perspective.” *Cellular and Molecular Life Sciences* 67 (18): 3131–37. doi:10.1007/s00018-010-0417-4.

Laney, Samuel R., Robert J. Olson, and Heidi M. Sosik. 2012. “Diatoms Favor Their Younger Daughters.” *Limnology and Oceanography* 57 (5): 1572–78. doi:10.4319/lo.2012.57.5.1572.

Lindner, Ariel B, Richard Madden, Alice Demarez, Eric J Stewart, and François Taddei. 2008. “Asymmetric Segregation of Protein Aggregates Is Associated with Cellular Aging and Rejuvenation.” *Proceedings of the National Academy of Sciences of the United States of America* 105 (8): 3076–81. doi:10.1073/pnas.0708931105.

López-Otín, Carlos, Maria A. Blasco, Linda Partridge, Manuel Serrano, and Guido Kroemer. 2013. “The Hallmarks of Aging.” *Cell* 153: 1194–1217. doi:10.1016/j.cell.2013.05.039.

Moore, D. L., G. A. Pilz, M. J. Arauzo-Bravo, Y. Barral, and S. Jessberger. 2015. “A Mechanism for the Segregation of Age in Mammalian Neural Stem Cells.” *Science* 349 (6254): 1334–38. doi:10.1126/science.aac9868.

Ni, Ming, Antoine L Decrulle, Fanette Fontaine, Alice Demarez, Francois Taddei, and Ariel B Lindner. 2012. “Pre-Disposition and Epigenetics Govern Variation in Bacterial Survival upon Stress.” *PLoS Genetics* 8 (12): e1003148. doi:10.1371/journal.pgen.1003148.

Proenca, Audrey M., Camilla Ulla Rang, Christen Buetz, Chao Shi, and Lin Chao. 2018. “Age Structure Landscapes Emerge from the Equilibrium between Aging and Rejuvenation in Bacterial Populations.” *Nature Communications* 9: 3722. doi:10.1038/s41467-018-06154-9.

Rang, Camilla U, Annie Y Peng, and Lin Chao. 2011. “Temporal Dynamics of Bacterial Aging and Rejuvenation.” *Current Biology* 21 (21): 1813–16. doi:10.1016/j.cub.2011.09.018.

Rang, Camilla U, Annie Y Peng, Art F Poon, and Lin Chao. 2012. “Ageing in *Escherichia coli* Requires Damage by an Extrinsic Agent.” *Microbiology* 158 (Pt 6): 1553–59. doi:10.1099/mic.0.057240-0.

Rang, Camilla Ulla, Audrey Menegaz Proenca, Christen Buetz, Chao Shi, and Lin Chao. 2018. “Minicells as a Damage Disposal Mechanism in *Escherichia coli*.” *MSphere* 3 (5): e00428-18.

Rokney, Assaf, Merav Shagan, Martin Kessel, Yoav Smith, Ilan Rosenshine, and Amos B. Oppenheim. 2009. “*E. coli* Transports Aggregated Proteins to the Poles by a Specific and Energy-Dependent Process.” *Journal of Molecular Biology* 392 (3). Elsevier Ltd: 589–601. doi:10.1016/j.jmb.2009.07.009.

Rose, Michael R. 1991. Evolutionary Biology of Aging. New York: Oxford University Press.

Sabate, Raimon, Natalia S. De Groot, and Salvador Ventura. 2010. “Protein Folding and Aggregation in Bacteria.” *Cellular and Molecular Life Sciences* 67 (16): 2695–2715. doi:10.1007/s00018-010-0344-4.

Steiner, Ulrich K., Adam Lenart, Ming Ni, Peipei Chen, Xiaohu Song, François Taddei, Ariel B. Lindner, and James W. Vaupel. 2017. “Two Stochastic Processes Shape Diverse Senescence Patterns in a Single-Cell Organism.” *BioRxiv*. doi:http://dx.doi.org/10.1101/105387.

Stewart, Eric J, Richard Madden, Gregory Paul, and François Taddei. 2005. “Aging and Death in an Organism That Reproduces by Morphologically Symmetric Division.” *PLoS Biology* 3 (2): e45. doi:10.1371/journal.pbio.0030045.

Wang, Ping, Lydia Robert, James Pelletier, Wei Lien Dang, Francois Taddei, Andrew Wright, and Suckjoon Jun. 2010. “Robust Growth of *Escherichia coli*.” *Current Biology* 20 (12). Elsevier Ltd: 1099–1103. doi:10.1016/j.cub.2010.04.045.

Winkler, Juliane, Anja Seybert, Lars König, Sabine Pruggnaller, Uta Haselmann, Victor Sourjik, Matthias Weiss, Achilleas S Frangakis, Axel Mogk, and Bernd Bukau. 2010. "Quantitative and Spatio-Temporal Features of Protein Aggregation in *Escherichia coli* and Consequences on Protein Quality Control and Cellular Ageing." *The EMBO Journal* 29 (5): 910–23. doi:10.1038/emboj.2009.412.

Yang, Da, Anna D. Jennings, Evalynn Borrego, Scott T. Retterer, and Jaan Männik. 2018. "Analysis of Factors Limiting Bacterial Growth in PDMS Mother Machine Devices." *Frontiers in Microbiology* 9 (MAY): 1–12. doi:10.3389/fmicb.2018.00871.

CHAPTER 3

A link between aging and persistence

3.1 Abstract

Despite the variety of strategies microorganisms have evolved to resist antibiotic treatments, most chronic infections are caused by subpopulations of susceptible bacteria in a transient state of dormancy. This phenotype, known as persistence, arises due to a natural and ubiquitous heterogeneity of growth states in bacterial populations, having been observed in *Escherichia coli*, *Mycobacterium tuberculosis*, *Staphylococcus aureus*, and many others. Nonetheless, the origin and unifying mechanism of this dormancy remains unknown, with several unrelated pathways being able to trigger persistence. Through single-cell microscopy and microfluidic techniques, we show that asymmetric damage partitioning, by producing deterministic phenotypic heterogeneity in bacterial populations, could be a driver of bacterial persistence. We demonstrate a relationship between the presence of protein aggregates, a marker for bacterial old poles, and the frequency of persister cells in a population. We also show the presence of deterministic asymmetry in the high-persistence mutant *hipA7*, widely used in antibiotic persistence research. Therefore, we propose asymmetric damage partitioning as the driver of the phenotypic heterogeneity leading to antibiotic persistence. Elucidating the link between asymmetry and persistence may provide a new perspective in the treatment of recalcitrant infections.

3.2 Introduction

Despite the variety of strategies microorganisms have evolved to resist antibiotic treatments, most chronic infections are caused by dormant subpopulations of susceptible bacteria. This phenotype, known as bacterial persistence, was first recognized upon the early clinical administrations of penicillin (Lee, Foley, and Epstein 1944). Although the magnitude of this public health concern was elusive at the time, *persisters* are ubiquitous among bacteria and represent the main cause of recalcitrant infections (van den Bergh, Fauvart, and Michiels 2017). These cells are present in the population prior to antibiotic treatment, evading the drugs through dormancy and generating a new susceptible population after treatment (Balaban et al. 2004; Levin and Rozen 2006; Lewis 2007). While the immune system alone is usually able to eliminate persisters left behind by antibiotics, these bacteria represent a serious concern in immunocompromised patients or in infections that evade immunity (van den Bergh, Fauvart, and Michiels 2017). Nonetheless, despite the identification of a wide variety of persistence mechanisms over the years, the current knowledge on this phenotype remains fragmented and often inconsistent.

Contrary to antibiotic resistance, where bacteria employ active evasion strategies, persistence derives from the heterogeneity of growth states in bacterial populations. This dormancy or slow growth represents a distinct physiological state often attributed to stochasticity, produced by variations in gene expression (Shah et al. 2006; N. Wu et al. 2015; Vázquez-Laslop, Lee, and Neyfakh 2006), toxin production (Rotem et al. 2010; Gerdes and Maisonneuve 2012), or accumulation of damaged components (Leszczynska et al. 2013; Y. Wu et al. 2012). Among the known persistence mechanisms, the effect of toxins produced by toxin-antitoxin modules has been studied in most detail. These modules are ubiquitous and highly redundant in bacteria, encoding toxins that repress cell growth and lead to dormancy (Gerdes and Maisonneuve 2012; Schuster

and Bertram 2013; Shah et al. 2006). Particularly, a high-persistence allele (*hipA7*) of the toxin HipA was observed in *Escherichia coli*, enhancing persistence rates by up to 1,000-fold due to a decreased interaction with the HipB antitoxin (Balaban et al. 2004; Schumacher et al. 2015; Germain et al. 2015; Korch, Henderson, and Hill 2003). The accumulation of HipA resulted in the stochastic transitioning between dormant and growing states, with persister frequencies increasing in stationary phase. The identification of a high-persistence mutant has allowed the observation of this phenotype through single-cell microscopy (Balaban et al. 2004; Mumcuoglu et al. 2008). However, studies following the onset of stochastic dormancy in bacterial lineages are still scarce.

Another important mechanism for the formation of persisters is the accumulation of non-genetic damage, which can produce deterministic heterogeneity in a population. Stressing factors, leading to oxidation or protein misfolding and aggregation, were shown to increase the frequency of persistent cells (Leszczynska et al. 2013; Y. Wu et al. 2012). Similarly, previous studies verified that mutations in certain chaperones impact the formation of persisters (Hansen, Lewis, and Vulić 2008; Leszczynska et al. 2013; Vázquez-Laslop, Lee, and Neyfakh 2006) and that the SOS response is essential for persister formation in response to fluoroquinolones (Dörr, Lewis, and Vulić 2009). Contrary to the idea of a stochastic switch between dormant and active growth states, previous research suggests a deterministic correlation between non-genetic damage and growth rates in rod-shaped bacteria (Lindner et al. 2008; Winkler et al. 2010; Stewart et al. 2005). Misfolded proteins accumulate in the form of aggregates, which become anchored at the cell poles (Coquel et al. 2013). Upon division each cell inherits a newly synthesized pole, formed at the fission site, and an old pole carrying damage accumulated by the mother. On the following generation, one daughter cell (*new daughter*) inherits the maternal new pole, carrying little damage, while its sibling (*old daughter*) inherits an old pole harboring larger damage loads (Fig 3.1A). This

asymmetric damage inheritance was shown to produce phenotypic heterogeneity, leading to deterministic aging and rejuvenation in bacterial populations (Stewart et al. 2005; Rang, Peng, and Chao 2011; Proenca et al. 2018). Although it was suggested that bacterial aging could lead to the formation of persister cells (Klapper et al. 2007; Aldridge et al. 2012), few studies have attempted to trace such parallel.

In this study, we propose a unifying explanation for antibiotic persistence by correlating this phenotype with bacterial aging. Through single-cell microscopy, we observed deterministic asymmetry in the *E. coli hipA7* mutant. By culturing *hipA7* populations in a microfluidic device, we verified a state of stable growth in both new and old lineages. Exponentially growing cultures of wild-type and *hipA7* were nearly identical in every growth aspect, and we did not observe a stochastic formation of persister cells in these experiments. Curiously, our results suggest that the high-persistence strain has a longer lag phase, surviving treatment when antibiotics are administrated before its exponential phase begins. We show that a pre-treatment with sub-inhibitory antibiotic concentrations can extend the lag phase in wild-type bacteria, increasing the frequency of persisters. Similarly, the induction of starvation or protein synthesis arrest produced persister cells from exponential cultures, suggesting that a clean growth arrest is necessary for survival through dormancy.

3.3 Results

3.3.1 Aging could explain antibiotic persistence

To quantify the phenotypic asymmetry produced by bacterial aging, we cultured populations of wild-type (WT) *E. coli* MG1655 in the mother machine microfluidic device. As demonstrated in the previous chapters, this device allows for stable growth over several

generations, while trapping the old lineage at the bottom of growth wells. In such conditions, with abundant nutrients and constant environment, old and new lineages reach distinct states of growth equilibrium (Figure 3.1B and Chapter 1). These equilibria are produced by the asymmetric partitioning of damage present in unstressed cells, leading to slower elongation rates and longer doubling times in old daughters. Lineages constantly inheriting old poles remain at the old lineage equilibrium, while the consecutive inheritance of new poles retains lineages at the new equilibrium. Because each mother bacterium in equilibrium produces a daughter belonging to the opposite equilibrium, these stable points are connected by processes of aging and rejuvenation.

As we have demonstrated in Chapter 2, the infliction of extrinsic damage through various sources has distinct consequences for old and new daughters. When rates of damage accumulation reach a certain threshold, old lineages lose equilibrium and arrest growth while new lineages retain proliferative immortality (Figure 3.1C). This threshold can be produced by phototoxic damage pulses with 3 s of exposure every 2 min, by 5 $\mu g.ml^{-1}$ Streptomycin, or by 43ºC heat stress (Figure 3.1D). While some new lineages also arrest division, old daughters consistently displayed a higher probability of becoming mortal at these conditions. Interestingly, these damage sources produced different effects over the elongation rate variance of our populations (Figure 3.1E). By partitioning the sums of squares into stochastic and deterministic (asymmetry and heritability) components, we observed that phototoxic damage produced the highest fraction of stochastic variance. Consequently, bacteria displayed constant elongation rates permeated by events of mortality. On the other hand, an increase in heritability was observed with Streptomycin, resulting in a progressive growth decline as shown by Figure 3.1D.

We hypothesize that this growth arrest could be related to the dormancy phenotype leading to antibiotic persistence. Since old lineages tend to arrest division with a lower damage threshold,

we hypothesize that there is a connection between old daughters and persister cells. On the next sections, we will explore the phenotypic heterogeneity produced by aging, enhanced by damaging agents, in the presence of antibiotic treatments.

3.3.2 Formation of persisters from exponentially growing populations

To investigate the development of antibiotic persistence in old lineages, we followed *E. coli* cells growing in the mother machine as they accumulated damage and arrested division. In order to induce the formation of protein aggregates, increasing the doubling time difference between siblings and decreasing elongation rates, we exposed the culture to light excitation applied in 2 min intervals. Although our previous results indicate that 3 s of exposure would induce division arrest in old daughters, we chose a lower exposure level to allow for a higher heterogeneity of growth states. Thus, we employed 1.5 s of light exposure for 16 h to induce damage accumulation, which was followed by the addition of 100 $\mu g.ml^{-1}$ of Streptomycin to the culture medium. The treatments were followed by a period of recovery, when no extrinsic damage was present.

Throughout the experiment, a total of 20 cells arrested growth for intervals between 4.2 and 25 h, 13 of which were old daughters (Figure 3.2A and 3.2B). Three of these cells became dormant before the addition of Streptomycin, a hallmark of bacterial persistence. Unfortunately, a total of 19 cells lysed during the recovery period without regaining growth activity (Figure 3.2C). One individual, which was the first to enter dormancy, remained stable for seven days after Streptomycin was removed from the system, without manifesting visible changes in cell size or integrity. Over several replicates of this experiment, employing distinct antibiotics (Streptomycin, Ampicillin, Nalidixic Acid) administered after various pre-treatments (light exposure, sub-

inhibitory antibiotic concentrations), we obtained the same outcome. While reaching loss of equilibrium and its consequent growth arrest consistently, no dormant cells regained proliferation spontaneously. We have also attempted to induce regrowth through the supplementation of growth medium with the chemical chaperone MOPS, replacement of LB by minimal media, and addition of mammalian gut signals. No pre-treatment, antibiotic drug, or recovery condition has promoted persister awakening for exponential cultures.

Since the fraction of persisters present in exponential cultures is dramatically low for an easy visualization of the phenotype within microfluidic devices, we attempted to reproduce a successful experiment performed in a batch culture. This study observed that an exponential culture treated with 50 $\mu g.ml^{-1}$ Tetracycline for 30 min exhibited high rates of persistence to 100 $\mu g.ml^{-1}$ Ampicillin. We performed this sequence of treatments in an exponentially growing culture in the mother machine device (Figure 3.2D and 3.2E), observing several dormancy events. Most dormant cells lysed during or after the antibiotic treatment 5 h window. However, after 6h of antibiotic removal three old lineages resumed growth. Throughout the device, considering 1650 growth wells, we observed a total of 160 persister lineages during the recovery period. Old lineages represented 83% of these persisters. The remaining 17% persisters represent wells in which the new lineages persisted, but the old lysed.

These results suggest that the trigger inducing dormancy influences the ability of a cell to resume growth after the antibiotic treatment. While damaging agents successfully induce dormancy in old lineages through increased damage inheritance, these cells are likely unable to repair such large damage loads. Tetracycline, on the other hand, induces a non-damaging protein synthesis arrest, inducing the production of persisters. These results suggest that environmental triggers are essential for the formation of persisters from exponentially growing cultures.

3.3.3 High persistence mutants display long-term growth stability

To increase the probability of observing persisters in microfluidic experiments, we employed the high-persistence *E. coli hipA7*. This mutation decreases the binding between the toxin HipA and its antitoxin, leading to increased dormancy rates. To observe a large population of this mutant, we cultured *hipA7* in the daughter device and compared to wild-type bacteria. Populations were imaged under stable unstressed conditions throughout the experiments.

The high-persistence mutant exhibited no anomalies in its growth physiology. Its elongation rates remained stable over time, with new daughters (0.029 ± 0.002 min^{-1}, n = 1565 cells) elongating faster than old daughters (0.028 ± 0.002 min^{-1}, n = 1505 cells; one-tailed t test, t = 13.37, df = 3063.1, $p < 0.001$; Figure 3.3A and 3.3B). *hipA7* displayed marginally slower growth than wild-type bacteria (Figure 3.3C), with a two-way ANOVA suggesting a significant effect of strain ($F = 51.390$; $p < 0.001$) and age ($F = 238.001$, $p < 0.001$) on elongation rates. This asymmetry was clearly visible on phase planes comparing the doubling times of a mother and its two daughters (Figure D and E). *hipA7* new daughters (23.843 ± 1.786 min, n = 1195 cells) exhibited shorter doubling times than their old siblings (24.573 ± 1.749 min, n = 1195 cells; one-tailed paired t test, t = 12.955, df = 1194, $p < 0.001$). Both lineages had a positive correlation with maternal doubling times, with new lineages showing a higher slope ($a = 0.443$, $p < 0.001$, $R^2 = 0.148$) than old lineages ($a = 0.349$, $p < 0.001$, $R^2 = 0.095$). Nonetheless, our stability analysis (see Chapter 1) performed on these slopes indicated that both lineages displayed stable growth equilibrium (Figure 3.3F), with the condition $a^2 + \sigma_1^2 = 1$ being largely satisfied. Thus, we found no evidence for loss of proliferation due to unstable growth on *hipA7* lineages.

We hypothesized that an increased stochasticity in growth physiology could lead to spontaneous persistence events. To address this hypothesis, we estimated the stochastic and

deterministic components of growth variance in wild-type and *hipA7* populations (see Chapter 2 and Chao et al. 2016). We normalized each pair of siblings by the estimated doubling time for a symmetric cell division, thus centering the population at a mean of zero. New and old subpopulations compose distinct distributions, with the distance between these distributions representing the doubling time variance produced by deterministic asymmetry (Figure 3.3G and 3.3H). The mean variance of the distributions, on the other hand, represents and estimate of stochastic variance. We observed no difference between wild-type and *hipA* populations in terms of deterministic or stochastic variance, suggesting that *hipA7* is not more likely to undergo spontaneous growth arrest. Therefore, *hipA7* mutants growing exponentially are physiologically equivalent to wild-type bacteria.

In only one aspect, *hipA7* displayed a remarkable distinction from wild-type *E. coli*. We observed that mutant cells loaded on a mother machine device had a longer lag phase (93.65 ± 26.37 min, n = 60 cells), with the first generation of cells taking longer than wild-type (62.60 ± 14.61 min, n = 60 cells; one-way ANOVA $F = 64.112$, $p < 0.001$) until the first division (Figure 4A). This large lag phase difference is especially crucial in the interpretation of previous studies where the antibiotic treatment occurred within the lag phase of *hipA7* (Balaban et al. 2004). While our attempts to produce *hipA7* persisters from exponentially growing populations yield the same negative results as for wild-type, we observed the formation of several persister lineages when 100 $\mu g.ml^{-1}$ Ampicillin was introduced 1 h after loading into the microfluidic device (data under collection). The cells that did not start exponential growth until the antibiotic treatment survived, resuming growth once the antibiotic was removed. Thus, the longer lag phase observed in *hipA7* mutants is the main differential in the formation of persister cells.

3.3.4 Stationary phase persisters

To explore the effect of stationary phase on persisters under single-cell microscopy, we cultured *E. coli* in agarose pads with Ampicillin. We employed the strain MG1655 containing yellow fluorescence protein (YFP) bound to the small chaperone IbpA, which acts as a marker for the subcellular localization of protein aggregates. Since protein aggregates eventually become anchored at the old cell poles (Chapter 2, Figure 2.1), we expect most cells containing large aggregates to be old daughters. We inoculated cells with 0, 1 or 2 $\mu g.ml^{-1}$ Streptomycin to induce the formation of protein aggregates in stationary cultures. Overnight cultures were then loaded into agarose pads containing 100 $\mu g.ml^{-1}$ Ampicillin and followed over 20 h, yielding measurements of cell area, protein aggregate area, and time until lysis.

We observed the classic bi-phasic killing of bacterial populations containing persister cells (Figure 3.4B). The rapid killing phase corresponds to the susceptible subpopulation, which is followed by the slower killing rate of the persistent subpopulation. Most antibiotic persistence studies limit the treatment window to 4-6 h, therefore we considered persisters the cells that survived beyond 5 h of treatment. The pre-treatment with 1 $\mu g.ml^{-1}$ Streptomycin led to a longer lag phase before the susceptible subpopulation started decaying (Figure 3.4B), which in this case was translated to a marginally higher persister frequency (Figure 3.4C). We further grouped the populations according to the presence of protein aggregates, observing the frequency of persisters among damaged or damage-free cells. In the 0 $\mu g.ml^{-1}$ control, we observed no distinction between groups, with cells containing aggregates showing 26.63% survival, and damage-free cells 23.71% ($X^2 = 0.362$, $p = 0.547$). However, the frequency of persisters in the 1 $\mu g.ml^{-1}$ Streptomycin pre-treatment was significantly higher among cells containing protein aggregates ($X^2 = 8.117$, $p = 0.004$; Figure 3.4D), relative to the 0 $\mu g.ml^{-1}$ control. This distinction could have emerged from

the increased damage accumulation promoted by Streptomycin, inducing the aggregation of proteins in the old poles. While the same trend was visible in the 2 $\mu g.ml^{-1}$ pre-treatment, with damaged cells exhibiting 54.8% persistence rates, there was no significant difference between groups ($X^2 = 0.504$, $p = 0.478$). We believe that the smaller sample size from this last treatment could explain this outcome (55 cells), and intend to replicate the experiment to further explore the trend.

Taking the presence of protein aggregates into the cellular context, we also considered the total cell area as a predictor of persistence. Overall, persisters exhibited a higher proportion of the cell occupied by aggregates (two-way ANOVA, $F = 11.92$, $p = 0.0006$), while this ratio did not change according to the Streptomycin treatment ($F = 2.65$, $p = 0.072$; Figure 3.4E). The cell area itself, however, was the most important factor in determining survival to 5 h of Ampicillin (Figure 3.4F). While a larger area was observed for the population pre-treated with 2 $\mu g.ml^{-1}$ Streptomycin (two-way ANOVA, $F = 173.43$, $p < 0.001$), susceptible cells also exhibited a larger initial area ($F = 174.54$, $p < 0.001$) than persisters. In our experimental design, cell size was the main indicator of whether an individual had reached stationary phase before the Ampicillin treatment.

Taken together, our results suggest that old daughters might exhibit higher rates of persistence. The higher rates of persisters among cells containing protein aggregates provides a preliminary evidence for this hypothesis, which we are now exploring through more sophisticated experiments. These observations also suggest that dormancy through starvation can effectively produce persisters, as opposed to non-culturable cells produced by our damaging treatments.

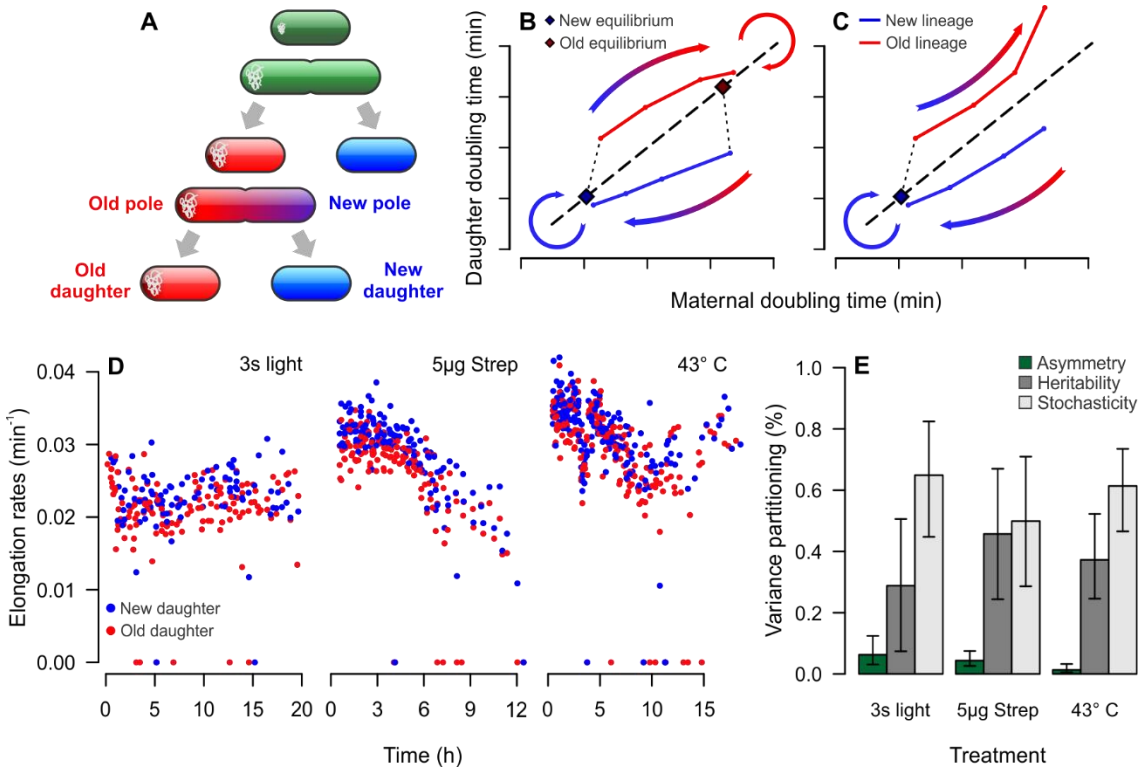

Figure 3.1 - Old lineages display higher probability of arresting division when exposed to extrinsic damage.
(A) Protein aggregates tend to accumulate in the old cell poles, leading to asymmetric damage inheritance. Cells inheriting conserved cell poles are called old daughters, while cells inheriting newly synthesized poles are new daughters. (B and C) Graphical representations of doubling times. (B) New and old lineages, consecutively inheriting either pole, remain in distinct growth equilibria when grown in unstressed conditions. These equilibria are connected by aging and rejuvenating lineages (gradient arrows). (C) When rates of damage accumulation reach a certain threshold, old lineages lose equilibrium and arrest growth, while new lineages are able to remain proliferative. (D) This loss of equilibrium was observed through the infliction of extrinsic damage by light exposure, Streptomycin and heat stress (see Chapter 2). (E) Damaging treatments caused different effects on the doubling time variance of bacterial populations, with light exposure producing the highest stochasticity and Streptomycin the highest deterministic variance.

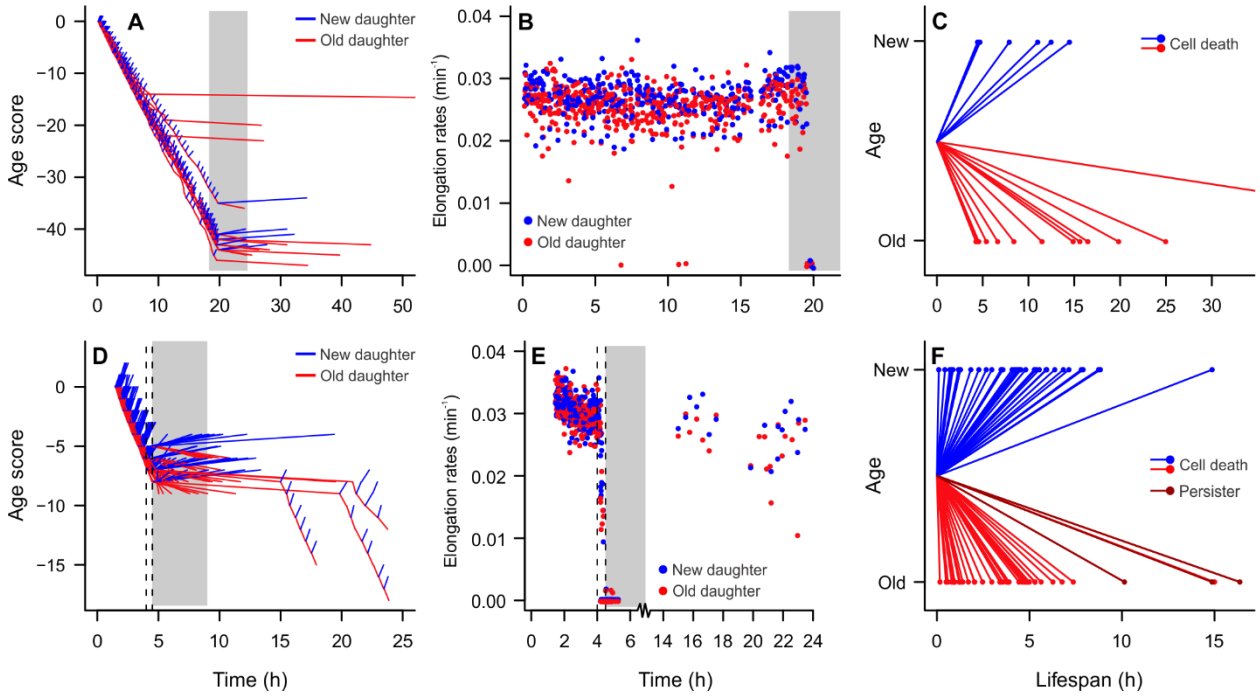

Figure 3.2 - Antibiotic persistence in exponentially growing cultures in microfluidic devices.
(A, B and C) The population was exposed to 1.5 s of light excitation every 2 min for 16 h, followed by treatment with 100 µg.ml^{-1} Streptomycin (gray area) for 5h. A higher frequency of dormant cells was observed among old daughters, although all but one dormant cells lysed over the course of 25 h. (D, E and F) An exponentially growing population was pre-treated with 50 µg.ml^{-1} Tetracycline (dashed lines) for 30 min, followed by exposure to 100 µg.ml^{-1} Ampicillin (gray area) for 5h. Three old lineages produced persisters, resuming growth after the antibiotic was removed.

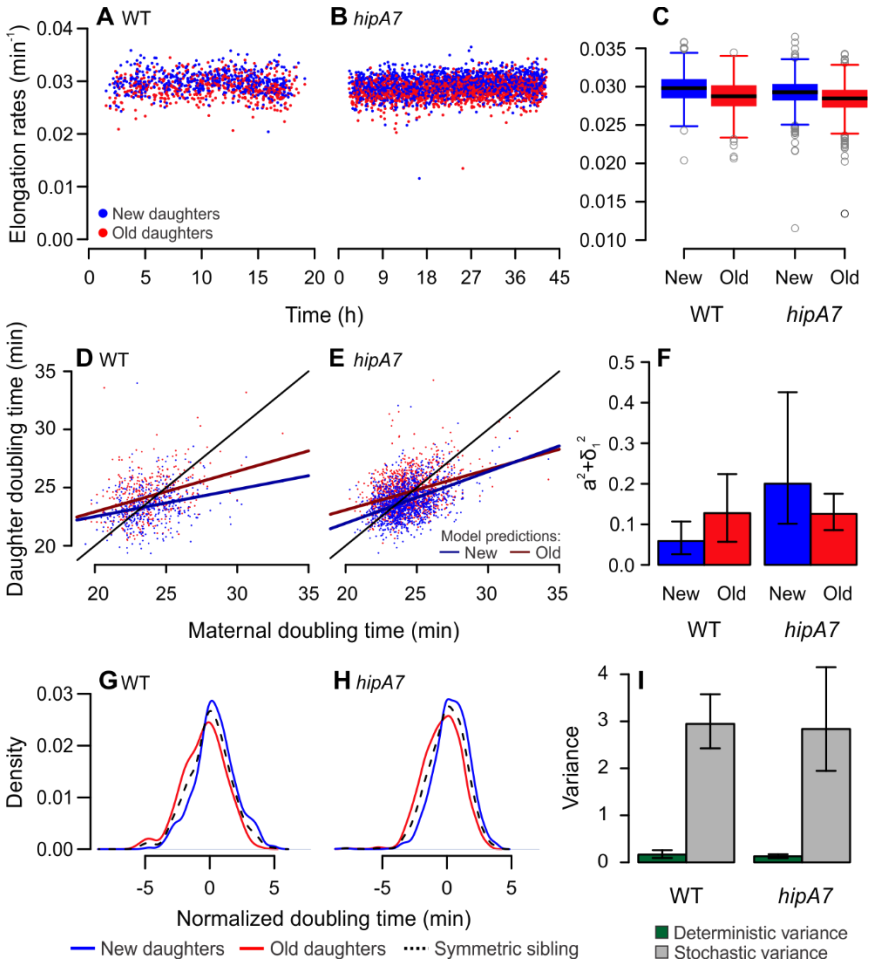

Figure 3.3 - Exponentially growing hipA7 are physiologically similar to wild-type *E. coli.*
(A and B) Elongation rates over time were constant for both strains, with no spontaneous dormancy events observed in the daughter device (see Chapter 1). (C) Doubling times of the wild-type strain were shorter than *hipA7*, and both strains exhibited asymmetry. (D and E) Phase planes show the separation of wild-type and *hipA7* into subpopulations of new and old daughters. The crossing between regression lines and the identity line represents a point of stable equilibrium to which new and old lineages regress. (F) All new and old lineages showed stable equilibrium, indicating that the toxin HipA did not induce dormancy in unstressed cells. (G and H) Normalized doubling time distrubutions used for the determination of stochastic and deterministic components of the doubling time variance. (I) Wild-type and *hipA7* displayed a similar stochastic variance.

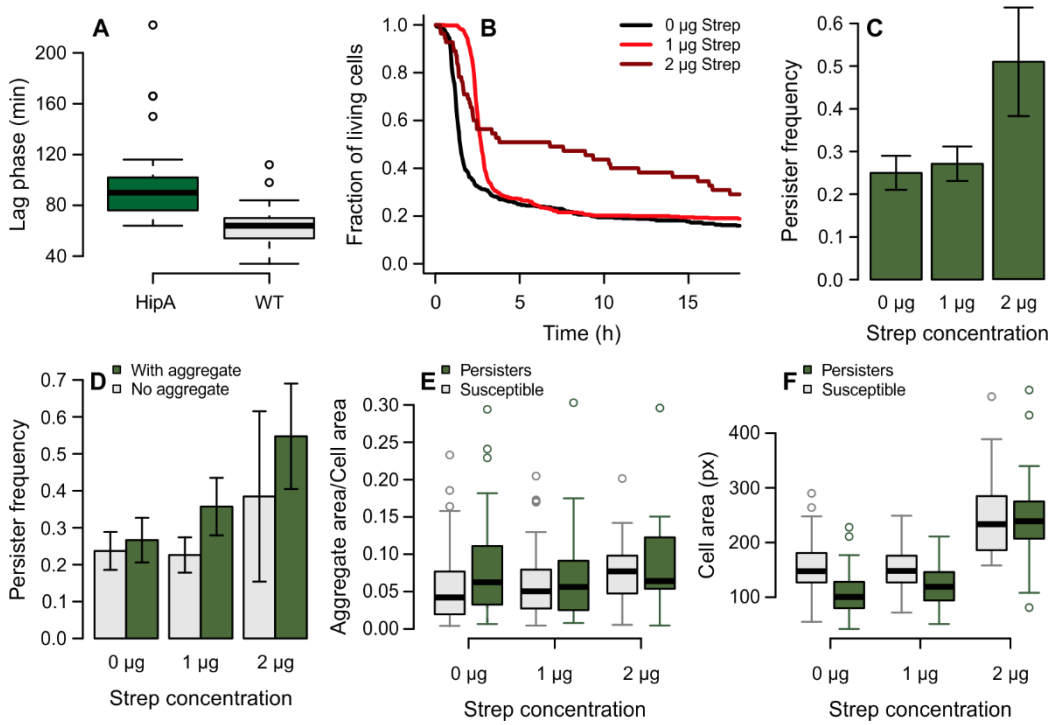

Figure 3.4 - Persistent bacteria observed in stationary phase cultures.
(A) In the mother machine device, *hipA7* mutants displayed a longer lag phase when compared to wild-type. When antibiotic treatments are performed within the lag window, persistence is observed. (B) Populations of *E. coli* MG1655 IbpA:YFP were pre-treated with 0,1 or 2 µg.ml^{-1} Streptomycin in overnight cultures. These cultures were inoculated into agarose pads containing 100 µg.ml^{-1} Ampicillin, showing declining survival over time. (C and D) Error bars represent 95% confidence intervals. (C) Persisters were determined as cells that survived at least 5 h of Ampicillin treatment. The highest frequency was observed for the 2 µg.ml^{-1} pre-treatment. (D) Cell containing protein aggregates displayed higher frequency of persisters, which might suggest a connection to old daughters. (E) The proportion of the cell occupied by a protein aggregate was higher for persisters. (F) The initial cell area is an indicator of whether a cell has entered dormancy, leading smaller cells to survive antibiotic treatment.

3.4 Discussion

Over the past years a wide variety of persistence mechanisms has been identified. The current consensus states that persister cells are present in a heterogeneous population prior to antibiotic treatment, representing a distinct physiological state of dormancy or slow growth (Balaban et al. 2019). This phenotype can be produced by variations in gene expression (Shah et al. 2006; N. Wu et al. 2015; Vázquez-Laslop, Lee, and Neyfakh 2006), toxin production (Rotem et al. 2010; Gerdes and Maisonneuve 2012), or accumulation of damaged components (Y. Wu et al. 2012; Leszczynska et al. 2013). However, the current knowledge on this phenotype remains fragmented, with most research groups focusing on specific protein pathways or toxins rather than looking for a general persistence framework. Moreover, these aspects of bacterial physiology are constantly interacting in living organisms, driving the dynamic emergence of persistence, responding to environmental cues and, ultimately, evolving due to selective pressures.

This study provided evidence for an alternative persistence framework, connecting the phenotype to properties observed in aging populations. We have shown that the dynamics of aging and rejuvenation that emerge in bacterial populations could produce dormant cells (Proenca et al. 2019), which would survive antibiotic treatment. In this scenario, both aging and persistence are produced by the same underlying phenotypic heterogeneity. Our results suggest that old lineages, which are susceptible to growth arrest, could display higher rates of persistence within a population. We have shown that old lineages can persist to Ampicillin when pre-treated with Tetracycline, and that cells containing protein aggregates — more likely to be old daughters — produce a higher persister frequency.

Antibiotic persistence represents a complex phenotype, combining deterministic and stochastic processes and responding to environmental cues. Our results have shown that nutrient

limitation or Tetracycline, which induces protein synthesis arrest, were successful in triggering persistence. Other treatments, including light excitation and oxidative damage, could not produce persisters from exponentially growing cells. Because these treatments can increase lag phase, it is possible that studies reporting exponential phase persisters were, in fact, detecting cells carried over from stationary cultures (Kim and Wood 2016). To conciliate environment and cell physiology, our future experiments will investigate the progression of aging as populations approach stationary phase. Damage accumulation likely plays a role in the determination of growth arrest or proliferation, producing phenotypic heterogeneity. Modulating nutrient availability within microfluidic devices could allow us to visualize the onset of dormancy in natural conditions, tracking damage accumulation and partitioning over generations.

Our future work will address persistence through a combination of experimental evolution, single-cell microscopy, and computational modeling. We will select bacterial populations for increased persistence rates, and investigate whether aging properties change in evolved populations. We will employ microscopy and microfluidic techniques to explore aging and persistence in stationary phase populations. Finally, we will apply this experimental data on the generation of computational models that capture the complexity of this system, producing predictions for the evolution of persistence. Antibiotic persistence is a complex public health concern, which we will continue to study through its multi-scale deterministic and stochastic properties.

3.5 Materials and Methods

3.5.1 Bacterial strains and growth conditions

Experiments were performed using K-12 *E. coli* MG1655. When the visualization of protein aggregates was necessary, MG1655 containing IbpA-YFP was used (A. Lindner, INSERM, France). The wild-type strain was compared to a high persistence mutant, MG1655 *hipA7* (kindly provided by K. Lewis, Northeastern University). Bacteria were grown overnight in LB medium (lysogeny broth) at 37^{o} C with agitation. Growth medium was supplemented with 1 or 2 µg/ml of Streptomycin for induction of protein aggregation, when required.

3.5.2 Microfluidic devices and treatment

Exponential growth experiments were performed using the mother machine or daughter device microfluidic chips. PDMS devices were fabricated through soft lithography from a master silicon wafer, produced by Nano3 (UC San Diego). The mother machine was based on the original design (Wang et al. 2010) and adapted by R. Johnson (Hasty Lab, UC San Diego). The daughter device was developed by O. Mondragón-Palomino (Hasty Lab, UC San Diego) (Mondragón-Palomino et al. 2011). Overnight bacterial cultures were concentrated and loaded into the devices through loading ports. For experiments with the HipA7 mutant, bacteria were kept warm during loading due to cold sensitivity. After loading, inlet and outlet 60 ml syringes were connected to the ports. When necessary, the inlet was replenished or replaced throughout the experiment.

Persister assays in microfluidic devices consisted of a 24 h control period, allowing cells to reach stable exponential growth, followed by a damaging treatment, antibiotic exposure, and recovery. Damaging treatments included light excitation (500 nm) and 1 µg/ml Streptomycin, with exposure lasting for 24 h. Alternatively, pre-treatment was replaced with 50 µg/ml Tetracycline

for 30 min. Antibiotic treatments were performed with 100 µg/ml Streptomycin or Ampicillin for 5 h unless otherwise indicated. Recovery treatments represented a reversion to control conditions, washing the inlet to remove the antibiotic and providing fresh medium.

3.5.3 Agarose pads for stationary cultures

Stationary culture experiments were performed in LB agarose pads (LB medium supplemented with 15g/L agarose). A 10 µl pad containing 100 µg/ml Ampicillin was prepared immediately prior to the experiment. Overnight cultures with 1 or 2 µg/ml Streptomycin were inoculated onto agarose and followed over time until lysis.

3.5.4 Time-lapse imaging and quantification

Cell movies were collected by a Nikon Eclipse Ti-S microscope, with imaging intervals controlled by NIS-Elements AR software. Mother machine and agarose pad phase images were obtained in 2 min intervals, while daughter device experiments were imaged every 20 s. When necessary for the visualization of protein aggregation or as a source of stress, fluorescence images were obtained through a FITC filter (500 nm), following 2, 10 or 20 min intervals.

These images were analyzed using the software ImageJ (NIH, https://imagej.nih.gov/ij), recording cell coordinates as Regions of Interest (ROI) and cell names as indicatives of lineage and cell pole inheritance. Cell lengths were determined immediately before and after each division and time of division was recorded. Elongation rates (r) and doubling times (ln(2)/r) were calculated from the data, and the resulting tables were entered in an R program (version 3.4.1) to determine maternity, sibling pairs and lineage trees. The ImageJ plugin MicrobeJ was used for detertion and segmentation of fluorescence images (Ducret, Quardokus, and Brun 2016).

3.6 Acknowledgements

We thank A. Lindner and K. Lewis for kindly providing bacterial strains. We would like to thank A. Qiu and X. Liu for data collection assistance.

Chapter 3, in part, is currently being prepared for submission for publication of the material. Proenca AM, Rang CU, Chao L. The dissertation author was the primary investigator and author of this material.

3.7 References

Aldridge, Bree B., Marta Fernandez-Suarez, Danielle Heller, Vijay Ambravaneswaran, Daniel Irimia, Mehmet Toner, and Sarah M. Fortune. 2012. "Asymmetry and Aging of Mycobacterial Cells Lead to Variable Growth and Antibiotic Susceptibility." Science 335 (6064): 100–104. https://doi.org/10.1126/science.1216166.Asymmetry.

Balaban, Nathalie Q., Sophie Helaine, Kim Lewis, Martin Ackermann, Bree Aldridge, Dan I. Andersson, Mark P. Brynildsen, Dirk Bumann, Andrew Camilli, James J. Collins, Christoph Dehio, Sarah Fortune, Jean-Marc Ghigo, Wolf-Dietrich Hardt, Alexander Harms, Matthias Heinemann, Deborah T. Hung, Urs Jenal, Bruce R. Levin, Jan Michiels, Gisela Storz, Man-Wah Tan, Tanel Tenson, Laurence Van Melderen, and Annelies Zinkernagel. 2019. "Definitions and Guidelines for Research on Antibiotic Persistence." Nature Reviews Microbiology. https://doi.org/10.1038/s41579-019-0196-3.

Balaban, Nathalie Q., Jack Merrin, Remy Chait, Lukasz Kowalik, and Stanislas Leibler. 2004. "Bacterial Persistence as a Phenotypic Switch." Science (New York, N.Y.) 305 (5690): 1622–25. https://doi.org/10.1126/science.1099390.

Bergh, Bram van den, Maarten Fauvart, and Jan Michiels. 2017. "Formation, Physiology, Ecology, Evolution and Clinical Importance of Bacterial Persisters." FEMS Microbiology Reviews 41 (3): 219–51. https://doi.org/10.1093/femsre/fux001.

Chao, Lin, Camilla Ulla Rang, Audrey Menegaz Proenca, and Jasper Ubirajara Chao. 2016. "Asymmetrical Damage Partitioning in Bacteria: A Model for the Evolution of Stochasticity, Determinism, and Genetic Assimilation." PLoS Computational Biology 12 (1): e1004700. https://doi.org/10.1371/journal.pcbi.1004700.

Coquel, Anne Sophie, Jean Pascal Jacob, Mael Primet, Alice Demarez, Mariella Dimiccoli, Thomas Julou, Lionel Moisan, Ariel B. Lindner, and Hugues Berry. 2013. "Localization of Protein Aggregation in Escherichia Coli Is Governed by Diffusion and Nucleoid Macromolecular Crowding Effect." PLoS Computational Biology 9 (4). https://doi.org/10.1371/journal.pcbi.1003038.

Dörr, Tobias, Kim Lewis, and Marin Vulić. 2009. “SOS Response Induces Persistence to Fluoroquinolones in Escherichia Coli.” PLoS Genetics 5 (12): e1000760. https://doi.org/10.1371/journal.pgen.1000760.

Gerdes, Kenn, and Etienne Maisonneuve. 2012. “Bacterial Persistence and Toxin-Antitoxin Loci.” Annual Review of Microbiology 66 (1): 103–23. https://doi.org/10.1146/annurev-micro-092611-150159.

Germain, Elsa, Mohammad Roghanian, Kenn Gerdes, and Etienne Maisonneuve. 2015. “Stochastic Induction of Persister Cells by HipA through (p)PpGpp-Mediated Activation of MRNA Endonucleases.” Proceedings of the National Academy of Sciences 112 (16): 5171–76. https://doi.org/10.1073/pnas.1423536112.

Hansen, Sonja, Kim Lewis, and Marin Vulić. 2008. “Role of Global Regulators and Nucleotide Metabolism in Antibiotic Tolerance in Escherichia Coli.” Antimicrobial Agents and Chemotherapy 52 (8): 2718–26. https://doi.org/10.1128/AAC.00144-08.

Kim, Jun Seob, and Thomas K. Wood. 2016. “Persistent Persister Misperceptions.” Frontiers in Microbiology 7 (DEC): 1–7. https://doi.org/10.3389/fmicb.2016.02134.

Klapper, I., P. Gilbert, B. P. Ayati, J. Dockery, and P. S. Stewart. 2007. “Senescence Can Explain Microbial Persistence.” Microbiology 153 (11): 3623–30. https://doi.org/10.1099/mic.0.2007/006734-0.

Korch, Shaleen B, Thomas A Henderson, and Thomas M Hill. 2003. “Characterization of the HipA7 Allele of Escherichia Coli and Evidence That High Persistence Is Governed by (p)PpGpp Synthesis.” Molecular Microbiology 50 (4): 1199–1213. https://doi.org/10.1046/j.1365-2958.2003.03779.x.

Lee, S. W., E. J. Foley, and Jeanne A. Epstein. 1944. “Mode of Action of Penicillin. I. Bacterial Growth and Penicillin Activity.” Journal of Bacteriology 48: 393–99. https://doi.org/10.1038/213183a0.

Leszczynska, Daria, Ewelina Matuszewska, Dorota Kuczynska-Wisnik, Beata Furmanek-Blaszk, and Ewa Laskowska. 2013. “The Formation of Persister Cells in Stationary-Phase Cultures of Escherichia Coli Is Associated with the Aggregation of Endogenous Proteins.” PloS One 8 (1): e54737. https://doi.org/10.1371/journal.pone.0054737.

Levin, Bruce R, and Daniel E Rozen. 2006. “Non-Inherited Antibiotic Resistance.” Nature Reviews. Microbiology 4 (7): 556–62. https://doi.org/10.1038/nrmicro1445.

Lewis, Kim. 2007. “Persister Cells, Dormancy and Infectious Disease.” Nature Reviews. Microbiology 5 (1): 48–56. https://doi.org/10.1038/nrmicro1557.

Lindner, Ariel B, Richard Madden, Alice Demarez, Eric J Stewart, and François Taddei. 2008. “Asymmetric Segregation of Protein Aggregates Is Associated with Cellular Aging and Rejuvenation.” Proceedings of the National Academy of Sciences of the United States of America 105 (8): 3076–81. https://doi.org/10.1073/pnas.0708931105.

Mondragón-Palomino, Octavio, Tal Danino, Jangir Selimkhanov, Lev Tsimring, and Jeff Hasty. 2011. “Entrainment of a Population of Synthetic Genetic Oscillators.” Science (New York, N.Y.) 333 (6047): 1315–19. https://doi.org/10.1126/science.1205369.

Mumcuoglu, M., C. Gabay, N. Q. Balaban, G. Engel, and O. Gefen. 2008. “Single-Cell Protein Induction Dynamics Reveals a Period of Vulnerability to Antibiotics in Persister Bacteria.” Proceedings of the National Academy of Sciences 105 (16): 6145–49. https://doi.org/10.1073/pnas.0711712105.

Proenca, Audrey M., Camilla Ulla Rang, Christen Buetz, Chao Shi, and Lin Chao. 2018. “Age Structure Landscapes Emerge from the Equilibrium between Aging and Rejuvenation in Bacterial Populations.” Nature Communications 9: 3722. https://doi.org/10.1038/s41467-018-06154-9.

Proenca, Audrey Menegaz, Camilla Ulla Rang, Andrew Qiu, Chao Shi, and Lin Chao. 2019. “Cell Aging Preserves Cellular Immortality in the Presence of Lethal Levels of Damage.” PLOS Biology 17 (5): e3000266.

Rang, Camilla U, Annie Y Peng, and Lin Chao. 2011. “Temporal Dynamics of Bacterial Aging and Rejuvenation.” Current Biology 21 (21): 1813–16. https://doi.org/10.1016/j.cub.2011.09.018.

Rotem, Eitan, Adiel Loinger, Irine Ronin, Irit Levin-Reisman, Chana Gabay, Noam Shoresh, Ofer Biham, and Nathalie Q. Balaban. 2010. “Regulation of Phenotypic Variability by a Threshold-Based Mechanism Underlies Bacterial Persistence.” Proceedings of the National Academy of Sciences of the United States of America 107 (28): 12541–46. https://doi.org/10.1073/pnas.1004333107.

Schumacher, Maria A., Pooja Balani, Jungki Min, Naga Babu Chinnam, Sonja Hansen, Marin Vulić, Kim Lewis, and Richard G. Brennan. 2015. “HipBA–Promoter Structures Reveal the Basis of Heritable Multidrug Tolerance.” Nature 524 (7563): 59–64. https://doi.org/10.1038/nature14662.

Schuster, Christopher F., and Ralph Bertram. 2013. “Toxin-Antitoxin Systems Are Ubiquitous and Versatile Modulators of Prokaryotic Cell Fate.” FEMS Microbiology Letters 340 (2): 73–85. https://doi.org/10.1111/1574-6968.12074.

Shah, Devang, Zhigang Zhang, Arkady Khodursky, Niilo Kaldalu, Kristi Kurg, and Kim Lewis. 2006. “Persisters: A Distinct Physiological State of E. Coli.” BMC Microbiology 6: 53. https://doi.org/10.1186/1471-2180-6-53.

Stewart, Eric J, Richard Madden, Gregory Paul, and François Taddei. 2005. “Aging and Death in an Organism That Reproduces by Morphologically Symmetric Division.” PLoS Biology 3 (2): e45. https://doi.org/10.1371/journal.pbio.0030045.

Vázquez-Laslop, Nora, Hyunwoo Lee, and Alexander A. Neyfakh. 2006. “Increased Persistence in Escherichia Coli Caused by Controlled Expression of Toxins or Other Unrelated

Proteins." Journal of Bacteriology 188 (10): 3494–97. https://doi.org/10.1128/JB.188.10.3494.

Wang, Ping, Lydia Robert, James Pelletier, Wei Lien Dang, Francois Taddei, Andrew Wright, and Suckjoon Jun. 2010. "Robust Growth of Escherichia Coli." Current Biology 20 (12): 1099–1103. https://doi.org/10.1016/j.cub.2010.04.045.

Winkler, Juliane, Anja Seybert, Lars König, Sabine Pruggnaller, Uta Haselmann, Victor Sourjik, Matthias Weiss, Achilleas S Frangakis, Axel Mogk, and Bernd Bukau. 2010. "Quantitative and Spatio-Temporal Features of Protein Aggregation in Escherichia Coli and Consequences on Protein Quality Control and Cellular Ageing." The EMBO Journal 29 (5): 910–23. https://doi.org/10.1038/emboj.2009.412.

Wu, Nan, Lei He, Peng Cui, Wenjie Wang, Youhua Yuan, Shuang Liu, Tao Xu, Shanshan Zhang, Jing Wu, Wenhong Zhang, and Ying Zhang. 2015. "Ranking of Persister Genes in the Same Escherichia Coli Genetic Background Demonstrates Varying Importance of Individual Persister Genes in Tolerance to Different Antibiotics." Frontiers in Microbiology 6: 1–11. https://doi.org/10.3389/fmicb.2015.01003.

Wu, Yanxia, Marin Vulić, Iris Keren, and Kim Lewis. 2012. "Role of Oxidative Stress in Persister Tolerance." Antimicrobial Agents and Chemotherapy 56 (9): 4922–26. https://doi.org/10.1128/AAC.00921-12.

CONCLUSIONS AND FUTURE DIRECTIONS

The study of aging in bacterial systems can provide valuable insights on the conserved processes involved in the ubiquitous fitness decline observed in biological organisms over time. Morphologically identical bacterial cells were shown to partition non-genetic damage with asymmetry upon division (Stewart et al. 2005; Lindner et al. 2008). Thus, through an unexpected physiological mechanism, asymmetric bacteria satisfy a core requirement of the Evolutionary Theory of Aging, namely exhibiting an effective separation between soma and germline (Kirkwood 2008). This observation expanded the possibilities of using bacteria as simple model organisms for the study of a complex phenotype such as aging, along with its progression along cell lineages.

To investigate the progression of bacterial aging, however, long-term microscopy techniques are essential. Early studies were successful in detecting the asymmetric phenotype by following bacterial colonies for a limited number of generations (Stewart et al. 2005; Rang et al. 2012), but the advancement of single-cell microscopy techniques required the tracking of longer cell lineages in a stable environment. The use of microfluidic devices for the study of bacterial physiology offered the ideal method for this goal (Wang et al. 2010; Ferry, Razinkov, and Hasty 2011; Mondragón-Palomino et al. 2011). Most outstanding, the mother machine microfluidic design allowed for the tracking of bacterial old lineages for hundreds of generations (Wang et al. 2010). However, contrary to the earlier observations of aging, old daughter lineages grown in the mother machine exhibited constant growth physiology, showing no signs of fitness decline over time. Although modeling and data-fitting could identify hypotheses reconciling these opposing results (Chao 2010; Rang, Peng, and Chao 2011) and the advantage of being asymmetric (Chao et

al. 2016), the ideas of bacterial aging versus its long-term growth stability remained controversial in the field.

Chapter 1 of the present dissertation offered a synthesis of physiological immortality and aging occurring in the same cellular context (Proenca et al. 2018). By following new and old cell lineages in microfluidic devices, we demonstrated that bacterial populations stabilize around two points of growth equilibrium. While remaining in equilibrium, both new and old lineages displayed physiological immortality through continuous proliferation with stable elongation rates. Since cells in equilibrium still divide with asymmetry, producing one daughter of the opposite polarity each generation, the stable points become connected by constant processes of aging and rejuvenation as lineages transition from one equilibrium to the other. These processes occur in unstressed populations, thus indicating the formation of deterministic age structures in bacterial populations.

Chapter 2 contextualized these findings through the framework of cellular aging, identifying the factors operating on the transition between proliferative immortality and mortality. The larger field of aging has long focused on multicellular organisms, which offer a direct parallel with human physiology. Whereas relevant hallmarks of aging have been identified (López-Otín et al. 2013) and largely studied, defining aging in the cellular context, the interaction between these hallmarks cannot be easily observed in a complex system. We showed that bacteria can offer a simple model for the study of cellular aging and its progression. Through the infliction of extrinsic damage, we demonstrated the disruption of growth equilibrium leading to a transition between immortality and mortality in single cell lineages. Moreover, because of asymmetric damage partitioning, we showed that old lineages reach their mortality threshold whereas new lineages

remain proliferative within the same population. Thus, cellular aging can lead to a differential cell lineage fate depending on damage inheritance.

Finally, Chapter 3 of this dissertation investigated the application of phenotypic heterogeneity produced by asymmetry in the context of antibiotic treatments. We focused on antibiotic persistence, a phenotype by which bacteria survive treatment by entering a dormant state prior to antibiotic exposure (Balaban et al. 2004; Levin and Rozen 2006; Maisonneuve and Gerdes 2014). Since old lineages are more likely to arrest proliferation, we investigated the connection between asymmetric damage inheritance and antibiotic persistence. This work suggests a new application of bacterial aging studies, suggesting the connection between phenotypic heterogeneity and serious public health concerns.

Future directions of this work include the furthering of antibiotic studies and the identification of intracellular mechanisms involved in the generation of asymmetry. Through the study of single gene deletion mutants, such as performed in Chapter 2, molecular pathways that are essential for an effective partitioning of damaged components could be identified. Furthermore, the investigation of bacteria other than *E. coli* and *C. crescentus* for the aging phenotype could determine aspects of cellular physiology that are necessary for the separation between soma and germline. While this work offered insights on the deterministic aspects of bacterial aging and its consequences for cell fate determination, we are certain the field will continue to move forward in the establishment of bacteria as model organisms for the ubiquitous manifestations of the aging phenotype.

References

Balaban, Nathalie Q., Jack Merrin, Remy Chait, Lukasz Kowalik, and Stanislas Leibler. 2004. "Bacterial Persistence as a Phenotypic Switch." Science (New York, N.Y.) 305 (5690): 1622–25. https://doi.org/10.1126/science.1099390.

Chao, Lin. 2010. "A Model for Damage Load and Its Implications for the Evolution of Bacterial Aging." PLoS Genetics 6 (8): e1001076. https://doi.org/10.1371/journal.pgen.1001076.

Chao, Lin, Camilla Ulla Rang, Audrey Menegaz Proenca, and Jasper Ubirajara Chao. 2016. "Asymmetrical Damage Partitioning in Bacteria: A Model for the Evolution of Stochasticity, Determinism, and Genetic Assimilation." PLoS Computational Biology 12 (1): e1004700. https://doi.org/10.1371/journal.pcbi.1004700.

Ferry, M S, I a Razinkov, and Jeff Hasty. 2011. Microfluidics for Synthetic Biology: From Design to Execution. Methods in Enzymology. 1st ed. Vol. 497. Elsevier Inc. https://doi.org/10.1016/B978-0-12-385075-1.00014-7.

Kirkwood, T. B. L. 2008. "Understanding Ageing from an Evolutionary Perspective." Journal of Internal Medicine 263 (2): 117–27. https://doi.org/10.1111/j.1365-2796.2007.01901.x.

Levin, Bruce R, and Daniel E Rozen. 2006. "Non-Inherited Antibiotic Resistance." Nature Reviews. Microbiology 4 (7): 556–62. https://doi.org/10.1038/nrmicro1445.

Lindner, Ariel B, Richard Madden, Alice Demarez, Eric J Stewart, and François Taddei. 2008. "Asymmetric Segregation of Protein Aggregates Is Associated with Cellular Aging and Rejuvenation." Proceedings of the National Academy of Sciences of the United States of America 105 (8): 3076–81. https://doi.org/10.1073/pnas.0708931105.

López-Otín, Carlos, Maria A. Blasco, Linda Partridge, Manuel Serrano, and Guido Kroemer. 2013. "The Hallmarks of Aging." Cell 153: 1194–1217. https://doi.org/10.1016/j.cell.2013.05.039.

Maisonneuve, Etienne, and Kenn Gerdes. 2014. "Molecular Mechanisms Underlying Bacterial Persisters." Cell 157 (3): 539–48. https://doi.org/10.1016/j.cell.2014.02.050.

Mondragón-Palomino, Octavio, Tal Danino, Jangir Selimkhanov, Lev Tsimring, and Jeff Hasty. 2011. "Entrainment of a Population of Synthetic Genetic Oscillators." Science (New York, N.Y.) 333 (6047): 1315–19. https://doi.org/10.1126/science.1205369.

Proenca, Audrey M., Camilla Ulla Rang, Christen Buetz, Chao Shi, and Lin Chao. 2018. "Age Structure Landscapes Emerge from the Equilibrium between Aging and Rejuvenation in Bacterial Populations." Nature Communications 9: 3722. https://doi.org/10.1038/s41467-018-06154-9.

Rang, Camilla U, Annie Y Peng, and Lin Chao. 2011. "Temporal Dynamics of Bacterial Aging and Rejuvenation." Current Biology 21 (21): 1813–16. https://doi.org/10.1016/j.cub.2011.09.018.

Rang, Camilla U, Annie Y Peng, Art F Poon, and Lin Chao. 2012. “Ageing in Escherichia Coli Requires Damage by an Extrinsic Agent.” Microbiology 158 (Pt 6): 1553–59. https://doi.org/10.1099/mic.0.057240-0.

Stewart, Eric J, Richard Madden, Gregory Paul, and François Taddei. 2005. “Aging and Death in an Organism That Reproduces by Morphologically Symmetric Division.” PLoS Biology 3 (2): e45. https://doi.org/10.1371/journal.pbio.0030045.

Wang, Ping, Lydia Robert, James Pelletier, Wei Lien Dang, Francois Taddei, Andrew Wright, and Suckjoon Jun. 2010. “Robust Growth of Escherichia Coli.” Current Biology 20 (12): 1099–1103. https://doi.org/10.1016/j.cub.2010.04.045.